ROBUST CONTROLLER SPECIFICATION AND DESIGN FOR A RUN-OF-MINE MILLING CIRCUIT

by

Ian Keith Craig

A thesis submitted to the Faculty of Engineering, University of the Witwatersrand, Johannesburg, in fulfilment of the requirements for the degree of Doctor of Philosophy.

Johannesburg, 1993.

DECLARATION

I declare that this thesis is my own, unaided work. It is being submitted for the Degree of Doctor of Philosophy in the University of the Witwatersrand, Johannesburg. It has not been submitted before for any degree or examination in any other university.

16 day of February 1993

ABSTRACT

A new approach to the problem of designing a control system for a run-of-mine (ROM) milling circuit is described. The ROM mill control problem is formalized in terms of a general linear system synthesis and analysis framework. Using this framework, μ-synthesis and analysis is applied to a model of an industrial ROM milling circuit. The milling circuit uncertainty structure is obtained from plant perturbation tests. Correlations of plant parameter uncertainties and the choice of the location of uncertainty weights within the plant transfer function matrix structure, are discussed. Some comments are made as to possible sources of the plant uncertainties, and practical measures that can be taken to minimize them. The choice of performance weighting functions is discussed with regard to the economic and process-related importance of each plant output and issues of implementation such as the sampling rate to be used. A μ-controller is obtained which provides robust performance in the face of significant model uncertainties. This controller is tested on a real industrial ROM milling circuit. It is shown that the μ-controller could be made to work on an industrial plant. Practical problems encountered are discussed, and reasons are given as to why the behaviour of the physical system differs form that observed in computer simulations.

ABSTRACT

A new approach to the problem of designing a control system for a run-of-mine (ROM) milling circuit is described. The ROM mill control problem is formalized in terms of a general linear system synthesis and analysis framework. Using this framework, μ-synthesis and analysis is applied to a model of an industrial ROM milling circuit. The milling circuit uncertainty structure is obtained from plant perturbation tests. Correlations of plant parameter uncertainties and the choice of the location of uncertainty weights within the plant transfer function matrix structure, are discussed. Some comments are made as to possible sources of the plant uncertainties, and practical measures that can be taken to minimize them The choice of performance weighting functions is discussed with regard to the economic and process-related importance of each plant output and issues of implementation such as the sampling rate to be used. A μ-controller is obtained which provides robust performance in the face of significant model uncertainties. This controller is tested on a real industrial ROM milling circuit. It is shown that the μ-controller could be made to work on an industrial plant. Practical problems encountered are discussed, and reasons are given as to why the behaviour of the physical system differs form that observed in computer simulations.

To my loving wife

Andrie

ACKNOWLEDGEMENTS

I am very grateful to my thesis supervisor Prof. Ian MacLeod for his guidance, support and encouragement during recent years. His contagious positive approach and sound judgement is greatly appreciated.

I would also like to thank my colleagues at Mintek who helped to create an environment which is conducive to doing high quality research. They include Victor Babarovich Hansen, Roger Henning, Dave Hulbert, Philip M[illegible]er, Gunter Metzner and Tiberius Viljoen. Their friendship and professionalism are greatly appreciated. A special word of thanks to Roger Henning and Dave Hulbert for proof reading this document.

I am especially privileged to have had Dave Hulbert as mentor and colleague. His pioneering work in the field of milling control is undisputed, and his humility and sense of excellence is an example to all. I will never forget the comment which he made when his multivariable controller worked fist time on the plant, "*If the theory says it must work, it must work!*".

Finally I would like to thank Mintek for the opportunity of conducting this research, and for sending me to Boston to do an SM at MIT.

CONTENTS

LIST OF FIGURES

Figure **Page**

LIST OF TABLES

Table **Page**

LIST OF SYMBOLS

R	field of real numbers
R_+	non-negative real numbers
jR	the imaginary axis
C	field of complex numbers
C_+	complex numbers with non-negative real parts
C^{nxm}	space of complex matrices of dimension n x m
A^T	transpose of matrix A
A^*	complex conjugate transpose of matrix A
A^{-1}	inverse of matrix A
$\lambda_i(A)$	the i^{th} eigenvalue of a matrix A
$\overline{\lambda}(A)$	the maximum eigenvalue of a matrix A
$\sigma_i(A)$	the i^{th} singular value of a matrix A
$\overline{\sigma}(A)$	the maximum singular value of a matrix A
$\rho(A)$	the spectral radius of a matrix A
$\mu(A)$	the structured singular value of matrix A
sup	least upper bound
inf	greatest lower bound
diag	diagonal
iff	if and only if
t/h	metric ton per hour

m^3/h	cubic meters per hour
L_∞	Banach space of matrix-valued functions which are (essentially) bounded on jR
H_∞	functions in L_∞ with bounded analytic continuation to the right half plane
$\|M\|_\infty$	L_∞/H_∞ norm
	$= \operatorname{ess}\sup_{\omega \in R} \overline{\sigma}[M(j\omega)]$ if $M \in L_\infty(jR)$ or $H_\infty(jR)$

NOMENCLATURE

CFF	cyclone-feed flow
FDLTI	finite-dimensional and linear-time-invariant
LOAD	mass of material in a mill
LTI	linear-time-invariant
MFS	mill-feed solids
MIMO	multi-input-multi-output
MIW	mill-inlet water
NP	nominal performance
NS	nominal stability
PSE	particle-size estimate/estimator
ROM	run-of-mine
RP	robust performance
RS	robust stability
SAG	semi-autogenous
SFW	sump-feed water
SISO	single-input-single-output
SLEV	sump level

CHAPTER 1

INTRODUCTION

1.1 Overview

1.1.1 Motivation and background

In the mineral processing industry, milling is normally the first stage of a metallurgical extraction process. Milling is not only the most expensive unit operation of such a process, but the quality of the milling circuit product is crucial to the ability of the downstream processes to separate the valuable material from the gangue. Improving milling efficiency could lead to a reduction in the cost of milling, but even larger financial benefits are obtained through the beneficial effects that better milling has on downstream extraction processes.

The selection of the structure of a milling circuit, and the selection and sizing of equipment are very important in determining the quality of the product produced. In addition once these factors are fixed, process control is needed to aid plant personnel in operating the milling circuit in an optimum manner, as disturbances that do inevitably occur are of such a nature that they cannot be eliminated by good plant design alone.

Feedback control systems thus play an important role in the operation of a milling circuit. For example, large economic benefits can be obtained by reducing fluctuations in important plant variables, and feedback can be used to reject disturbances which cause these process fluctuations [1]. A control system can also provide a basis for process optimization, so that resources can be utilized in an optimum manner. The plant can be open-loop unstable, in which case feedback can be utilized to provide stability. However, one of the most important factors which hampers the implementation of feedback control and optimization schemes on milling plants, is the uncertain nature of the underlying metallurgical process.

In order to synthesize a controller for the real plant, a dynamic model which describes the interaction between important plant input and output variables is needed. There is, however, an inherent discrepancy between this mathematical model and the plant, as no physical system can be modeled exactly. Thus in order to completely describe a physical system, the model should also include an uncertainty description which describes the set of all possible plant variations that can occur in practice. The uncertainty description should captivate plant parameter variations, neglected high frequency dynamics, neglected time delays, and approximations made during the modelling process. The uncertainty description must be mathematically tractable, in order to fit into the controller synthesis and analysis framework.

Given a plant model plus an uncertainty description, the control engineer can design a control system for the plant, such that some performance criterion is satisfied. Nominal stability is obtained automatically in most modern controller synthesis methods. A possible controller design approach is then to use suitable analysis tools to determine whether or not the plant-controller combination is robust (in terms of stability and performance), to the plant uncertainty. Thus the analysis test tells the designer if the controller is able to stabilize the plant, and deliver the required performance, in the presence of the plant uncertainty.

Maintaining closed-loop stability and performance in the presence of uncertainty has been the driving force behind the development of control theory for most of the twentieth century (e.g., [2] and [3]). The concepts of gain and phase margin were developed by classical designers to quantify stability robustness for single-input-single-output (SISO) systems. More recently criteria have been proposed for multi-input-multi-output (MIMO) systems in which closed-loop stability is maintained in the presence of a single unstructured norm-bounded uncertainty. These criteria were formulated in terms of a singular value frequency-domain inequality on the closed-loop transfer function [4]. This work was extended to include multiple model uncertainties appearing at different locations in the plant and feedback loop. Such structured uncertainty can arise from multiple unstructured uncertainty blocks and parameter uncertainty. Doyle developed an analysis framework based on the structured singular value to asses the stability and performance of linear-time-invariant (LTI) feedback systems in the presence of structured uncertainty [5]. Numerous attempts to develop a robust synthesis methodology which utilizes the μ-analysis framework (e.g., [6] and [7]) have been made. These developments paved the way for addressing the run-of-mine (ROM) milling controller synthesis and analysis problem in a formal framework, and will be elaborated upon later in this thesis. (ROM milling is autogenous or semi-autogenous (SAG) milling of ore that has not been sized or crushed, except perhaps in regard to very large rocks.)

Milling circuits used in the mineral processing industry, grind ore to a fine product, and the quality of this product determines the ability of the down-stream processes to extract the maximum possible benefit from the processed ore. A milling circuit can thus be said to operate in an optimized manner when it is producing a high-quality product at the maximum possible rate and efficiency. Producing a high-quality product implies that some form of product-size control is required, whereas maximizing the rate at which this product is produced requires a form of grinding media control.

A first step toward the optimization of a milling circuit was the introduction of an instrument to continuously measure the quality of the milling-circuit product on-line. This was made possible by the development of an ultrasound-based particle-size estimator (PSE) in the 1970's [8]. The next step in achieving optimized milling-circuit operation was the control of the milling-circuit product, utilizing the measurements provided by a PSE. Milling circuits are inherently multivariable due to the highly interactive nature of the process dynamics, and multivariable controller design techniques have to be applied to effectively control the product size to a setpoint. Various successful attempts were made during the early 1980's at product-size control for conventional milling circuits ([9],[10]). These multivariable product-size controllers are reported to have been taken into continuous use on the milling circuits for which they were designed.

Since the introduction of ROM milling in 1958 [11], most of the mining industry's efforts have been directed towards grinding-media control, rather than product-size control (e.g. [12]). Product-size control of ROM milling circuits is more difficult than for conventional milling since the main grinding medium and the feed rate of the ore to the mill are not independent. Due to the ROM nature of the feed material, there is also very little or no control over the size and hardness of the grinding medium. This results in significant uncontrolled disturbances entering the circuit. Hulbert *et al.* [13] showed that product-size control of an industrial ROM milling circuit is possible. For this implementation the inverse Nyquist array (INA) method [14] was used to design a MIMO controller for the milling circuit.

In the hands of an experienced control engineer who has a good understanding of the process to be controlled, the INA synthesis method (and other MIMO synthesis techniques derived from classical methods, for e g., [15] and [16]) can result in useful controllers for MIMO systems. Considerable skill, intuition, and effort is however required on the part of the designer when using synthesis methods that are currently applied to ROM milling circuits, as they do not accommodate performance specifications or the significant model uncertainties that are present in ROM models in a rigorous manner. Great care has to be taken to ensure that the resulting closed-loop system is robust to model un- ..inties, as the way in which the uncertainties impact on the system is not transparent [4].

Considerable time is required, using current methods, to establish a control system on an industrial ROM milling circuit. It can take anything from three to twelve months for such a system to materialize. As time is money, the resulting control system could be very expensive.

In view of the above, it is worthwhile to consider an alternate MIMO synthesis and analysis technique for ROM milling circuit controllers. Such a technique should address the weaknesses of methodologies that are currently applied to ROM milling circuits, i.e., it should

- deal with model uncertainties in a formal manner
- deal with performance specifications in a formal manner
- provide necessary and sufficient conditions for robust stability and performance
- formalize the intuitive design decisions of the experienced control engineer

A formal ROM milling controller synthesis and analysis framework that address the issues raised above could reduce the time and skill required, and thus also the cost, to establish a controller on an industrial ROM milling circuit. It would thus make advanced control and optimization strategies more affordable by the mineral processing industry. It is for these reasons that such a framework is developed in this document.

1.1.2 Contribution of the thesis

The main contributions made in this thesis are as follows: for the first time, the ROM milling circuit control problem is formalized in terms of a general synthesis and analysis framework, and a μ-controller which results from the proposed approach is tested on an actual industrial ROM milling circuit.

The dynamics of a ROM milling circuit exhibit large uncertainties which are mainly due to size distribution and hardness changes in the feed material. A simple, practically viable method is proposed for obtaining a milling circuit uncertainty description from plant perturbation tests. Correlations of plant parameter uncertainties are discussed together with the location of uncertainty weights within the plant transfer function matrix structure. Specific attention is given to motivating the choice of uncertainty and performance weights from a practical point of view. The choice of performance weighting functions is discussed with regard to the economic and process-related importance of each plant output, and issues of implementation such as the sampling rate to be used.

An approach for applying the μ-methodology to the resulting finite-dimensional and linear-time-invariant (FDLTI) model of an industrial ROM milling circuit is demonstrated. Given the plant model, a model uncertainty description, and performance specifications, the μ-methodology results in a closed-loop system that is guaranteed to achieve nominal stability and performance, and stability and performance robustness with respect to the model uncertainty. The order of this controller is reduced to make it suitable for implementation.

Experimental implementation of the resulting μ-controller on an industrial ROM milling circuit is discussed. The results show that such a controller could be made to work on an industrial plant. Practical problems encountered during tests are analyzed, and reasons are given as to why the behaviour of the physical system differs form that observed in computer simulations.

1.1.3 Organization of the thesis

This thesis is organized into six chapters. In the remainder of the first chapter previous work done in the area of milling control and robust control, is reviewed.

Chapter 2 provides the theoretical background required for the rest of the thesis. The structured singular value is introduced, and a formal structure for controller synthesis and analysis is established.

The ROM milling circuit under consideration is described in Chapter 3. It is in this chapter, together with Chapter 5 in which the main contribution of this thesis can be found. The objectives of milling control are discussed, and the plant model with its uncertainty description are given. The selection of uncertainty weights and performance specifications are motivated from a practical point of view. Finally, the ROM milling circuit model with its uncertainty description is put into a general synthesis and analysis framework.

The ROM milling circuit controller synthesis and analysis is done in Chapter 4. In this chapter the μ-synthesis and analysis procedure is applied to the milling circuit with its uncertainty and performance weights as established in Chapter 3. Weight iterations are done in order to meet the performance robustness requirement. The order of the controller that results from the μ-synthesis process is reduced to ease its practical implementation. The reduced order controller is analyzed for robustness using μ-analysis and linear time simulations.

Chapt 5 describes the practical implementation of the μ-controller on an industrial ROM milling circuit. The platform on which the controller was implemented, is discussed. Results of initial plant tests are presented which indicate that the μ-controller design needs to be modified. One set of plant identification tests, which led to a redesign of the μ-controller, are described. Results achieved with this final controller are also presented and discussed.

Conclusions and recommendations are given in Chapter 6. In this chapter a summary of the most important results of this thesis is given. An assessment of the study is done where the significance and limitations of the work are discussed. Finally some suggestions are made for future research.

1.2 Previous Work and Related Literature

1.2.1 Milling control

The control and optimization strategies for ROM and SAG milling reported in the literature concentrate their efforts mainly on grinding media control. These methods are essentially based upon adjusting the mill feed-rate (and possibly composition) in order to achieve a certain power draw from the mill motor. Flook and Plasket [17] propose the use of a Williamson-type controller [18] to control the mill feed-rate to maximize power demand, as they claim that this maximizes both throughput and fineness of grind. Pauw *et al.* [19] report a multivariable peak-seeking controller which maximizes power by utilizing the addition of water and pebbles to pebble mills. They state that this strategy optimizes the pebble load and bulk density of the load so that the mill operates at maximum efficiency. Herbst *et al.* [20] use Kalman filtering techniques to estimate certain milling parameters on-line, from which the feed-rate necessary to achieve a desired power draw is determined. Mular [21] reports on an attempt to the control product size of a SAG milling circuit using single variable techniques, but it appears that these efforts have been abandoned.

Hulbert [1] reports on the state of the art in milling control. He states that the most appropriate control strategies for milling are those that not only stabilize the milling process, but are also aimed at optimizing the economics of the plant as a whole. This daunting task is perhaps best approached by defining a series of sub-objectives which are compatible with the overall aim of optimizing the plant's economic performance. The particle size of the product of a milling circuit and the throughput of solids are of major importance when specifying sub-objectives. This is because these two variables are closely related to the quality of the product, and the efficiency of operation. Towards this end, Hulbert *et al.* [13] pioneered the control of product particle-size for ROM milling in 1987. The process dynamics were found to be highly interactive, which necessitated the use of multivariable controller design techniques. This controller was subsequently optimized to combine particle-size control with grinding media control in order to maximize the efficiency of the milling circuit [22]. Efforts were also made to extend the range over which particle size can be controlled. For this purpose the inlet water feed to the mill was used as an additional "steady-state" control action, and a hydrocyclone underflow angle meter was used to extend the range of the feed flow to the cyclone [23].

Milling circuit models, and ROM models in particular, generally contain significant uncertainties which complicate the controller synthesis process. Various attempts have been made to address this problem by using real-time recursive filters to estimate uncertain plant parameters ([24],[25]). More recently, Metzner and MacLeod [26] investigated the application of multivariable adaptive control to ROM milling, in order to accommodate the time-varying nature of a ROM mill's dynamics.

1.2.2 Robust linear control

The problem of designing a feedback system that is robust with respect to model uncertainties has received considerable attention in recent times. In fact, robustness has become somewhat of a buzzword in the control community with thousands of papers having been published on the subject of robust control (e.g. [27] and [28] and the references cited therein). Two types of model uncertainties are usually singled out, i.e., parametric or structured uncertainty, and dynamic or unstructured uncertainty. Synthesis and analysis techniques can be categorized according to which type of uncertainty they address.

As far back as 1945 Bode [2] argued that the inclusion of plant uncertainty is a fundamental aspect of feedback theory. This aspect was also addressed by Horowitz in his 1963 book [3], and led him to developed the so-called quantitative feedback theory (QFT) which utilizes templates that represent, at a particular frequency, the gain and phase changes associated with parameter variations as a region on a Nichols chart (see [29] and references cited therein). From these templates a loop-transfer function is derived via graphical techniques. This procedure has been shown to provide closed-loop stability and specified performance over the possible range of parameters. Although SISO QFT seems to be a reasonable synthesis method, it would appear that QFT cannot be easily generalized to the MIMO case in order for it to be a practical MIMO design tool [30].

Laughlin *et al.* [31] proposed a SISO controller design technique that can be applied to a process described by a transfer function with real parameter variations. All the possible variations of the transfer function are pictured as model uncertainty regions on the complex plane. The internal model control (IMC) method [32] is then used to map the uncertainty regions to the Nyquist plane for stability and performance analysis. This method can unfortunately not be generalized to the MIMO case, as more than one element in the MIMO loop-transfer function matrix can be influenced by a common source of uncertainty. This method is impractical for MIMO controller design because arbitrary conservativeness is introduced if elements are considered to have independent uncertainties when they are in fact correlated.

Robustness measures such as the MIMO stability margin [33] and the structured singular value [5] have been proposed to deal with both parametric and unstructured uncertainty. These measures can potentially be conservative in the case of real parametric uncertainty, as real parameters are essentially replaced with complex ones when they are calculated.

Various attempts have been made at dealing with systems that contain both real parametric and unstructured uncertainties. Wei and Yedavalli [34] propose a method for the robust stabilization of minimum phase SISO plants having both parametric and unstructured uncertainty. Hollot *et al.* [35] use Kharitonov-like results to treat parametric uncertainty and unmodeled high frequency dynamics for SISO systems in a unified framework. Kharitonov's theorem provides a necessary and sufficient condition for the stability of a polynomial whose coefficients vary independently in given bounded intervals. One only needs to check the stability of four vertex polynomials to guarantee the stability of the entire family. The results of this theorem have generated significant interest in the control community since it was introduced to the Western literature by Barmish in 1982 (see [36] and the references cited therein). Fan *et al.* [37] compute the structured singular value in the case of mixed real parametric and complex uncertainty for MIMO systems. Sánches Peña and Sideris [38] propose a stability and performance analysis method which determines the robustness of a MIMO system with possible related real uncertain parameters and structured complex uncertainty. These efforts discussed above mainly address the analysis of control systems uncertain systems, and should be encouraged as they broaden the type of uncertainty structure that can be addressed. However, the problem of synthesizing controllers for MIMO plants with real parametric and structured uncertainties, remains largely unsolved.

Adaptive control has been proposed as a solution to the robust control problem, as such controllers are designed to overcome parameter uncertainty. The idea of identifying the plant uncertainties on-line is certainly very appealing, but unfortunately, adaptive controllers have great difficulty in dealing with unstructured model uncertainty [39]. Significant advances have been made in the field of robust adaptive control (adaptive control in the presence of unstructured model uncertainty) in recent times [40], but it would appear that a theory which provides general robust stability and performance guarantees in an adaptive control context, is still a long way off.

1.2.3 The μ-methodology

For the time being, the μ-methodology developed by Doyle ([5], [6], [41], and [42]) appears to be the most promising approach to the controller synthesis and analysis problem for application to a ROM milling circuit. Several application studies, in which this methodology was used, have been reported in the literature. Doyle *et al.* [43] designed a lateral axis flight control system for a space shuttle during reentry. Smith *et al.* [44] apply μ-synthesis to a laboratory scale two-tank control problem, and experimentally compare the resulting μ-controller to a loop shaping controller. Skogestad *et al.* [45] designed a control system for a high-purity distillation column. They show that an acceptable performance/robustness trade-off cannot be obtained for this ill-conditioned plant by using simple loop-shaping techniques. Steinbach *et al.* [46] apply μ-analysis to a five degrees of freedom electromechanical positioning device to be used in optical recording.

A technique currently available to solve the μ-synthesis problem is referred to as DK iteration [42]. This technique exploits the fact that the structured singular value is a scaled version of the singular value with a block structured scaling matrix. The aim of the DK iteration scheme is to find a stabilizing controller K and a diagonal scaling matrix D such that the H_∞-norm of the scaled closed-loop transfer function is less than or equal to unity (, the condition for robust performance is satisfied). This is accomplished by alternately minimizing the scaled closed-loop transfer function with respect to either K or D while holding the other constant. For a fixed scaling D, a standard H_∞ control problem results which can be solved for K using the techniques discussed in [47]. For a fixed controller K the minimization with respect to D is a convex optimization problem at each frequency. The result is a real diagonal matrix $D(\omega)$ of which the magnitude frequency response is fitted with a stable, minimum phase rational transfer function. The process is repeated until it converges.

Until fairly recently, the solution of the μ-synthesis problem using DK iteration was cumbersome due to the computational complexity of solving the associated H_∞ synthesis problem [48]. Glover and Doyle [49] introduced a solution to the H_∞ synthesis problem that involves only two algebraic Ricatti equations. This advance greatly improves the efficiency of the DK iteration technique.

The major problem with this μ-synthesis method is that the DK iteration is not guaranteed to find the globally optimal K and D, as individual convexity in the two parameters D and K do not imply joint convexity.

CHAPTER 2

BACKGROUND THEORY

This chapter provides the theoretical background required for the rest of the thesis. The structured singular value μ is defined and its use as an analysis tool is discussed in terms of stability, performance and robustness. The chapter is concluded with a discussion of the μ-synthesis procedure.

2.1 The Structured Singular Value

The structured singular value μ was developed by Doyle [5], and plays an important role in the analysis of feedback systems with structured uncertainty. Referring to the feedback structure in Figure 2.1, μ can be seen as a function of a complex matrix M which essentially "measures" the distance to singularity of M with respect to a set of complex structured perturbations Δ. μ Can thus be thought of as a tool to analyze the "stability" of the closed-loop system in Figure 2.1. When I - MΔ remains nonsingular for all frequencies and for all Δ under consideration, the only solutions to the loop equations,

$$\begin{aligned} d &= Mz \\ z &= \Delta d \end{aligned} \tag{2.1}$$

are z = d = 0. The system could then be considered to be "stable". However if $I - M\Delta$ is singular, then there are infinitely many solutions to (2.1), and the norms $\|d\|$, $\|z\|$ of the solutions can be arbitrary large. The system can then be called "unstable".

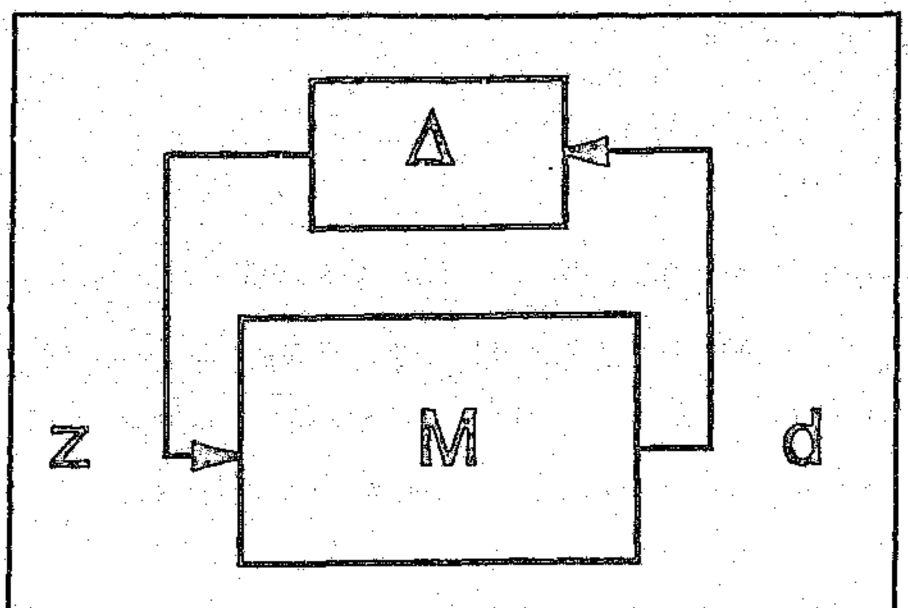

Figure 2.1: Feedback Structure

The positive real-valued function μ satisfies the following condition

$$\det (I-M\Delta)\neq 0 \ \forall \ \Delta\epsilon X, \ \bar{\sigma}(\Delta_i)<\gamma \quad \text{iff } \gamma\mu(M)\leq 1 \tag{2.2}$$

where X is the set of all complex perturbations with a specific block diagonal structure and spectral norm less than γ, i.e.,

$$X=\{diag(\Delta_1,\Delta_2,...,\Delta_\alpha)\,|\,\bar{\sigma}(\Delta_i)<\gamma\} \tag{2.3}$$

The function μ depends on the structure of Δ, but this dependency is typically not represented, for notational convenience. The function μ could thus be defined such that its inverse is equal to the smallest maximum singular value of Δ needed to make $(I - M\Delta)$ singular, i.e.,

$$\mu^{-1}(M) = \min_{\gamma} \{\gamma \,|\, \det(I - M\Delta) = 0 \text{ for some } \Delta \epsilon X\} \tag{2.4}$$

If no Δ exists such that $\det(I - M\Delta) = 0$, then $\mu(M) = 0$. Unfortunately the definition of μ does not satisfy the mathematical definition of a norm because it does not satisfy the triangle equality. This greatly complicates the feedback synthesis problem as the rich mathematical structure and results which accompany a norm are not available.

In what follows, Δ will be restricted to consist of block diagonal, complex matrices. Real parameter variations will not be treated directly, but can be incorporated into this structure by treating the variations as complex perturbations.

The definition (2.4) is in itself not useful for computing μ, as the implied optimization problem is nonconvex. Several properties of μ (see [5] for a detailed discussion) can however be proven which lead to methods for computing μ. The following choices of Δ show μ to be a generalization of the spectral radius and the spectral norm.

$$\begin{gathered} \Delta = \{\lambda I \,|\, \lambda \epsilon C\} \Rightarrow \mu(M) = \rho(M) = |\bar{\lambda}(M)| \\ \Delta = C^{NxN} \Rightarrow \mu(M) = \bar{\sigma}(M) \end{gathered} \tag{2.5}$$

thus

$$\rho(M) \le \mu(M) \le \bar{\sigma}(M) \tag{2.6}$$

The bounds of (2.6) are not sufficient on their own, as the gap between ρ and $\bar{\sigma}$ can be arbitrary large. They can however be refined by transformations on M that do not affect $\mu(M)$, but do affect ρ and $\bar{\sigma}$. Suppose that $\bar{U}$ and $\bar{D}$ are sets such that for any $\Delta \in X$,

$$\begin{aligned} U \in \bar{U} &\Rightarrow \bar{\sigma}(U\Delta) = \bar{\sigma}(\Delta) \\ D \in \bar{D} &\Rightarrow D^{-1}\Delta D = \Delta \end{aligned} \tag{2.7}$$

Then from the definition of μ it follows that,

$$\begin{aligned} U \in \bar{U} &\Rightarrow \mu(MU) = \mu(M) \\ D \in \bar{D} &\Rightarrow \mu(DMD^{-1}) = \mu(M) \end{aligned} \tag{2.8}$$

Based on (2.6), (2.7), and (2.8) it is shown in [5] that,

$$\sup_{U \in \bar{U}} \rho(MU) \leq \mu(M) \leq \inf_{D \in \bar{D}} \bar{\sigma}(DMD^{-1}) \tag{2.9}$$

For the case of nonrepeated complex blocks, the following sets can be defined,

$$\begin{aligned} &X = \{\mathrm{diag}(\Delta_1, \Delta_2, \ldots, \Delta_n) \,|\, \Delta_j \in C^{m_j \times m_j}\} \\ &\bar{U} = \{\mathrm{diag}(U_1, U_2, \ldots, U_n) \,|\, U_j^* U_j = I\} \\ &\bar{D} = \{\mathrm{diag}(d_1 I, d_2 I, \ldots, d_n I) \,|\, d_j \in R_+\} \end{aligned} \tag{2.10}$$

The bounds in (2.9) provide a means of computing μ. The lower bound can be shown to be an equality for all M and Δ. However, the optimization problem posed by the lower bound is not convex and therefore it might have multiple local maxima. A power algorithm is described by Packard *et al.* [50] which can be used to calculate this lower bound. Th formulation used is slightly different from (2.9), and the algorithm is apparently quite effective, even though convergence cannot be guaranteed.

It can also be shown that the upper bound in (2.9) is an equality for three of fewer blocks, or if M is real. The upper bound can be found more easily since the associated optimization problem has only global minima. The upper bound is thus useful for computing μ, and numerical evidence suggests that this bound is reasonably tight for four or more (complex) blocks. The worst known example has a ratio of μ over the bound of about 0.85.

Doyle [5] proposed a generalized gradient search procedure to minimize the upper bound in (2.9). This bound can also be calculated using a generalization of Osborne's routine [51]. Osborne's algorithm minimizes the Frobenius norm rather that the maximum singular value, and produce scalings that can be used to approximate the upper bound [52].

2.2 Analysis: Stability, Performance, and Robustness

The general framework for studying methods aimed at analysing performance and robustness properties of feedback systems, is shown in Figure 2.2. This framework has become standard in the H_∞ control community [42]. Any linear interconnection of inputs, outputs, commands, perturbations, and a controller can be arranged to fit this diagram. P is a FDLTI operator and is referred to as the design plant model. It consists of a nominal plant model, and uncertainty and performance weighting functions. The selection of weighting functions forms an integral part of the design process, and will be elaborated upon later in this sequel. K is the controller that has to be designed, and Δ is a FDLTI operator representing a perturbation on P due to uncertain plant dynamics. The vector time signals in Figure 2.2 are defined as:

v - exogenous inputs (reference signals, disturbances, and noise)

e - errors to be made small

u - controls

y - measurements

z - outputs from perturbation operator

d - inputs to perturbation operator

The block-diagram in Figure 2.2 contains the relationships shown in equation (2.11), where P_{ij} are transfer function matrices of appropriate dimensions.

$$\begin{bmatrix} d \\ e \\ y \end{bmatrix} = \begin{bmatrix} P_{11} & P_{12} & P_{13} \\ P_{21} & P_{22} & P_{23} \\ P_{31} & P_{32} & P_{33} \end{bmatrix} \begin{bmatrix} z \\ v \\ u \end{bmatrix} \tag{2.11}$$

with

$$\begin{aligned} u &= K\,y \\ z &= \Delta d \end{aligned} \tag{2.12}$$

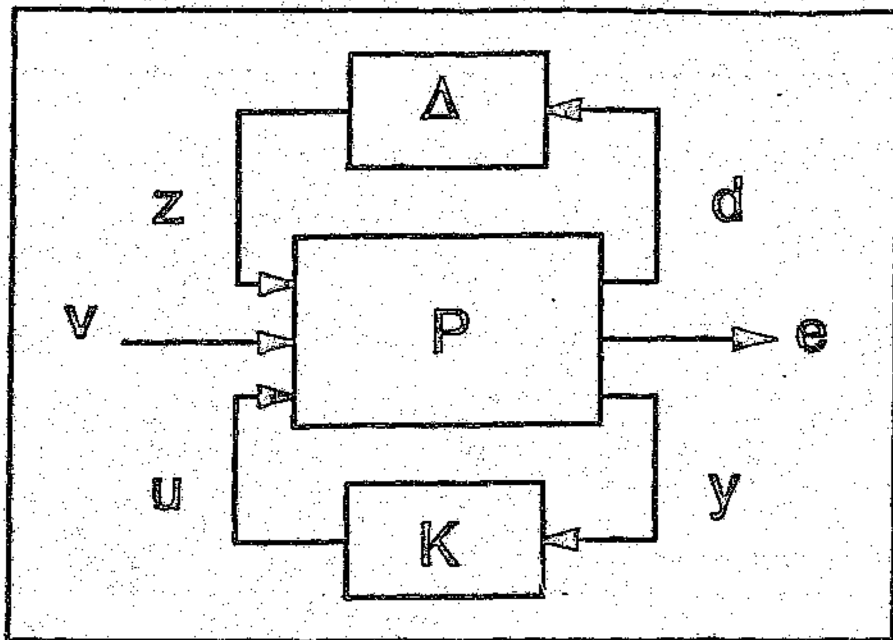

Figure 2.2: General Framework

For the purpose of analysis, the controller can be thought of as just another system component, and can be incorporated with the plant P via a lower linear fractional transformation to yield the closed-loop transfer function matrix M (Figure 2.3), i.e.,

$$M = F_l(P,K) = P_{11}+P_{12}K(I-P_{22}K)^{-1}P_{21} \tag{2.13}$$

with

$$\begin{bmatrix} d \\ e \end{bmatrix} = M \begin{bmatrix} z \\ v \end{bmatrix} \tag{2.14}$$

and

$$M = \begin{bmatrix} M_{11} & M_{12} \\ M_{21} & M_{22} \end{bmatrix} \tag{2.15}$$

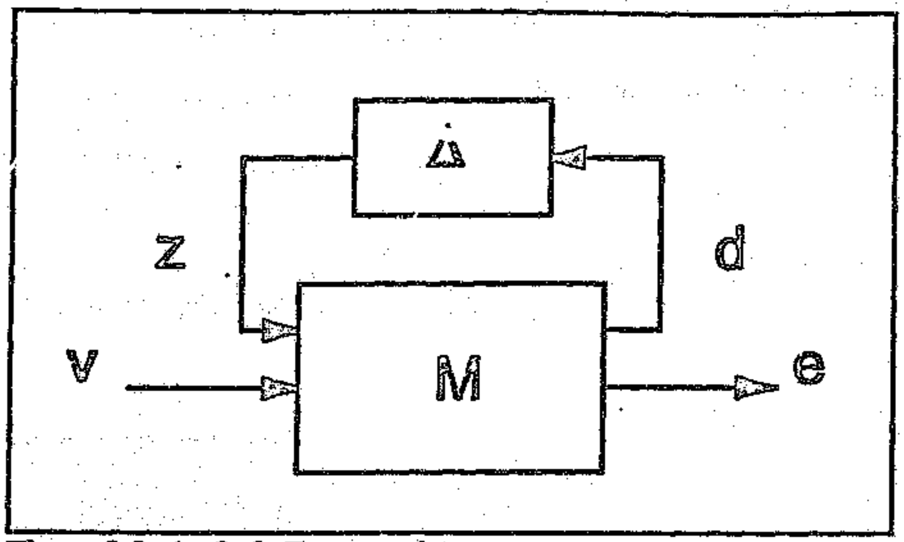

Figure 2.3: Analysis Framework

The analysis problem involves determining whether the error e remains in a desired set for sets of inputs v and perturbations Δ. Analysis methods differ on the assumptions made on the interconnection structure M in Figure 2.3, and the description of the sets to which the signals v and e belong. In the discussion followed here, M is assumed to be a FDLTI system represented by a rational transfer function. The transfer function from v to e can be expressed as the upper linear fractional transformation,

$$e = F_u(M,\Delta)v = [M_{22}+M_{21}\Delta(I-M_{11}\Delta)^{-1}M_{12}]v \tag{2.16}$$

It is worth noting at this stage that uncertainty modeled as Δ has a different effect on system performance from that of v, as for e.g., Δ can cause a nominally stable system to become unstable, whereas v cannot.

The remainder of this section concentrates on the conditions under which the system in Figure 2.2 will achieve nominal stability (NS), nominal performance (NP), robust stability (RS), and robust performance (RP). Nominal refers to the case when the particular system attribute (stability or performance) is satisfied when $\Delta=0$, and similarly, the term robust is used when Δ is present. The main result in each section will be expressed in terms of Doyle's General Analysis Theorem.

General Analysis Theorem (GAT) [42]

Performance is achieved for all Uncertainty

if and only if an analysis test is passed

The focus is thus on necessary and sufficient conditions for performance in the presence of uncertainty. In this context, uncertainty can be a combination of input signals, perturbations, and parameter variations, whereas performance is taken to be stability or stability plus a bound on the error e.

2.2.1 Nominal stability

A basic requirement for any controller is that it stabilize the nominal closed-loop system ($\Delta = 0$). Stability here will be taken to mean that the closed-loop system has no closed right-half plane poles. Nominal stability can be verified either in the time or the frequency-domain. In the time-domain, a closed-loop system is stable if and only if,

$$\mathrm{Re}\ \{\ \lambda_i[A_{cl}]\ \} < 0 \quad \forall\ i \tag{2.17}$$

where A_{cl} is the "A" matrix of the standard state-space description of the closed-loop system, and λ_i its eigenvalues. This time-domain stability test is easily performed on a computer, and is therefore often used.

A standard frequency-domain test for nominal stability is the MIMO Nyquist criterion. This test is rather cumbersome to perform in practice, but does play a key role in the development of a stability-robustness theorem (e.g. [4]). The MIMO Nyquist criterion relies on Cauchy's integral theorem and the Principle of the Argument to determine if any closed-loop poles are in the right-half of the s-plane. For a given controller, the stability of the closed-loop system can be established by plotting the Nyquist diagram of the loop-transfer function matrix, and examining the number of encirclements of the critical point.

Most modern synthesis methods make the nominal stability problem trivial in that stability is guaranteed. These methods are based on the parameterization of all stabilizing controllers conceived by Youla *et al.* [53]. For example, the standard H_∞ synthesis method finds a stabilizing controller to minimize the H_∞-norm of the (nominal) transfer function from exogenous inputs v to errors e (Figure 2.2).

2.2.2 Nominal performance

Nominal performance ($\Delta = 0$) is considered in this section in terms of bounds on e in the presence of uncertain bounded inputs v. Having defined the bounds on v and e, the nominal performance test boils down to a norm test applied to the appropriate transfer function matrix. Consider three different types of bounds on the signals v and e, i.e., that they are bounded in "average power", "total energy", or magnitude. If v is assumed to be a function of time such that it is square integrable on any finite interval, then the bounds on v can be obtained in terms of:

$$\begin{aligned}
\text{Power:}\quad & BP = \{v \mid \lim_{T\to\infty} \frac{1}{2T}\int_{-T}^{T} |v(t)|^2\, dt < 1\} \\
\text{Energy:}\quad & BL_2 = \{v \mid \|v\|_2^2 = \int_{-\infty}^{\infty} |v(t)|^2\, dt < 1\} \\
\text{Magnitude:}\quad & BL_\infty = \{v \mid \|v\|_\infty = \operatorname{ess}\sup_t |v(t)| < 1\}
\end{aligned} \tag{2.18}$$

where B denotes the unit ball. To simplify comparisons of different tests on M implied by alternative assumptions on v and e, these signals are temporarily assumed to be scalars. These bounds are scaled to 1 since any other scaling can be absorbed into the interconnection M. The use of scaling and weighting functions are of prime importance in the synthesis process, and will be elaborated upon later in this document.

For nominal performance the GAT can be stated as:

e ∈ Performance   for all   v ∈ Input set

if and only if   a norm test is passed

The performance and input sets are taken from (2.18), and the H_∞-norm will be used in the norm test. Table I summarizes the GAT for nominal performance for input and performance combinations where the H_∞-norm is applicable.

Table I: Norm Tests for Nominal Performance

v	e	
	Power	**Energy**
Power	$\|M\|_\infty$	∞
Energy	0	$\|M\|_\infty$
Magnitude	$\|M\|_\infty$	∞

In each case e is guaranteed to be an element of the performance set for any v in the input set if and only if the H_∞-norm is less than or equal to 1, e.g. for v and e of bounded power (BP), Nominal performance theorem (Power/Power) [42]

$$e \in BP \;\; \forall \;\; v \in BP \;\; \text{iff} \;\; \|M_{22}\|_\infty < 1 \tag{2.19}$$

The H_∞-norm is applied to M_{22}, which is the transfer function matrix connecting v and e. The 0 entry in Table I occurs because for any stable M, $v \in BL_2$ yield e of zero average power. The ∞ entries occur because the indicated combinations allow for unbounded outputs for bounded inputs when $M \neq 0$. When measuring performance in terms of the H_∞-norm, frequency dependent weights can be used to shape the spectral content of signals and to implement performance specifications such as command following, disturbance rejection and insensitivity to sensor noise. The real payoff for using the H_∞-norm however is that it allows for direct treatment of robust performance using μ.

2.2.3 Robust stability

In this section plant perturbations will be considered, and as they can destabilize a normally stable system, the issue of robust stability must be addressed. Perturbations are assumed to be complex so as to conform to current μ-synthesis theory. Real perturbations such as those arising from parametric variations in model coefficients can be covered by complex perturbations, at the expense of possible conservativeness [38].

The robust stability theorem for unstructured perturbations (Δ is assumed to be bounded but otherwise unknown), is given as,

Theorem (robust stability, unstructured) [4]

$$F_u(M,\Delta) \text{ is stable } \quad \forall\, \Delta \;,\; \bar{\sigma}(\Delta)<1 \qquad \text{iff} \quad \|M_{11}\|_\infty \le 1 \tag{2.20}$$

The H_∞-norm thus yields necessary and sufficient conditions for robust stability. Equation (2.20) is limited in the assumption that no structural information is available for Δ. In practical problems it is often preferable to represent uncertainties with multiple norm-bounded perturbations, occurring at different locations in the plant to be controlled. This could be accomplished by choosing Δ to be a member of a set such as,

$$X=\{\, \mathrm{diag}(\delta_1 I, \delta_2 I, \ldots, \delta_m I, \Delta_1, \Delta_2, \ldots, \Delta_n) \,|\, \delta_i \in C, \Delta_j \in C^{k_j \times k_j}\} \tag{2.21}$$

or its bounded subset,

$$BX = \{\, \Delta \in X \,|\, \bar{\sigma}(\Delta)<1\} \tag{2.22}$$

With Δ defined as in (2.22), (2.20) can be used to obtain sufficient conditions for robust stability, but the test could be arbitrarily conservative. In order to obtain a precise generalization of (2.20) to handle structured uncertainty, the structured singular value μ is needed. The robust stability theorem with structured uncertainty then becomes,

Theorem (robust stability, structured) [42]

$$F_u(M,\Delta) \text{ is stable} \quad \forall\ \Delta \in BX$$
$$\text{iff} \quad \|\mu(M_{11})\|_\infty \leq 1 \tag{2.23}$$
$$\text{where} \quad \|\mu(M)\|_\infty \triangleq \sup_\omega \mu[M(j\omega)]$$

2.2.4 Robust performance

The closed-loop transfer function from exogenous inputs v to errors e, $F_u(M,\Delta)$, must be small for all possible Δ for the robust performance requirement to be satisfied. Performance is thus considered with both noise and perturbations occurring simultaneously. The robust performance requirement can be stated as,

$$\|F_u(M,\Delta)\|_\infty \leq 1 \qquad \forall\ \Delta \in BX \tag{2.24}$$

This requirement can be interpreted as a stability condition on the perturbed system shown in Figure 2.4, and will be satisfied if and only if,

* $F_u(M,\Delta)$ is stable
* the system in Figure 2.4 is stable for all $\Delta_p \in BX$

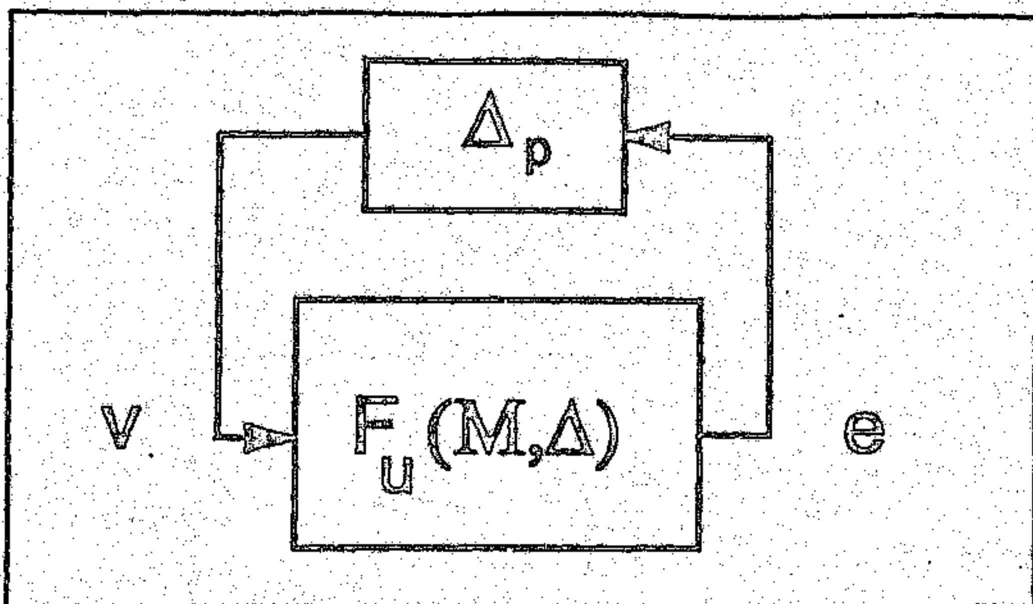

Figure 2.4: Perturbed Closed-loop System $F_u(M,\Delta)$ with Performance Block Δ_p

The robust performance problem can thus be recast as a robust stability problem with the performance specification represented as a "performance perturbation" Δ_p.

The analysis framework shown in Figure 2.3 can be combined with Figure 2.4 to give the general block structure for μ-analysis shown in Figure 2.5.

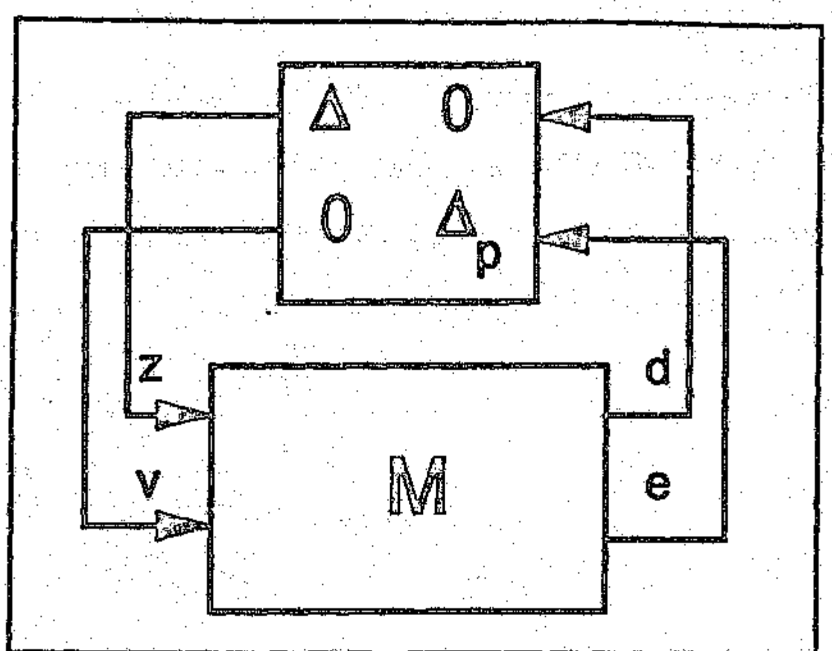

Figure 2.5: General Block Structure for μ-Analysis

Robust performance is achieved if and only if the system in Figure 2.5 is stable for all perturbations with the 2x2 block diagonal structure as indicated. The robust performance theorem can be stated as follows:

Theorem (robust performance) [42]

$$F_u(M,\Delta) \text{ is stable and } \quad \|F_u(M,\Delta)\|_\infty \le 1 \quad \forall\, \Delta \in BX \qquad \text{iff} \quad \|\mu(M)\|_\infty \le 1 \tag{2.25}$$

where μ is taken with respect to the structure,

$$XP = \{\, \mathrm{diag}(\Delta, \Delta_p) \,|\, \Delta \in X \,\} \tag{2.26}$$

This theorem gives necessary and sufficient conditions for simultaneous stability and performance robustness in the presence of a block structured perturbation. Performance is thus guaranteed over a whole set of possible plants. This is made possible by the equivalence of performance and robust stability when using the H_∞-norm. The use of μ is essential in this theorem as a block structured perturbation is required regardless of the model uncertainty structure Δ. Note that μ is computed for the full matrix M.

2.2.5 Concluding remarks

The analysis results presented here can be summarized as shown in Table II.

Table II: Analysis Results

Perturbation	Performance	
	Stability	$e \in BP$
$\Delta = 0$	No C_+ poles	$\|M_{22}\|_\infty \leq 1$
$\overline{\sigma}(\Delta) < 1$ (unstructured)	$\|M_{11}\|_\infty \leq 1$	$\|\mu(M)\|_\infty \leq 1$
$\Delta \in BX$ (structured)	$\|\mu(M_{11})\|_\infty \leq 1$	$\|\mu(M)\|_\infty \leq 1$

One might well ask why one should bother with μ-based analysis methods when there are powerful simulation packages on which a wide variety of plant models and performance specifications can be tested. The problem with using a simulator for analysis is that the system inputs and perturbations can only be considered one at a time. The μ-based methods focus on describing sets of signals and perturbations and drawing conclusions on worst-case performance on the entire set at once. However, in applying μ-based methods restrictive assumptions have to be made about the interconnection structure M, such as linearity.

Nonlinearities can only be treated as perturbations.

2.3 μ-Synthesis

This section addresses the problem of designing a feedback system that is robust with respect to modelling uncertainties. The synthesis problem is to specify a controller K to

- achieve nominal closed-loop stability
- satisfy nominal performance specifications
- provide stability and performance robustness with respect to all possible Δ.

In the μ-analysis framework described in the previous section, the synthesis problem reduces to finding a stabilizing controller K such that,

$$\|\mu(F_l(P,K))\|_\infty \leq 1 \tag{2.27}$$

with $F_l(P,K)$ given in (2.13), and μ taken with respect to the structure in (2.26). The design plant model P as shown in Figure 2.6 is a real-rational, proper transfer function matrix, and is not necessarily stable. P must of course be stabilizable and detectable for a stabilizing controller K to exist. It is assumed that P_{12} has at least as many rows as columns, and vice versa for P_{21}. This is sufficient to ensure that the controllers are proper.

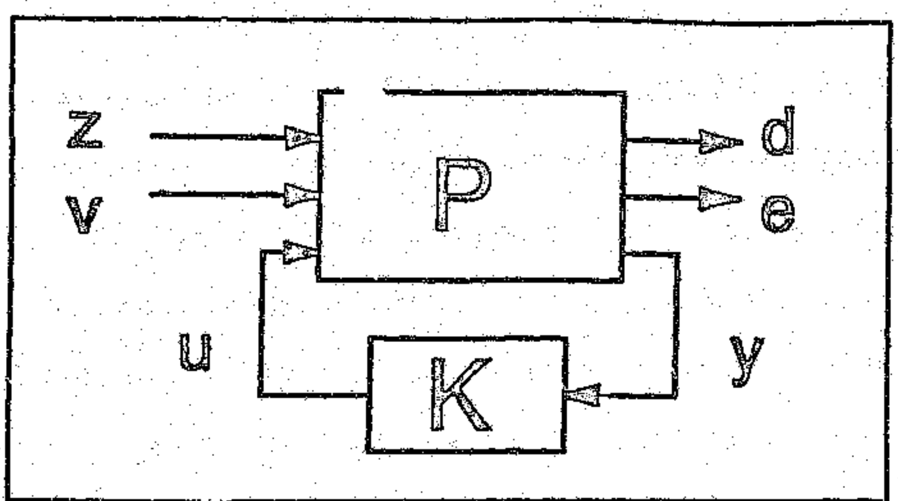

Figure 2.6: Synthesis Framework

The μ-synthesis problem can be solved using DK iteration which exploits the fact that the structured singular value is a scaled version of the singular value with a block structured scaling matrix. The aim of the DK iteration scheme is to find a stabilizing controller K and a diagonal scaling matrix D such that the H_∞-norm of the scaled closed-loop transfer function is less than or equal to unity. (The scaling matrix forces the H_∞-minimization to concentrate on μ across frequency rather than the maximum singular value ($\bar{\sigma}$).) Thus the condition for robust stability and performance is satisfied when,

$$\|DF_l(P,K)D^{-1}\|_\infty \leq 1 \tag{2.28}$$

One method to achieve this aim is to alternately minimize equation (2.28) for either K or D while holding the other constant. For a fixed scaling D the left-hand side of equation (2.28) is a standard H_∞ control problem which can be solved for K using well known techniques [47]. For a fixed controller K the minimization with respect to D is a convex optimization problem at each frequency. The result is a real diagonal matrix $D(\omega)$ at each frequency of which the magnitude frequency response is fit with a stable, minimum phase rational transfer function. Note that the phase of D does not effect the norm in (2.28). The process is repeated until it converges, or until the condition for robust stability and performance in (2.28) is satisfied. Unfortunately, individual convexity in the two parameters D and K does not imply joint convexity, and thus the DK iteration scheme is not guaranteed to converge to the global optimal K and D. The DK iteration process can be broken down into the steps shown in Figure 2.7.

After an initial H_∞-design is done, $\mu(F_l(P,K))$ is computed and the optimal scaling matrix D is determined at each frequency. If the robust performance condition in (2.28) is met, the process is terminated. If not, [illegible] of each element of $D(\omega)$ is fitted to a stable and minimum-phase transfer [illegible] problem is then scaled with a stable minimum phase transfer matrix D [illegible]ture. Another H_∞-design is done which yields a controller K which minimizes the left hand side of the expression in (2.28), and the whole process is repeated until the robust performance condition is met. Other stop criterions, such as those proposed by Lundström *et al.* [64], can be used when robust performance cannot be met for the specific choice of weighting functions. They propose two stop criterions, an iteration and a "flatness" criterion. The iteration criterion suggests that the iteration be stopped when the difference between the current and previous μ values is smaller than a certain tolerance. The flatness criterion states that the iterations be stopped when the μ-versus-frequency plot is "flat" over the bandwidth of interest.

μ-Synthesis will not be of much use to the control engineer without the necessary software to solve (2.2?). Fortunately a Matlab toolbox [54] has recently appeared which makes the DK iteration procedure executable without extensive programming.

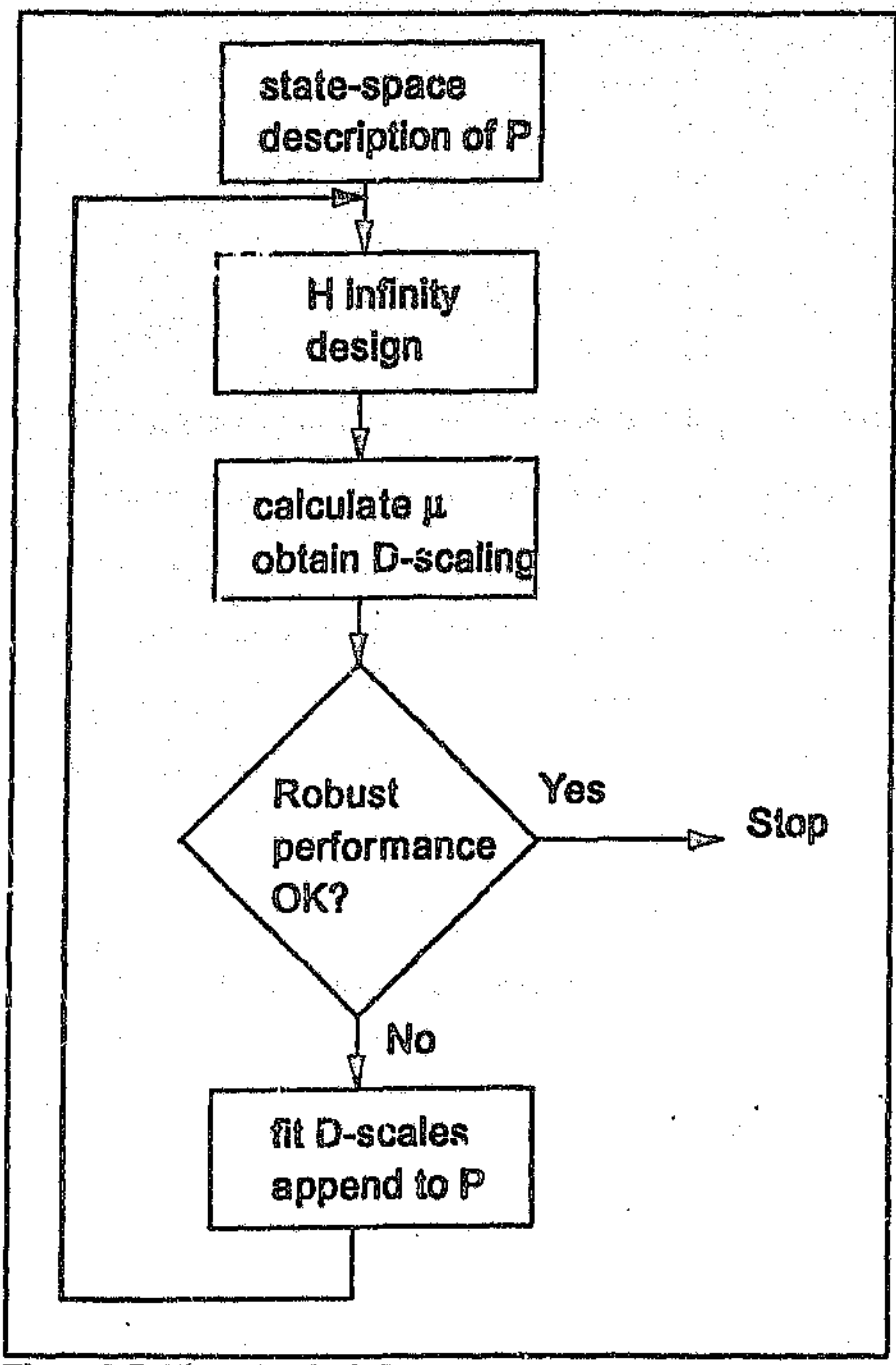

Figure 2.7: The μ-Synthesis Process

CHAPTER 3

ROM MILL CONTROL

This chapter introduces the ROM milling circuit under consideration. The milling circuit is described, and the objectives of milling control are discussed. The plant model with uncertainty description is given, and the selection of uncertainty weights and performance specifications are motivated from a practical point of view. Finally the ROM milling circuit model with its uncertainty description is put into a general synthesis and analysis framework.

3.1 ROM Milling Circuit Description

A Run-of-Mine circuit with single-stage classification, as shown in Figure 3.1, is discussed.

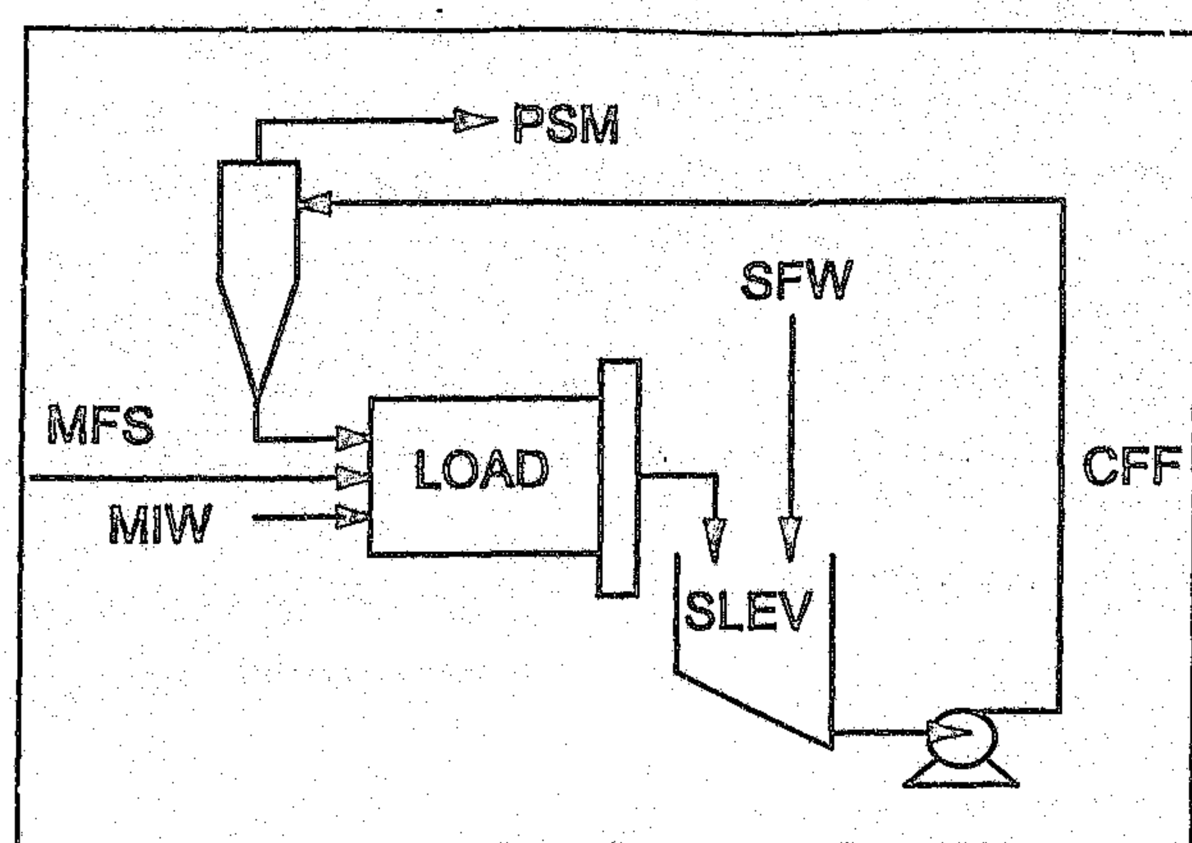

Figure 3.1: A typical ROM milling circuit

The circuit grinds about 100 t/h of gold-bearing ore to give a product containing 70 to 75% particles with size smaller than 75μm. The ROM mill is operated in closed-circuit with a hydrocyclone, and the product is pumped to thickeners. The gold is subsequently extracted by a leaching process. The mill is 9 m long and 5 m in diameter, and is supported by pressurized-oil circumferential bearings. It is operated at 90% of critical speed [55], and has lifter bars and solid white-iron liners. Pulp flows out of the mill through an end-discharge grate and is discharged into a sump, where it is mixed with dilution water. The diluted pulp is pumped to a hydrocyclone with an internal diameter of 1 m. The underflow from the cyclone, additional water, and fresh ore are fed into the mill.

The plant output variables to be controlled are the level of slurry in the sump (SLEV), the mass of material in the mill (LOAD), and the product particle-size (PSE). These variables are controlled by manipulating plant input variables such as the feed rate of water to the sump (SFW), the feed rate of solids to the mill (MFS), and the flowrate of slurry to the cyclone (CFF). An additional input, the feed rate of water to the mill inlet (MIW), will not be used in the design of the dynamic controller. It can, however, be used as a steady-state control action to extend the range over which the PSE can be controlled [23].

3.2 Objectives in Mill Control

An appropriate control strategy for milling should not only stabilize the milling process, but should also be aimed at optimizing the economics of the plant as a whole [1]. This task can be approached by defining a series of sub-objectives which are compatible with the overall aim of optimizing the plant economic performance. Possible sub-objectives related to milling circuit performance are:

(i) to improve the quality of the product

(i1) by increasing the fineness of grind

(i2) by decreasing product size fluctuations

(ii) to maximize throughput

(iii) to minimize steel consumed per ton of fines produced

(iv) to minimize power consumed per ton of fines produced, etc.

The size of the product (or grind) of a milling circuit and the throughput of solids are of major imp... ance when specifying sub-objectives. A combined measure of th ~ variables gives a good indication of milling circuit performance, as they are closely related to the quality of the product and the efficiency of operation. A typical throughput/grind relationship is illustrated in Figure 3.2. This relationship shows for example that a fine grind is accompanied by a low throughput, i.e., there is a trade-off between objectives (i1) and (...).

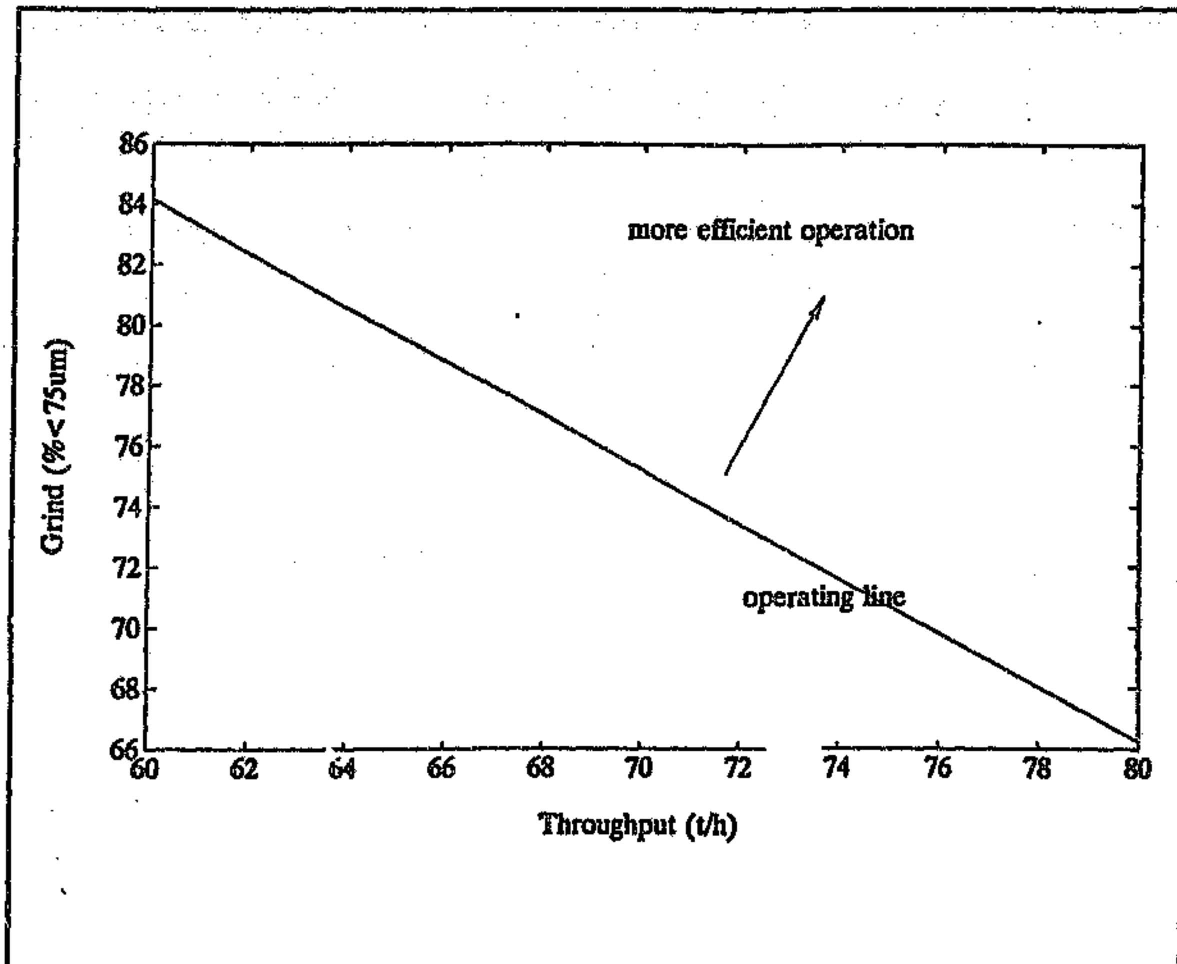

Figure 3.2: Typical Throughput/Grind Trade-off for a ROM Milling Circuit

The size of the milling circuit product is crucial to the downstream extraction process. In general, more gold will be extracted at a finer product size (objective (i1)). In fact, it is not only the average size that is important, but also the standard deviation of the size. The economic importance of this factor of product-size control is often overlooked, possibly due to the experimental difficulties in obtaining a grind versus residue relationship. Craig *et al.* [22] showed that the relationship between grind and residue is nonlinear, with the implication that the increase in residue by grinding coarser is not balanced by the decrease in residue that result from grinding finer. Such a relationship is shown in Figure 3.3, and implies that decreased product size fluctuations will result in increased gold recovery. As undergrinding can result in significant gold losses, a milling control strategy should have as one of its goals to reduce the fluctuations in the product particle-size (objective (i2)).

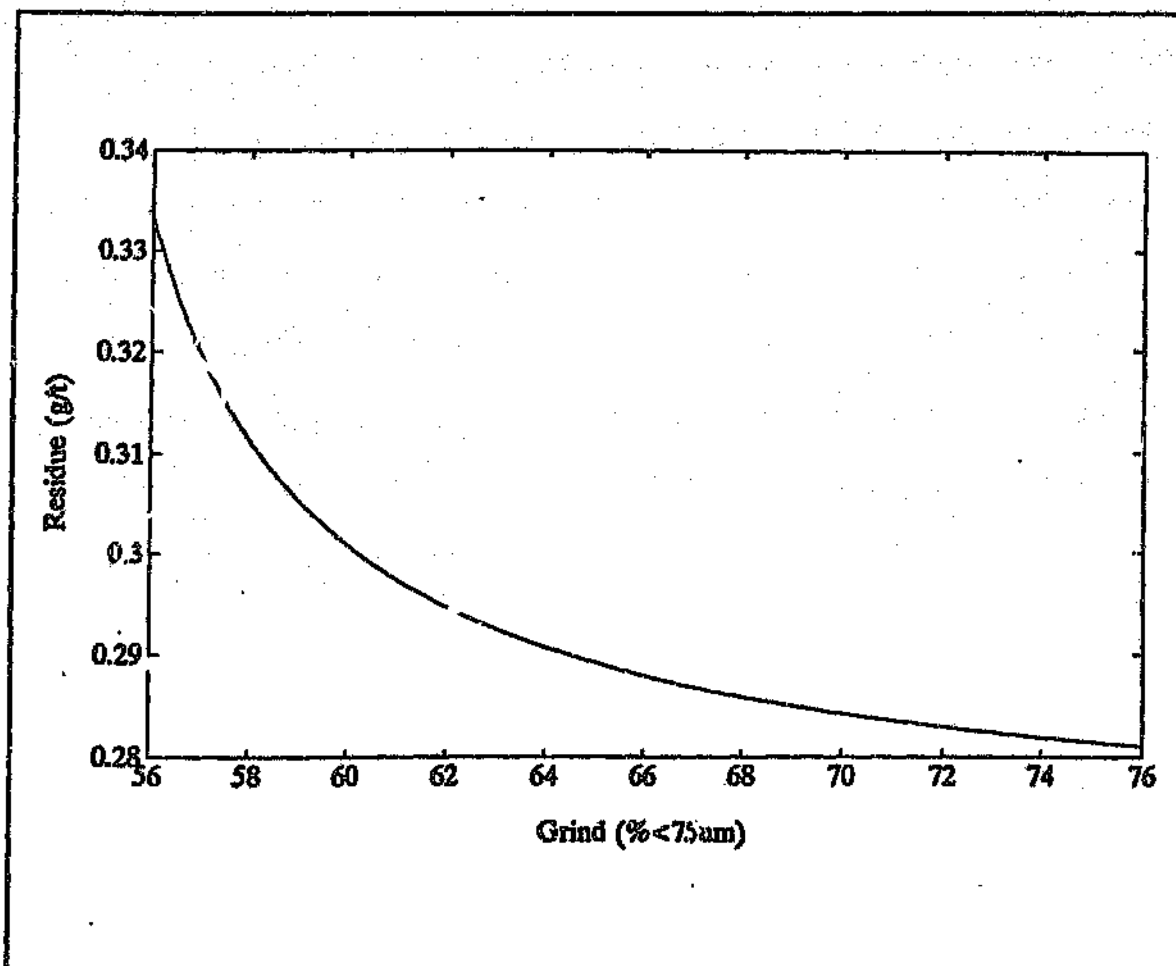

Figure 3.3: A Typical Grind/Residue Relationship

In general the throughput of a ROM mill is maximized when the mill draws maximum power from the mill motor. Given the value of the milling circuit product versus the cost of electricity, objective (iv) is generally not considered important. Objectives (i) to (iii) are all interrelated. Steel is added to the ROM mill feed [illegible] order to increase throughput, and to partly stabilize the grinding conditions inside the mill. A controller which reduces product particle-size fluctuations will improve the quality of the milling circuit product, and could at the same time reduce the need for steel to stabilize the grinding conditions. If throughput is not of overriding importance, objective (iii) will be addressed when objective (i2) is met.

For a particular set of operating conditions, the process will operate along the line shown in Figure 3.2. It is however possible by operating under different conditions, to move the line in the direction of more efficient process operation. A possible control strategy could be to c[illegible] the product size to a setpoint, and to maximize the throughput at that particular siz[illegible]point by optimizing the process operating conditions [22]. Such a strategy addresses both objective (i) and (ii). The effect of this strategy is illustrated in Figure 3.4. This figure shows that the throughput/grind operating line is shifted by the control strategy in the direction of more efficient plant operation.

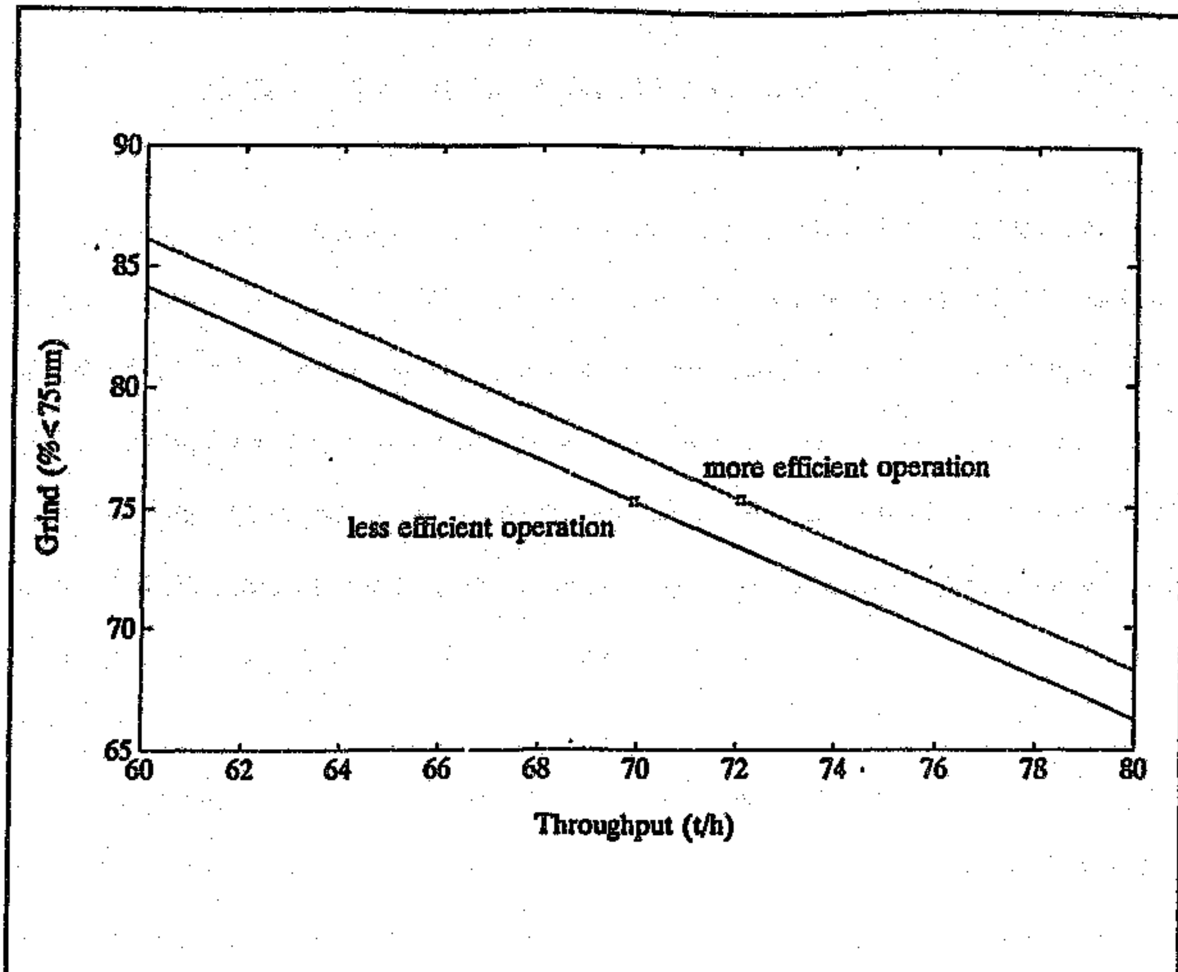

Figure 3.4: Control Strategy Improving Operating Efficiency

The particle-size setpoint can be chosen to correspond with throughput targets set by plant management, or if throughput is not a consideration, to achieve the finest possible grind. Throughput maximization could possibly be achieved by adjusting the mill load setpoint to a point where maximum power is drawn from the mill motor [22]. The search for this optimal load setpoint needs to be dynamic as the optimal setpoint changes with, for e.g., changing ore characteristics.

The objectives discussed in this section will be used as a basis for choosing milling circuit performance specifications in Section 3.6.

3.3 Obtaining a Plant Model for Controller Synthesis

For control purposes a plant model is required that predicts, with reasonable accuracy, the dynamic responses of the milling circuit. Such a model is usually required to have a specific structure that conforms with the synthesis method to be used. For example, the milling circuit is inherently multivariable, as any one of the plant inputs has an effect on more than one plant output. A MIMO controller thus has to be designed to control the plant outputs. As MIMO controller design methods such as μ-synthesis are only readily available for FDLTI systems, a FDLTI model for the milling circuit is needed.

A nominal FDLTI model of the milling circuit is however not enough. It should be accompanied by an uncertainty description which describes the set of all possible plant variations that can occur in practice. The structure of plant uncertainties is an issue in MIMO systems, where the location of uncertainties (for e.g., plant input vs. plant output), and the internal structure of the uncertainty blocks, can have a major influence on the effective set of plant variations used for controller synthesis.

There are two basic ways of obtaining plant models, i.e., from the laws of nature, or from experimental data. These will now be discussed in more detail.

3.3.1 From the laws of nature

The process of obtaining plant models from the laws of nature is referred to as modelling, and the resulting models are called mechanistic models. The development of mechanistic models which describe milling processes, have received considerable attention in the literature [56]. Such models usually describe the milling process with selection and breakage functions, with the concept of breakage formulated as a stochastic process [57]. Modelling the behaviour of an autogenous mill is considered to be difficult for the following reasons Two breakage functions must be determined, as two mechanisms of breakage, i.e., abrasion and crushing breakage, are considered to occur in autogenous mills [58]. In addition, the rates of breakage of particles change because the mill load changes as the ore changes. Also the mill load is dependent on the breakage rates, the breakage functions, and the discharge rates. The grinding capacity of autogenous mills is thus dependent on the feed ore characteristics, unlike for example a ball mill for which the grinding capacity is almost constant.

Mechanistic models which attempt to describe the behaviour of ROM mills are usually nonlinear and involve hundreds of variables. Their success in describing a ROM mill's dynamics depend to a large extent on functional forms given to functions that describe rates and distributions of breakage. It is not practical to measure such model inputs on an industrial milling circuit, with the result that they are normally chosen through intuition. It is therefore not surprising that even complex mechanistic models are unable to describe the nominal dynamics of a ROM milling circuit adequately enough such that it is suitable for controller design.

3.3.2 From experimental plant data

The process of obtaining plant models from experimental plant data is referred to as system identification. Such models are called black-box models, and are derived to fit measured responses of milling circuits. These models are made sufficiently complex to accurately describe important plant inputs/outputs relationships in the bandwidth of interest.

The system identification process can be broken up into four stages: experiment design, choice of model structure, selection of criterion of fit, and model evaluation [59]. The outcome of such a process is usually a nominal plant model which can predict what the plant outputs will be, given the plant inputs. Such a model comes with a "quality tag" which describes the estimated deviations from the true model description in the parameter or frequency domain. The deviations can be used to construct an uncertainty description for the plant, which can then be used for controller synthesis. This quality tag might however not be enough, as it is derived under the assumption that the truth model is available in the model set, which for an ROM milling circuit it is not. The actual milling circuit is nonlinear and time-varying, which implies that the model uncertainty description must be adjusted in order to accommodate these phenomena.

In the case of an ROM milling circuit, the nonlinearities that occur are largely unknown, and will manifest themselves as linear model parameter variations. The effect of such nonlinearities could be kept small by performing identification experiments in the operating region where the plant is approximately linear.

The dynamics of milling circuit change over time due to factors such as the ageing of measurement and actuating equipment, cyclone spigot wear, liner and grid wear, and unmeasured disturbances acting on the circuit in the form of changing feed ore characteristics. Time-varying behaviour is also induced by routine maintenance actions such as relining or cyclone spigot changes.

The degree to which a milling circuit's dynamics changes with time, can be captured by performing identification experiments over an extended time period, in order to cover all possible plant operating conditions. The parameter variations of an average model which best describe all the data sets derived from such experiments could then be used to construct an uncertainty description which captures the time-varying nature of the milling circuit.

3.4 Plant Model and Uncertainty Framework

From the discussion in the previous section it is evident that milling circuits are in general nonlinear and time-varying systems. Research has however shown that it is possible to represent such systems with FDLTI models for controller design purposes [13]. The nonlinear and time-varying nature of a milling circuit can be accounted for in the uncertainty description that accompanies the linear model [60]. Optimization schemes could also be employed to exploit the nonlinear circuit behaviour in order to achieve certain economic objectives [22].

The model used in this study was derived from perturbation tests done on the plant

[13]. At least five perturbations tests were conducted for each plant input, and the responses of the plant outputs were observed. The results from these tests were used for the derivation of linear dynamic models for each plant input/output pair. Model structures were assumed for each input/output pair that best describe its behaviour. Each model was then given a weighting according to the quality of the fit and the conditions under which the relevant perturbation test was performed. All the model parameters were then averaged, w   le parameters of the "better" models weighted more heavily according to the relevant weighting factor. From this process the following model resulted:

$$\begin{bmatrix} \Delta PSE \\ \Delta LOAD \\ \Delta SLEV \end{bmatrix} = \begin{bmatrix} g_{11} & g_{12} & g_{13} \\ g_{21} & g_{22} & g_{23} \\ g_{31} & 0 & g_{33} \end{bmatrix} \begin{bmatrix} \Delta SFW \\ \Delta MFS \\ \Delta CFF \end{bmatrix} \tag{3.1}$$

with g_{11}, g_{12}, g_{13}, g_{21}, and g_{23} of the orm

$$g_{ij} = \frac{k_{ij}}{\tau_{ij}s+1} e^{-\theta_{ij}s} \tag{3.2}$$

and g_{22}, g_{31}, and g_{33} of the form

$$g_{ij} = \frac{k_{ij}}{s} e^{-\theta_{ij}s} \tag{3.3}$$

Using the standard deviation of each model parameter derived from the plant perturbation tests, the relative uncertainty in each transfer function element can be described as:

$$k_{ij}: \quad \begin{bmatrix} 35\% & 14\% & 31\% \\ 16\% & 11\% & 65\% \\ - & - & - \end{bmatrix} \tag{3.4}$$

$$\tau_{ij}: \quad \begin{bmatrix} 19\% & - & 18\% \\ 60\% & - & 40\% \\ - & - & - \end{bmatrix} \tag{3.5}$$

$$\theta_{ij}: \quad \begin{bmatrix} - & - & 27\% \\ 43\% & - & - \\ - & - & - \end{bmatrix} \tag{3.6}$$

The dashes indicate that for the particular parameter in question, the relative uncertainty is insignificant, or the parameter itself is zero.

There is no doubt that changes in the ROM feed size distribution and hardness are the major cause of the sizeable parameter uncertainties shown in (3.4) to (3.6) [61]. From a control point of view, one should be careful to distinguish between the MFS, which refers the mill feedrate of ROM material, and the composition and hardness of the feed. Even though the feedrate could be constant, a change in feed size distribution could cause drastic changes in the operation of the milling circuit. Such unmeasured disturbances partly manifest themselves as the parameter variations shown above.

A typical Witwatersrand ROM feed has a top size of about 300 mm square mesh [55], and in ROM milling such large rocks are essential for efficient grinding to take place. It is however not uncommon for feed ore to consist mostly of fines (smaller than about 10 mm square mesh). In such cases what little grinding media that there is, is supplemented with ferrous media such as steel balls. In fact, it is common practice for plant personnel to periodically add steel balls to the ROM feed at a fixed rate such as 0.8 kg/t of fresh feed. Steel addition has the effect of smoothing out the variations in the ROM feed, and prevents the model parameter variations from becoming even larger than they are already.

The Bond Work Index, which is a [illegible]e of ore hardness, can possibly range between 17 and 20 kWh/t for ore from the same shaft [62]. Work index variations can be even more pronounced at large mines where ore from different shafts (at which different reefs are mixed) are sent to a specific mill in order to fully utilize milling capacity. Such variations can also contribute to model parameter variations.

Another source of uncertainty in the linear milling circuit model is the fact that an essentially nonlinear system is approximated by a linear model. For example the different models for the PSE/CFF relationship from which the aggregate model g_{13} is obtained, exhibit classical nonlinear behaviour such that the gain and time constant are linearly related to the base-level of the PSE from which the perturbation step was made. For the other models, however, there is no simple relationship between the perturbation step base-levels and the model parameters.

3.5 The Selection of Uncertainty Weights

In the μ-synthesis framework, model uncertainties are represented by norm bounded perturbations and weighting functions. For example, uncertainty is often reflected at the plant output. The set of all possible plants G_s is then described by a nominal plant model G_n, and a frequency dependent output uncertainty weight W, i.e.,

$$G_s = \{G_n(I + W\Delta) \,|\, \sigma(\Delta) \le 1\} \tag{3.7}$$

Such a description is referred to as a multiplicative output uncertainty description and is shown in block-diagram form in Figure 3.5.

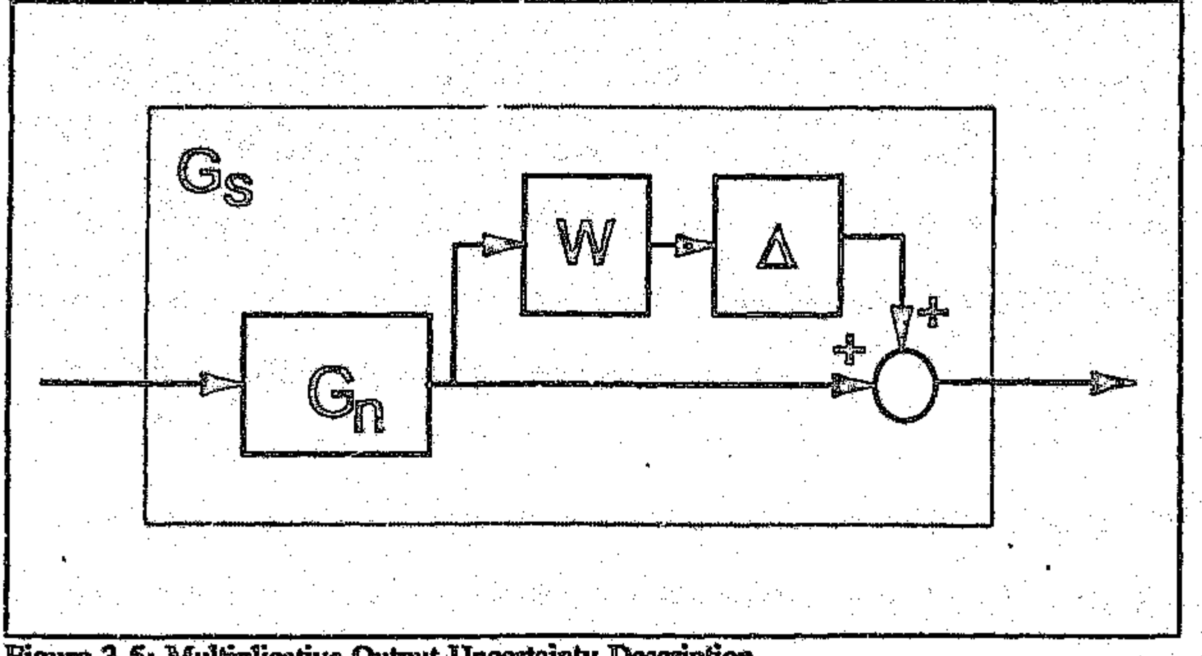

Figure 3.5: Multiplicative Output Uncertainty Description

Another useful uncertainty description is the inverse multiplicative perturbation where

$$G_s = \{(I + W\Delta)^{-1} G_n \,|\, \sigma(\Delta) \le 1\} \tag{3.8}$$

In block-diagram form this system can be represented as shown in Figure 3.6.

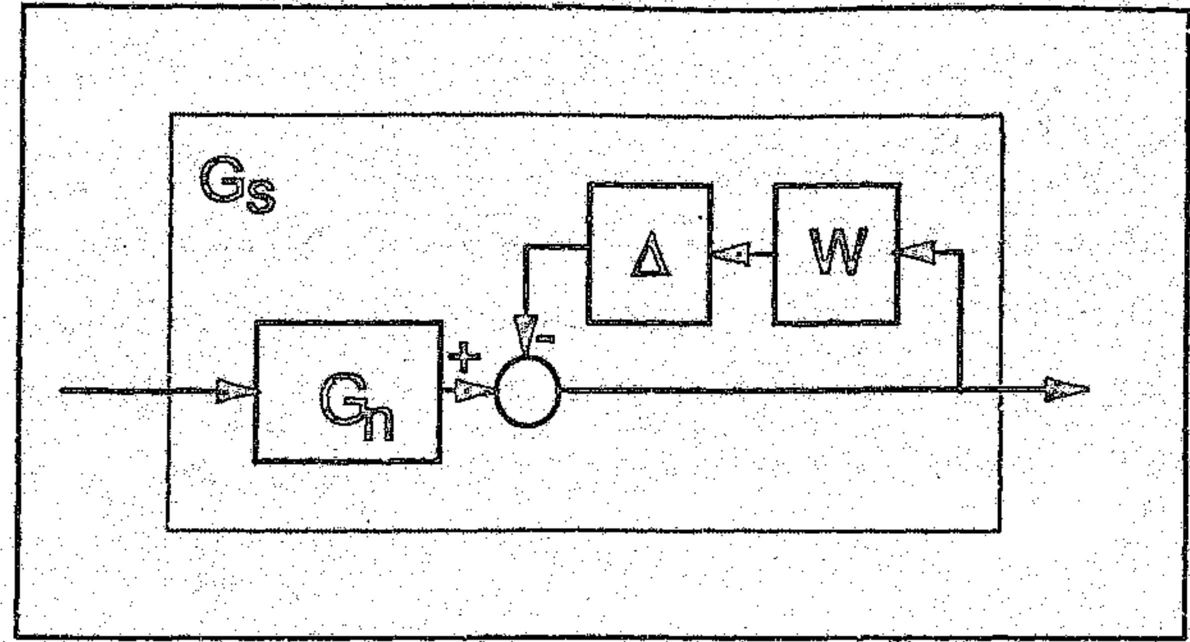

Figure 3.6: Inverse Multiplicative Output Uncertainty

The milling circuit model contains gain, time constant and time delay uncertainties. These uncertainties can be reflected in numerous ways. The simplest way would be to account for the each uncertainty independently. However, the H_∞ framework is a worst-case approach, and in general one should not include too many sources of uncertainty as it becomes highly unlikely for the worst-case to occur in practice.

In the case of a milling circuit there is undoubtedly some correlation between the parameter uncertainties, especially when these parameters depend directly upon the rheology of the slurry inside the mill. For example one would expect the uncertainties in the LOAD/SFW and LOAD/CFF models to be correlated. The time constants for these models are more or less equal to the hold-up time of the mill given by

$$\tau = RC \tag{3.9}$$

where C is the volume of material inside the mill, and R the inverse of the slurry discharge rate. In regard to (3.5), it would thus make sense to group these two time constant uncertainties (g_{21} (60%) and g_{23} (40%)) into one LOAD output uncertainty. Similarly the time constants for the PSE/SFW and PSE/CFF models are in the order of the sump hold-up time. The uncertainties for these time constants (g_{11} (19%) and g_{13} (18%)) could thus be lumped together as a PSE output uncertainty.

A time constant uncertainty for a first-order transfer function such as g_{11}, can be expressed as an inverse multiplicative uncertainty as shown in Figure 3.6 [52]. Assume that $\bar{\tau}$ is the nominal time constant and that r_τ is the relative uncertainty of τ such that,

$$|\tau - \bar{\tau}| < r_\tau \bar{\tau} \tag{3.10}$$

τ can then be written in terms of a norm bounded perturbation as,

$$\tau = \bar{\tau}(1 + r_\tau \Delta_\tau) , \qquad |\Delta_\tau| \le 1, \qquad \Delta_\tau \in \Re \tag{3.11}$$

Referring to (3.2), τ can be expressed as an inverse multiplicative perturbation on the "plant" (as shown in Figure 3.6), with

$$\begin{gathered} \frac{1}{\tau s + 1} = \frac{1}{\bar{\tau} s + 1} \, \frac{1}{1 + w_\tau \Delta_\tau} \\ \text{with} \qquad w_\tau = \frac{r_\tau s}{s + 1/\bar{\tau}} \end{gathered} \tag{3.12}$$

The gain uncertainty associated with the MFS (g_{12} (14%) and g_{22} (11%)) can be accounted for as an input uncertainty for this input. For the rest of the parameter uncertainties, there are no clear physically motivated guidelines as to where and how they should be represented in the uncertainty framework. For these uncertainties the most convenient representations are chosen without being overly conservative. The gain and time-delay uncertainties of the LOAD/SFW (k 16% and θ 43%) and PSE/CFF (k 31% and θ 27%) are grouped together to form one uncertainty representation per model, using the technique developed by Laughlin *et al.* [63]. This technique translates variations in transfer function coefficients into an approximate equivalent complex plane uncertainty representation. Using the transfer function described in (3.2), the real valued gain and time-delay uncertainty can be aggregated into a single complex valued multiplicative output uncertainty description with weighting function

$$W = \left| \frac{|\bar{k}|+\Delta k}{|\bar{k}|} e^{\Delta\theta s} - 1 \right| \tag{3.13}$$

with $(\bar{k} - \Delta k) \leq k \leq (\bar{k} + \Delta k)$; $\quad \bar{k}$ = nominal gain

$(\bar{\theta} - \Delta\theta) \leq \theta \leq (\bar{\theta} + \Delta\theta)$; $\quad \bar{\theta}$ = nominal time-delay

Note that if the exponential term in (3.13) is approximated by a Padé approximation, the resulting weight will be unstable. The unstable pole can however be removed by multiplying the weight with the appropriate all-pass function.

The gain uncertainties in the PSE/SFW and LOAD/CFF models, and the one associated with the MFS, can be accounted for using multiplicative weighting functions

(Figure 3.5) of the form

$$W = \frac{k\%(s + \omega_b)}{s + 100*\omega_b} \tag{3.14}$$

with k% - gain uncertainty in per cent

ω_b - the frequency at which the gain uncertainty becomes larger than k%

The bandwidth of these weighting functions are chosen to conform with the sampling interval (10 sec.) used in the plant identification process. The block-diagram of the resulting plant with uncertainty description is shown in Figure 3.7. The gain weighting functions in Figure 3.7 are,

$$\begin{aligned} w_1 &= \frac{15(s + \omega_b)}{s + 100*\omega_b} \\ w_3 &= \frac{11(s + \omega_b)}{s + 100*\omega_b}; \qquad \omega_b = 1/16 \\ w_5 &= \frac{15(s + \omega_b)}{s + 100*\omega_b} \end{aligned} \tag{3.15}$$

and the combined gain and time-delay weighting functions,

$$w_2 = \frac{2.16*\frac{\Delta\theta}{2}s + 0.16}{\frac{\Delta\theta}{2}s + 1}; \qquad \Delta\theta = 0.43*\bar{\theta}$$

$$w_4 = \frac{2.15*\frac{\Delta\theta}{2}s + 0.15}{\frac{\Delta\theta}{2}s + 1}; \qquad \Delta\theta = 0.27*\bar{\theta} \qquad (3.16)$$

The time constant weighting functions are,

$$w_6 = \frac{0.19*s}{s + \omega_b}; \quad w_7 = \frac{0.4*s}{s + \omega_b}; \qquad \omega_b = 1/16 \qquad (3.17)$$

In the weights w_1, w_4, and w_5, 15% uncertainty in the gains were used, instead of 35%, 31%, and 65% respectively. As discussed in Chapter 4, this was done in order to achieve robust performance. Robust stability is however guaranteed when the gain uncertainties associated with these weights are 27%, 31%, and 65% respectively.

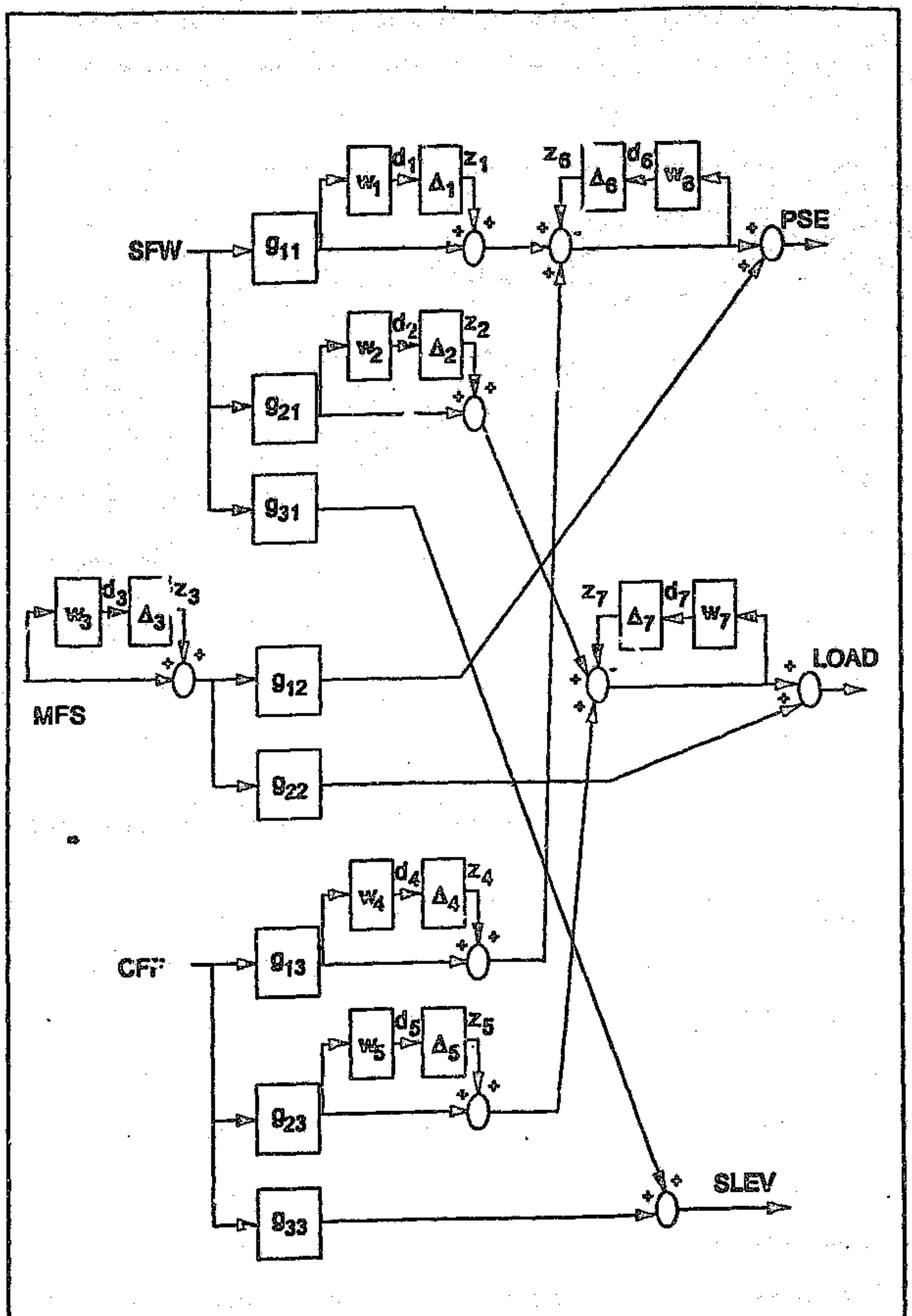

Figure 3.7: Nominal Plant with Uncertainty Description

The frequency response of the weighting functions are shown in Figure 3.8.

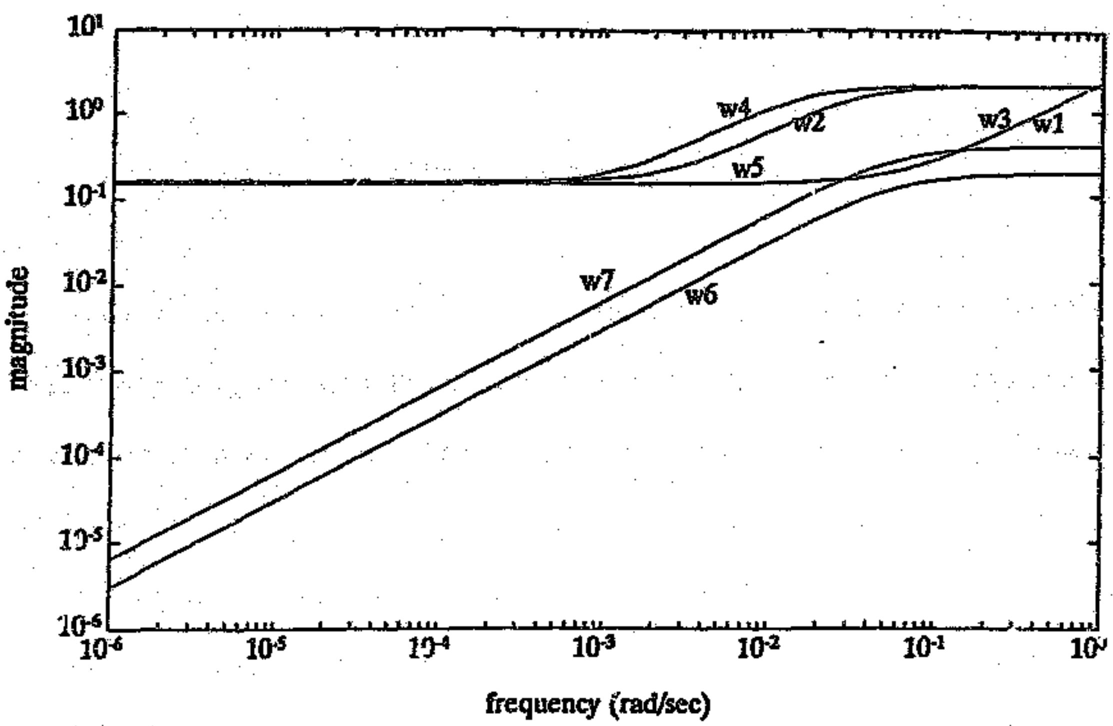

Figure 3.8: Frequency Response of the Weighting Functions

The uncertainty description shown in Figure 3.7 concentrates on the low-frequency dynamics of the milling circuit. Unmodeled high-frequency dynamics, such as those resulting from the actuators or the rotation of the mill, are not addressed specifically. They can however be "taken care of", from a robustness point of view, by constraining the bandwidth of the closed-loop system with carefully chosen performance specifications. In fact the uncertainty weights described in this section also play a role in constraining the closed-loop bandwidth. For example the gain uncertainty weight w_3 in (3.15), shows that the gain uncertainty is up to 11% at low-frequencies, but can increase to 100% or more at frequencies beyond 0.5

rad/sec. With such band-limiting weighting functions, a controller designed to achieve robust stability and robust performance, will naturally limit the bandwidth of the closed-loop system.

3.6 Performance Specifications and Weight Selection

In the μ or H_∞-synthesis framework performance specifications are expressed in the frequency domain as weighting functions on relevant transfer functions. As explained in Lundström *et al.* [64], there are three basic approaches to the selection of performance weights, i.e., the loop shaping approach (e.g. [65], [66], and [67]), the frequency-by-frequency approach [43], and the power spectrum approach [42]. These approaches differ mainly on the physical interpretation given to the H_∞-norm of M in Figure 2.3. The interpretation of the H_∞-norm which leads to the power spectrum approach, is illustrated in Table I. Here it is shown that the H_∞-norm is, for e.g., the induced norm from bounded-power spectrum inputs to bounded-power spectrum outputs in the time-domain. This approach considers the entire frequency spectrum, and the performance weights chosen can be interpreted as shaping the spectral content of the relevant input and output signals.

The loop shaping and frequency-by-frequency approaches can best be illustrated in terms of the singular value decomposition (SVD) [68]. An SVD can be done at each frequency of interest to provide a singular value gain-band for a system as a function of frequency. It also provides directional information in the form of the left and right singular vectors. In fact, the complex directions of the singular vectors, which correspond to sinusoidal vectors with relative phase shift among their elements, can be used to determine minimum and maximum input and output amplification directions. For example, a unit input sinusoid at a particular frequency, which is in the direction of the right singular vector associated with the maximum singular value, will at sinusoidal steady-state result in an output sinusoid, with maximum possible amplitude, in the direction of the left singular vector associated with the maximum singular value.

The loop shaping approach utilizes the definition of the H_∞-norm, and essentially boils down to choosing performance weighting functions which bound the gain-band (minimum and maximum singular value) of the transfer function in question. With this approach the performance weighting functions are chosen as direct bounds on important transfer functions such as the closed-loop and sensitivity transfer function matrices. Thus "classical" performance specifications such as bandwidth and disturbance rejection specifications can be set in a multivariable framework.

The frequency-by-frequency approach considers the sinusoidal system response, thereby exploiting the gain information provided by the singular values as well as the directional information contained in the singular vectors. Although the two SVD-type approaches differ in concept, the distinctions between them tend to become somewhat vague when they are applied in practice.

The performance weights chosen in this document can be interpreted using all three approaches described above. Performance weighting functions W_y and W_u are chosen as bounds on the error and control signals respectively. This could be taken as a loop shaping approach, but in fact the approach used here goes beyond conventional singular value loop shaping, as the controller will be designed to minimize μ over the bandwidth of interest [69]. Using μ conditions for robust performance avoid overstating actual requirements that could occur when singular value conditions are used.

The inverse of the error weight W_y can be thought of as bounding the maximum singular value of the sensitivity transfer function matrix S(s), and similarly, the inverse of the control weight W_u, acts as a bound on the transfer function R(s)=K(s)S(s). The NP condition (2.19) then becomes,

$$\|M_{22}\|_\infty \leq 1$$
$$\text{where} \quad M_{22} = \begin{bmatrix} W_y S \\ W_u R \end{bmatrix} \tag{3.18}$$

$|W_y(j\omega)|$ can be thought of as determining the degree of disturbance attenuation at each frequency ω, whereas $|W_u(j\omega)|$ can be interpreted as reflecting the largest anticipated additive plant perturbations [65].

Performance specifications for a ROM milling circuit are determined by the economic and process-related importance of the outputs PSB, LOAD, and SLEV. The specifications for each of these outputs will be expressed in terms of a scalar weight w_{yi} [64] with structure:

$$w_{yi} = \frac{1}{M}\,\frac{\tau_{cl}\,s + M}{\tau_{cl}\,s + A} \quad ; \quad = \frac{1}{\omega_B} \quad ; i=1,2,3 \tag{3.19}$$

with A - disturbance rejection factor, or steady-state offset less than A

ω_B - closed-loop bandwidth higher than ω_B

M - amplification of high-frequency noise less than M

The weights on the errors can then be combined in a single diagonal weight such as,

$$W_y = diag\{w_{y1}, w_{y2}, w_{y3}\} \tag{3.20}$$

3.6.1 PSE error weight

Objective (i) in Section 3.2 gives an indication as to how PSE performance specifications should be chosen. This objective states that it is important to control the PSE to a certain average size (the finer the better), and to reduce the product size fluctuations. The reduction of size fluctuations is important because even though two grind time records may have the same mean, the one with the larger standard deviation will result in higher gold losses. From an economic point of view, it is thus important to keep the standard deviation of the PSE as low as possible.

Product particle size is very difficult to measure on-line, and the best resolution that can be expected from a PSE is in the order of 5% of the range of measurement. As there is no point in controlling the PSE to less than the resolution of the instrument, it is reasonable to require that the PSE loop (both nominal and perturbed) should reject output disturbances by a factor of 20-to-1 (at least at low frequencies). This specification also implies that the normalized steady-state tracking error due to a reference step input should be less than 0.05. The frequency up to which this specification must hold is limited not only by the sampling frequency and the speed of the actuators' response, but also by averaging that occurs within the instrument itself. However, as discussed in the following chapter, model uncertainties turn out to be the limiting factor on the achievable bandwidth of the PSE loop. For the PSE error weight (w_{y1}) the following parameters are chosen,

$$A = 0.05, \ M = 2, \text{ and } \tau_{cl} = 900$$

Note that these specifications account for noise but not for bias.

3.6.2 LOAD error weight

The LOAD loop does not have such a clear-cut economic criterion in terms of disturbance rejection or steady-state tracking error. What is important however is the time this loop takes to settle after a setpoint step-change. The steady-state relationship between the LOAD and the solids throughput is approximately parabolic. There is thus an optimum LOAD operating point at which the milling circuit throughput is maximized. This optimum operating point changes with time, largely due to changes in the feed ore hardness and composition [22]. Thus in order to keep the milling circuit operating at the optimum load, a "steady-state" throughput optimization strategy is needed to step the LOAD in the "right" direction in a peak-seeking fashion. The speed of response of the LOAD loop limits the time interval between LOAD setpoint changes, as requested by the throughput optimizer. The longest practically viable time interval that can be tolerated by the optimizer, is in the region of one hour. It is thus required of the LOAD loop to settle within an hour after a setpoint step-change has been made. The steady-state tracking error specification for the LOAD loop is not that critical, and can be of the order of 10%. With reference to equation (3.19), a LOAD error weight (w_{y2}) with the following parameters will suffice,

$$A = 0.1,\ M = 2,\ \tau_{cl} = 1800$$

If the LOAD loop can adhere to the specifications described above, a throughput optimization strategy will be able to move the process in the direction of more efficient operation, as shown in Figure 3.4.

3.6.3 SLEV error weight

The absolute level of the slurry in the sump, SLEV, is not important as long as it lies between safe operating limits, i.e., it should not be close to overflowing or running dry. If the sump is close to empty, the sump pump can suck air which will result in erratic CFF behaviour. If the sump overflows, the result will not be disastrous, but this could lead to lengthy clean-up sessions. In addition, the operating staff might lose confidence in the control system being used. In these extreme cases the linear plant model will of course not be valid.

Mill sumps come in all shapes and sizes, but they usually all have an inclined floor to prevent the build-up of "sandbanks". The linear plant model only holds as long as the SLEV does not go below the level at which the floor incline starts. In some mill sumps this level could be at 50% of capacity. The level of such sumps should then be controlled between 50 and 100% of capacity.

The mill sump can be seen as a buffer which can absorb milling circuit disturbances such as surges in the mill discharge. In fact, Hulbert *et al.* [13] used error squared control on the SLEV loop, i.e., significant control action is only taken when the difference between the SLEV and its setpoint becomes large. Such large errors could possibly occur due to spillage pumping which occur at irregular intervals.

The point is that the SLEV control does not have to be tight, and thus reasonable steady-state tracking errors can be tolerated. With reference to equation (3.19), this discussion indicates that a SLEV error weight (w_{y3}) with the following parameters can be chosen,

$$A = 0.2,\ M = 2,\ \tau_{cl} = 1800$$

The frequency response of the inverses of the three error weights are shown in Figure 3.9.

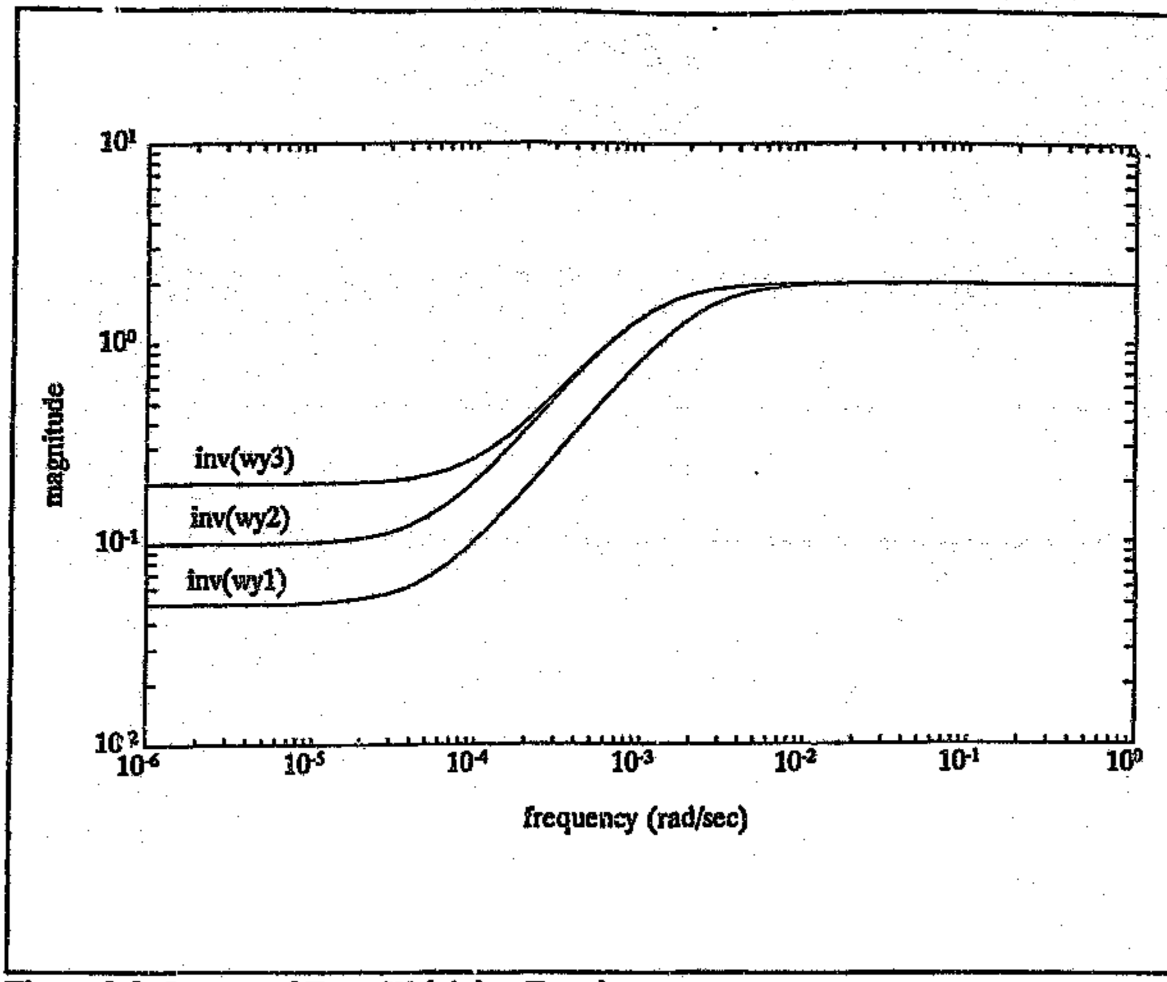

Figure 3.9: Inverse of Error Weighting Function

3.6.4 Control weight

The weight on the controls W_u was not chosen with the idea of making the closed-loop robust to some additive plant uncertainty, but rather to limit the rate of change of the control inputs. This is done such that the digital implementation of the controller does not become an issue. Fast actuator movement is thus inhibited by the weight W_u, which is small at low frequencies whilst increasing at higher frequencies. This weight is chosen to reach its maximum about a decade below the sampling frequency. This ensures that the controller do not request control input changes which are faster than what the implemented system can deliver. With a sampling interval of 10 seconds, this weight is chosen as,

$$W_u = w_u \, I_3$$

$$w_u = \frac{16s + 0.01}{16s + 1} \tag{3.21}$$

The frequency response of the control weight W_u, is shown in Figure 3.10.

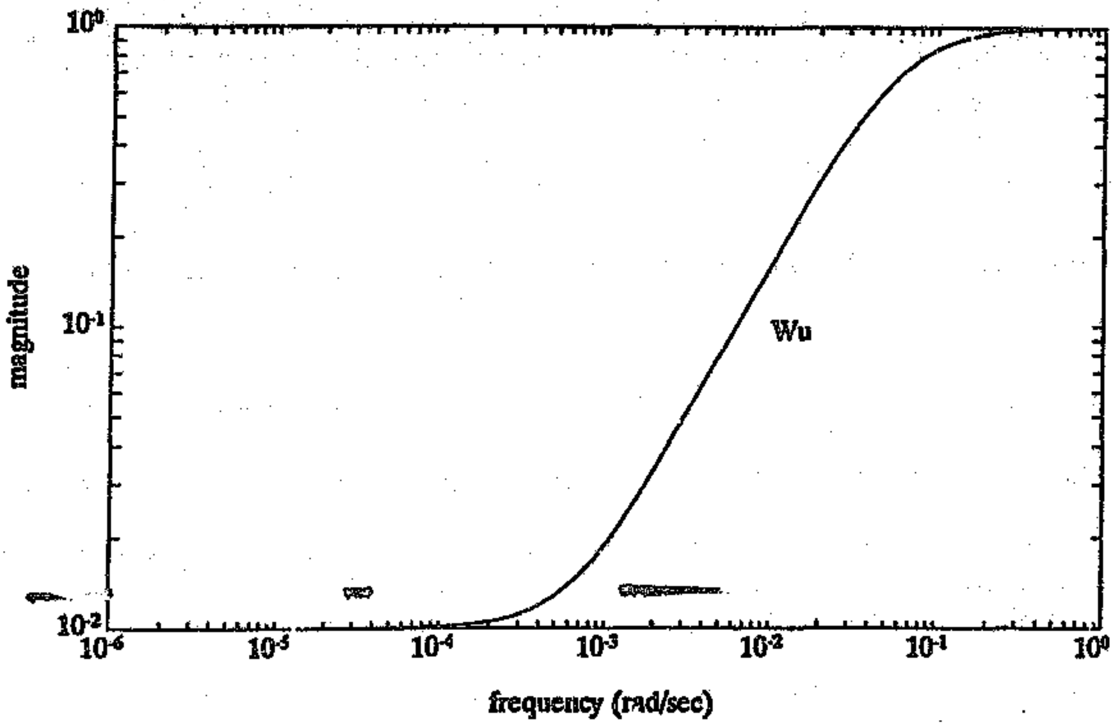

Figure 3.10: Frequency Response of the Control Weight

It is of course possible to weight some of the controls heavier than others. For example one could allow the CFF to change much faster than the MFS by specifying different bandwidths for the appropriate weights. This will however not be done here.

3.6.5 Other possibilities

Other sources of disturbances such as measurement noise, although they do exist, are not considered to be of sufficient importance, when compared to disturbances caused by changes in ore feed composition and hardness, to warrant the inclusion of associated weights. The more weights there are, the more states the final controller will have, and the longer it will take to compute. Also, by including too many sources of disturbances and noise, it becomes very unlikely in an H_∞-norm setting for the worst case to occur in practice.

3.7 ROM Milling Circuit and the General Synthesis and Analysis Framework

The error weight (W_y) and control weight (W_u) can be superimposed on the plant with its uncertainty description (Figure 3.7), to form the general synthesis and analysis framework of Figure 2.2. The result is shown in Figure 3.11. In this figure, Δ represents the norm bounded perturbations that form part of the model uncertainty description. The perturbation inputs and outputs are represented by z and d respectively. e Represents the weighted controls and errors, whereas v represents the setpoints.

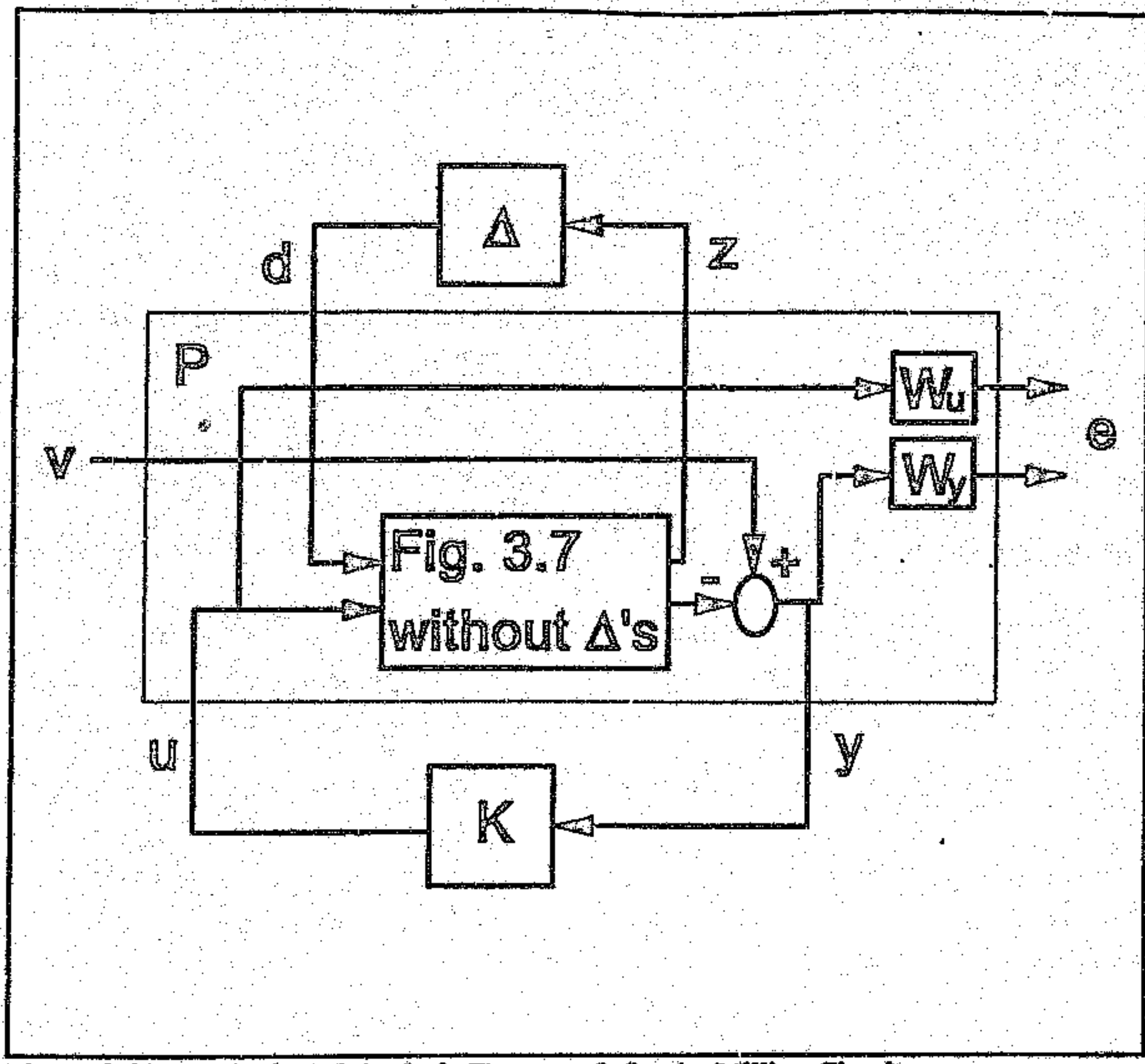

Figure 3.11: Synthesis and Analysis Framework for the Milling Circuit

The vector time signals in Figure 3.11 can be represented as,

$$
\begin{aligned}
z &= [z_1, z_2, \ldots, z_7]^T \\
d &= [d_1, d_2, \ldots, d_7]^T
\end{aligned}
\qquad (3.22)
$$

and

$$e = \begin{bmatrix} W_u \, u \\ W_y \, y \end{bmatrix} \tag{3.23}$$

with

$$\begin{aligned} u &= [SFW \ MFS \ CFF]^T \\ y &= v - \begin{bmatrix} PSE \\ LOAD \\ SLEV \end{bmatrix} \end{aligned} \tag{3.24}$$

The perturbations are given by,

$$\Delta = diag(\Delta_1, \Delta_2, \ldots, \Delta_7) \tag{3.25}$$

CHAPTER 4

MILLING CIRCUIT CONTROLLER DESIGN

In this chapter the μ-synthesis and analysis procedure is applied to the milling circuit with its uncertainty and performance weights as shown in Figure 3.11. Weight iterations are done in order to meet the performance robustness requirement. The order of the controller that results from the μ-synthesis process is reduced to ease its practical implementation. The reduced order controller is analyzed for robustness using μ-analysis and linear time simulations.

4.1 Controller Design

The controller design process described here is illustrated in Figure 2.7. Before the start of the design process, one needs to conduct the laborious but straight-forward task of obtaining a state-space description for the block P in Figure 3.11. In order to do this, the time-delays were approximated by first-order Padé approximations in order to make P a rational transfer function matrix. (These delays can be approximated arbitrarily well in the low frequency region, but at higher frequencies some additional model uncertainty is introduced [70]). The result is a system with 13 inputs, 16 outputs, and 26 states. The

26 states are made up of the states of the plant (13), the uncertainty weights (7), and the performance weights (6).

An initial H_∞-controller design was done without any scaling. This design provides a controller, with the same order as that of the plant plus weights, which minimizes the H_∞-norm over a set of stabilizing controllers, of the transfer function matrix between a 10 x 1 vector of inputs and a 13 x 1 vector of outputs. The input vector consists of perturbation inputs (7 x 1) and setpoints (3 x 1), whereas the output vector consists of perturbation outputs (7 x 1), weighted control signals (3 x 1), and weighted errors (3 x 1). Thus with reference to (2.14), the H_∞-design yields a stabilizing controller which minimizes $\| M \|_\infty$, where M is the closed-loop transfer function matrix from inputs,

$$\begin{bmatrix} z \\ v \end{bmatrix} \tag{4.1}$$

to outputs,

$$\begin{bmatrix} d \\ e \end{bmatrix} \tag{4.2}$$

The minimum γ value achieved for this initial design is shown in Table III.

Table III: Design Results

H_∞ design	$\gamma_{min} = \|DF_l(P,K)D^{-1}\|_\infty$	Weight Orders
Initial	1.78	-
1st iteration	1.095	1:3:1:1:3:2:2
2nd iteration	4.54	1:3:1:1:3:2:2
3rd iteration	1.161	1:3:3:1:3:2:2
4th iteration	1.038	1:3:1:1:1:2:2
5th iteration	1.038	1:3:1:1:1:2:2

The next step in the design process consists of a μ-analysis of the closed-loop system $F_l(P,K)$ with respect to the block structure of Figure 2.5. This uncertainty block has 8 complex sub-blocks of which 7 are scalars arising from the plant uncertainty, and one 6 input, 3 output "performance block". For a fixed controller K, the calculation of μ provided the frequency dependent D scaling matrices (one scaling for each of the uncertainty weights) which minimizes the norm,

$$\|DF_l(P,K)D^{-1}\|_\infty \tag{4.3}$$

At this stage the performance and robustness properties of the closed-loop transfer function M were evaluated. Nominal performance (2.19) and robust stability (2.20) were achieved, but the robust performance criterion (2.25) was not met. It is not surprising that robust performance was not acceptable at this stage, as no μ-minimization has yet been done.

The D-scales were thus fitted with stable, minimum phase rational functions, after which they were absorbed into the generalized plant P. The scaled version of P was then used in a subsequent H_∞-design. The H_∞-design was now tricked into minimizing $\mu(M)$ over frequency instead of $\overline{\sigma}(M)$ because the D-scaling matrix that was absorbed into P, forces the H_∞-minimization to concentrate on μ across frequency rather than the maximum singular value ($\overline{\sigma}$). As shown in Table III, this design iteration resulted in a reduction in γ_{min}, i.e., form 1.78 to 1.095. (The number of significant figures for γ_{int} and γ_{min} is determined by the tolerance used in the H_∞-minimization. Typically, larger tolerances are used for the initial H_∞ design.)

μ-Analysis of the closed-loop system showed that nominal performance and robust stability were achieved, but that robust performance was not satisfactory at this stage (NP test $\|M_{22}\|_\infty < 0.85$, RS test $\|\mu(M_{11})\|_\infty < 0.4$, and RP test $\|\mu(M)\|_\infty < 1.78$). In fact, it was only after another three design iterations that robust performance of the closed-loop system was considered to be acceptable. (For the purposes of this thesis robust performance is considered to be acceptable when $\mu(M)$ is smaller than 1.05.) The DK iteration process was repeated five times, resulting in the minimum γ values shown in Table III. The fifth iteration was done to ensure that γ_{min} achieved in iteration four was indeed the minimum that could be reached.

The second and third iterations show that the DK iteration, as implemented in the Matlab toolbox, does not always converge monotonically. This phenomenon was also observed by Lundström *et al.* [64]. After the fourth and fifth iterations, the condition in (2.28) was (approximately) met, and the process was terminated. In fact it was found that there no change in the γ_{min} value resulting from the fourth and fifth iterations. Also, after five iterations the μ-versus-frequency plot was more or less flat up to 0.01 rad/sec, in line with the "flatness stop criterion" discussed by Lundström *et al.* [64].

It is interesting to note that the numerical calculations to compute the design described above take about 50 minutes to perform on a 33 MHz 486 PC.

4.2 Weight Iterations

The design discussed above is the end result of an extensive process in which designs were done with different combinations of uncertainty and performance weighting functions and parameters. It was necessary to iterate on the weights in order to achieve acceptable μ-values for performance robustness. Care was however taken not to reduce the plant uncertainty description such that it becomes an unrealistic description of the real plant.

The weight iteration process is summarized in Table IV. This table shows the uncertainty and performance weighting parameters that were changed in order to achieve robust performance. It also indicates whether nominal performance (NP), robust stability (RS), and robust performance (RP) were achieved for a particular design. The weighting parameters arrived at in the final design are the same as those given in Chapter 3. Only the parameters that were changed in the design process are shown. The other parameters can be found in Sections 3.5 and 3.6. The parameter γ_{init} indicates the minimum γ value that was achieved after the initial H_∞-design. The end result of the μ-synthesis process (DK iteration) is γ_{min}, and the value in brackets underneath γ_{min} indicates the number of DK iterations that were attempted. For some designs no DK iterations were done as the initial H_∞-design indicated that a particular parameter(s) will not play a significant role in achieving

Table IV: Weight Iterations

Design No.	w_1	w_3	w_4	w_5	w_{yl}	γ_{init}	γ_{min}	NP	RS	RP
1	k%=35	k%=11 in	k%=31 θ%=27	k%=65	τ_{cl}=1800 M=3	3.43	3.23 (1)	No	No	No
2		k%=1				3.43				
3		k%=11	k%=10			3.36	2.57 (1)	No	Yes	No
4			k%=31 θ%=10			3.43				
5	k%=10		θ%=27			3.10	2.44 (1)	No	Yes	No
6	k%=35			k%=10		1.85	1.65 (1)	No	Yes	No
7		out		k%=65		3.43	1.85 (2)	Yes	No	No
8	k%=15			k%=15		1.33	1.128 (4)	Yes	Yes	No
9			k%=15			1.19	0.997 (1)	Yes	Yes	Yes
10					τ_{cl}=900(w_{yl}) M=2	1.52	1.038 (3)	Yes	Yes	Yes
final		in				1.78	1.038 (5)	Yes	Yes	Yes
RS test	k%=27		k%=31	k%=65			1.7	Yes	Yes	No

robust performance.

The uncertainties represented by the uncertainty weights in design 1, are as shown in (3.4) to (3.6). For this design, γ_{min} of 3.23 was achieved after one DK iteration. NP, RS, and RP were not achieved. The RS measure $\mu(M_{11})$ peaked below 1.2. This design indicated that other combinations of uncertainty weighting parameters had to be chosen in order to achieve RP.

For designs 1 to 9, the bandwidth of the PSE loop was made 1/1800 in order to make it easier to meet the robust performance specification. The parameter τ_{cl} in the error weights w_{yi} was thus made 1800 as indicated. The high frequency noise amplification factor M in the error weights w_{yi} (3.19), was made 3 for all three the error weights up to design 9, after which is was decreased to 2 in design 10.

The effect of the gain uncertainties on robust performance were investigated in designs 2, 3, 5, and 6. Design 2 shows that a substantial reduction in the gain uncertainty associated with weight w_3 does not reduce the γ_{init} value found in design 1. In design 3 a reduction from 31% to 10% in the gain uncertainty associated with weight w_4 reduced γ_{init} from 3.43 to 3.36, and γ_{min} from 3.23 to 2.57 after one DK iteration. For this DK iteration, NP and RP were not achieved. RS was achieved as $\mu(M_{11})$ peaked below 0.85. Design 5 shows that a reduction from 35% to 10% in the gain uncertainty associated with weight w_1 reduced γ_{init} from 3.43 to 3.10, and γ_{min} from 3.23 to 2.44 after one DK iteration. NP and RP were not achieved, whereas RS was with $\mu(M_{11})$ peaking below 0.6. Design 6 shows that a reduction from 65% to 10% in the gain uncertainty associated with weight w_5 reduced γ_{init} from 3.43 to 1.85, and γ_{min} from 3.23 to 1.65 after one DK iteration. NP and RP were not achieved, whereas RS was with $\mu(M_{11})$ peaking below 1.0. Design 4 shows that a reduction in the time delay uncertainty associated with weight w_4 does not reduce the γ_{init} value found in design 1.

For design 7 the input uncertainty weight w_3 was removed from P in Figure 3.11. This change in the uncertainty structure was not detected by the initial H_∞ design, as it does not take the structure of the uncertainty into account. The DK iteration however shows that this change to the uncertainty structure caused a substantial reduction in γ_{min} from 3.23 (design 1) to 1.98 (1st iteration) and 1.85 (2nd iteration). This design illustrates the conservativeness that can result when using unstructured uncertainty blocks. Also this input uncertainty has a substantial effect on RP, whereas the two output uncertainties w_6 and w_7 have a very small effect on RP. This confirms to some extent the findings of Skogestad *et al.* [45], which state that input uncertainties put much more constraints on controller design than does output uncertainties.

Designs 5 and 6 illustrates that the weights w_1 and w_5 have a substantial influence on RS and RP respectively. With w_3 removed, the gain uncertainties associated with these weights were reduced to 15% in design 8, and four DK iterations resulted in a γ_{min} value of 1.128. NP and RS were achieved. In design 9 the gain uncertainty associated with w_4 was also reduced to 15%. This resulted in a γ_{init} value of 1.19, and a γ_{min} value of 0.997 after one DK iteration, i.e., NP, RS, and RP were achieved. The ease with which RP was achieved in this design (only one DK iteration), suggested that the performance specifications, that of the PSE loop in particular, could be made tighter.

In design 10, the bandwidth of the PSE loop was increased to 1/900, and the high frequency noise amplification factor M was reduced to 2 for all three error weights. A γ_{min} value of 1.038 was achieved in this design, i.e., NP, RS, and RP were achieved.

μ-Analysis was performed using the controller that resulted from design 10. Instead of using the six uncertainty weights on which the controller design was based, all seven the uncertainty weights (w_3 included) were used in the analysis. This analysis suggested that RP could be achieved when all seven uncertainty weights are included in the design process. The final design shown in Table IV includes all the uncertainty weights, and is also the design that is described in Section 4.1.

RP can thus only be guaranteed for a subset of the uncertainty set described by the weights used in design 1. As the H_∞ framework is a worst-case approach, the final μ-controller will achieve RP in most cases as it is highly unlikely for the worst case to occur in practice. RS is guaranteed for a larger subset of uncertainties, as shown in the last entry in Table IV. RS is guaranteed for the full gain uncertainties of w_4 and w_5, and for 27% (instead of 35%) gain uncertainty in w_1. In this case $\mu(M_{11})$ peaked at 0.99 whereas the RP measure $\mu(M)$ peaked at 1.7.

4.3 Controller Reduction

The design process discussed in section 4.1 results in a controller with 48 states. The number of states of the controller is dependent on the number of states of the plant (13), the uncertainty weights (7), the performance weights (6), and the rational functions fitted to the D-scales (11). The 48 controller states thus result from the 26 states of P (plant plus weights) and the 22 states of the D and D^{-1} scaling realizations. There is one scaling realization for each of the seven uncertainty weights. The orders of the realizations of these weights are 1, 3, 1, 1, 1, 2, and 2 respectively, and the total order of these weighting realizations make up the 11 D-scale states.

A 48 state controller is unsuitable for implementation, as it would tie up too many computing resources. There are a few options that can be followed when a controller of reduced order is required. The design plant model P can be reduced before the actual controller design is done. Such a design would then yield a reduced order controller. The other alternative is to use the full order design plant model in the controller design. The resulting full order controller is then reduced after the design has been completed [71]. This approach will be followed here.

The order of the controller was reduced as much as possible without losing the achieved level of robust performance. A model reduction routine, which calculates the optimal Hankel norm approximation of a balanced controller realization [72], reduced the 48 states of the controller to 13 (equal to the number of plant states) without a significant change in the level of performance robustness achieved.

Singular value plots of the full and reduced order controller are shown in Figure 4.1. The singular values of the reduced order controller are indicated with *'s. Two μ plots of M (both upper and lower bound) are shown in Figure 4.2. In the one case M contains the

48 state controller, and its μ-plots are indicated by a solid and a dashed line. In the other case M contains the 13 state controller, and its μ-plots are indicated by °'s. The controller singular value plots show that the singular values of the full and reduced order controllers only differ in the smallest two singular values, particularly at low and high frequencies. The μ-plots show that this difference has a slight influence on robust performance, particularly in the low frequency region. Robust performance is however still acceptable.

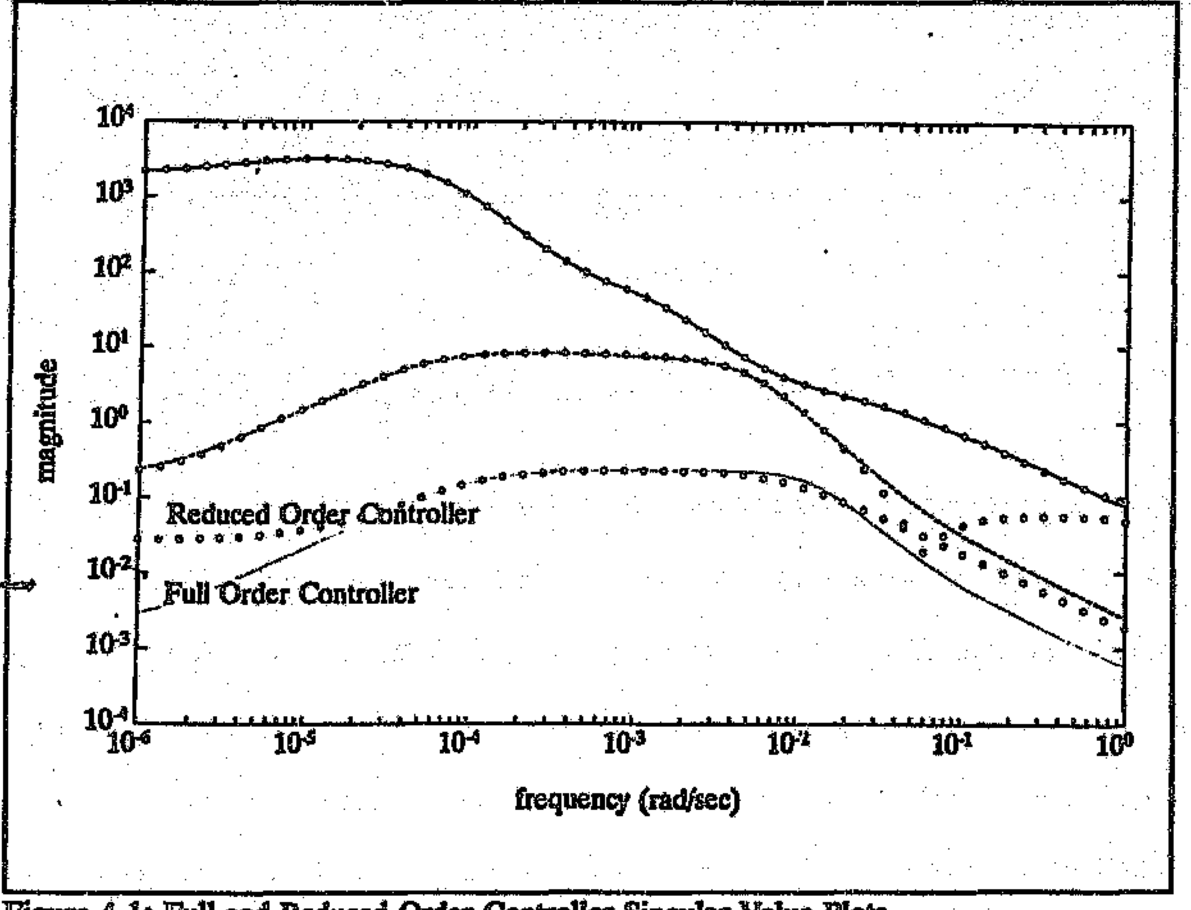

Figure 4.1: Full and Reduced Order Controller Singular Value Plots

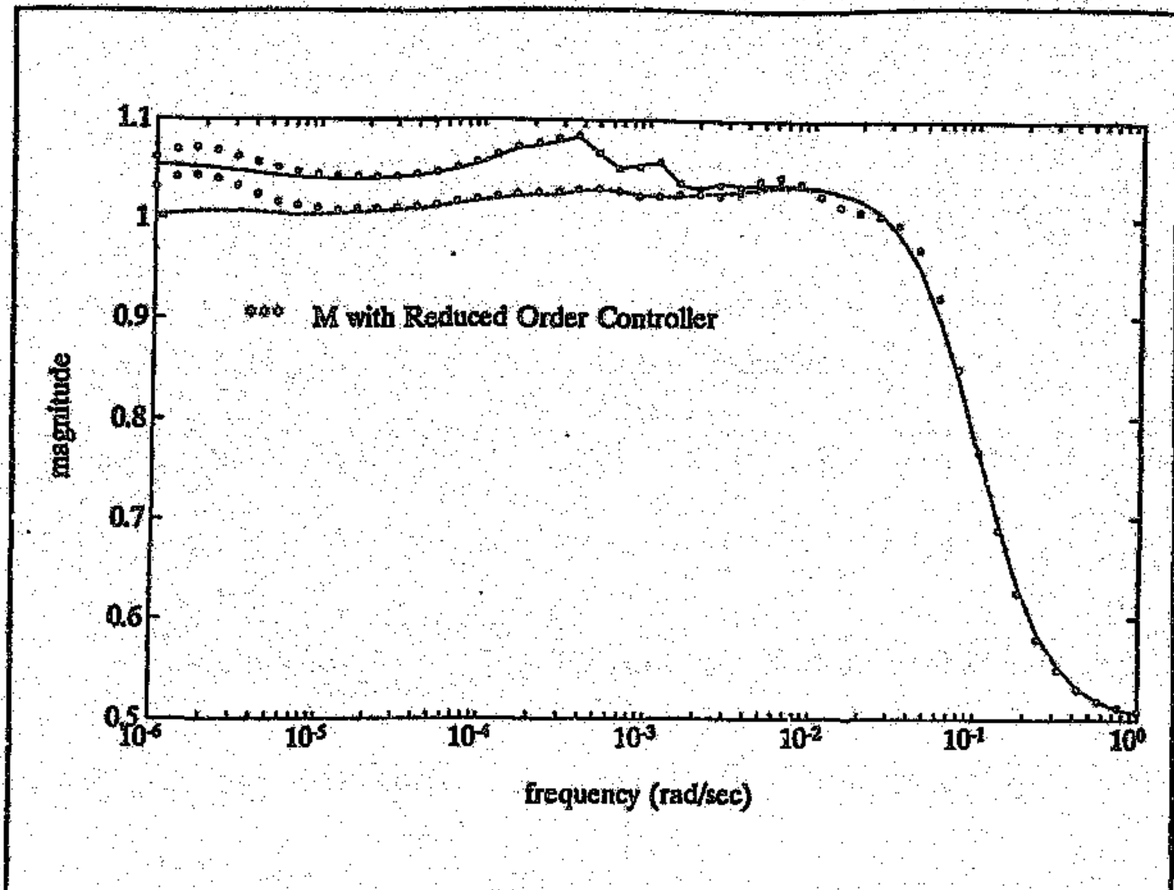

Figure 4.2: μ-Plots of M with Full and Reduced Order Controllers

The effect of the controller reduction is illustrated in the time-domain by a linear simulation of the closed-loop system as shown in Figure 4.3. This figure shows the response of the system to a unit step in the LOAD setpoint. There are no visible differences in transient responses of the PSE and LOAD. A slight but insignificant difference can be observed in the SLEV response. No difference can be observed when comparing the plant input transients generated by the reduced and full order controllers. The reduced order controller is thus used in the analysis that follow.

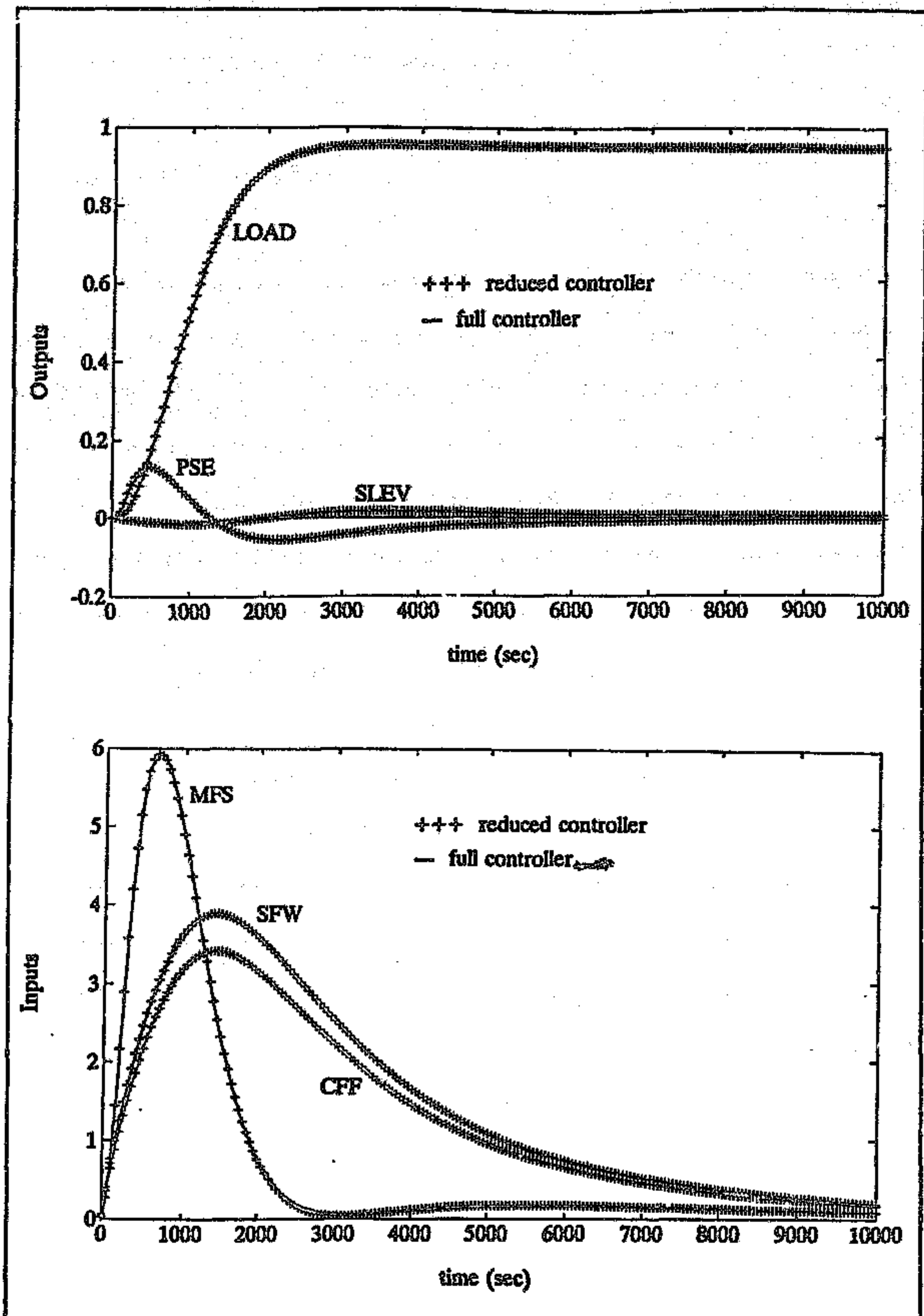

Figure 4.3: Time Simulation with Full and Reduced Order Controllers

4.4 Performance and Robustness Analysis

4.4.1 μ-Analysis

In this section, μ-analysis, as discussed in Section 2.2, is applied to the closed-loop system M. M is thus analyzed for nominal performance, robust stability, and robust performance. Nominal stability is guaranteed by the μ-synthesis methodology. Nominal performance is achieved when the singular values of the transfer function between v and e (M_{22}) are below unity for all frequencies. Robust stability is achieved when μ of the transfer function between z and d (M_{11}), with respect to the block structure Δ of (2.26), has a peak value below one for all frequencies. Robust performance is achieved when the μ-versus-frequency plot of M, with respect to the block structure in Figure 2.5, peaks below unity.

Figure 4.4 shows the plots of $\mu(F_l(P,K))$ (both upper and lower bound), as well as the μ plot of M_{11} for robust stability and the $\overline{\sigma}$ plot of M_{22} for nominal performance. The controlled system achieves nominal performance and robust stability as indicated. Robust performance is almost achieved, with the μ plot of M, with respect to the block structure in Figure 2.5, peaking at a value of 1.038. This peak value is γ_{min} that was achieved after the fourth DK iteration. The bounds on $\mu(M)$ shown in Figure 4.1 and Figure 4.4, are slightly higher than γ_{min} found after the fourth DK iteration. This phenomenon was also encountered by Lundström *et al.* [64] when using the μ-Analysis and Synthesis Toolbox [54].

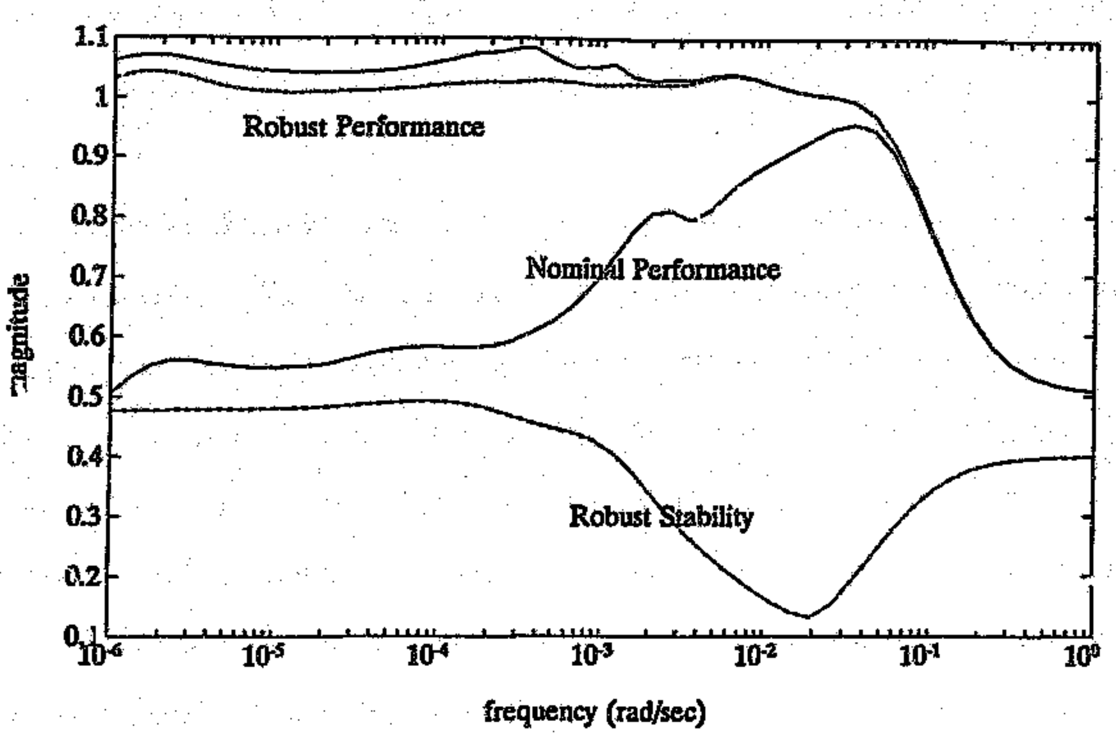

Figure 4.4: Performance and Robustness Analysis of the Controlled System

4.4.2 Linear time simulations

μ-Analysis draws conclusions as to the worst-case performance for the entire sets of input signals and perturbations at once. Figure 4.4 can thus be thought of as a summary of linear simulations responses that result from all possible combinations of input signals and perturbations defined earlier. Of all these combinations, one . combination (a LOAD step change), and one perturbation combination will be highlighted to illustrate the performance of the closed-loop system in the time-domain. A LOAD step change is chosen to test wether the LOAD performance specification is met. The perturbation combination is chosen to illustrate the effect that practical events such as a fine feed ore, and the addition of steel balls could have on the performance of the control system.

In the first simulation, the nominal closed-loop system ($\Delta=0$) is subjected to a unit step change in the LOAD setpoint, and the resulting input and output responses are observed in Figure 4.3. The LOAD performance specification is met as it settles in the required time (3600 sec.), and its steady-state error is less than 10%. This simulation shows that there is some transient interaction between the LOAD and PSE loops. This interaction results from the fact that the μ-controller was designed to be robust to significant plant uncertainties. If the plant were to contain no uncertainties, then a controller could be designed to invert the plant at all frequencies in the bandwidth of interest, which will result in perfect decoupling with no interaction between the plant outputs. In practise this is never a viable option, as uncertainties (and other plant characteristics such as non minimum phase zeros) put a constraint on the degree of plant inversion that can be achieved.

An attempt was made to simulate practical events that can result in plant parameter changes such as those discussed in Chapter 3. The result of a size distribution change in the MFS is considered. Such a change can result from changes in mining practice, segregation in storage bins and stockpiles, and chute and feeder blockages [61]. These changes can be long-term, as in the case of changes in mining practice, or short-term, as in the case of segregation in storage bins.

In the case of the feed ore becoming fine, a shortage of grinding medium in the mill will result, and the throughput of the milling circuit will drop. A particle will then spend more time in the mill before it is small enough to leave the circuit in the cyclone overflow, i.e., the effective mean residence time of the mill will increase. Certain parameters in the linear plant model which are dependent on the mean residence time of the mill [73], i.e., the time constant τ in g_{21} and g_{23}, and the gain k in g_{23}. The uncertainty in these parameters is represented by the weight w_7 in the case of the time constants, and by the weight w_5 in the case of the gain.

A practical event that decreases the mill residence time, is the addition of steel balls to the MFS. This will increase the rate of grinding and hence the milling circuit's throughput, with a resulting decrease in the mill residence time. The time constants in g_{21} and g_{23}, and the gain in g_{23} will thus decrease as a result.

Two linear simulations were conducted in which the time constant (τ) uncertainty in g_{21} and g_{23}, and the gain (k) uncertainty in g_{23} were alternately increased (fine MFS) and decreased (steel perturbation) by 40% and 15% respectively. This represents the maximum possible perturbations on these parameters, for which the μ-controller will guarantee robust performance, as specified by the weights w_5 and w_7. A unit step change in the LOAD setpoint was made, and the resulting responses of the perturbed systems are shown in Figure 4.5. This figure shows that the μ-controller is able to meet the performance specifications in the face of the perturbations describe above.

The gain (k) uncertainty in g_{23} was subsequently increased to 65%, which is the maximum uncertainty for this parameter, as indicated in (3.4). Table IV indicated (RS test) that for such a perturbation, RS is achieved, but that RP can no longer be guaranteed. Figure 4.6 shows two linear simulations for which the time constant (τ) uncertainty in g_{21} and g_{23}, and the gain (k) uncertainty in g_{23} were alternately increased (fine MFS) and decreased (steel perturbation) by 40% and 65% respectively. As before, a unit step change in the LOAD setpoint was made. This figure shows that the performance of the closed-loop system deteriorates somewhat in the "steel-perturbation case", as the LOAD takes longer to reach its setpoint. For this perturbation, the μ-controller performs reasonably well in the face of sizeable parameter changes.

4.5 Concluding Remarks

Figure 4.4 and the linear time simulations shown here do not reflect simulation responses resulting from a realistic (non-linear) dynamic ROM simulator. Due to the complexity of the dynamics of a ROM mill, such a simulator is unfortunately not available. The real test for the μ-controller is its practical implementation, the results of which are given in Chapter 5.

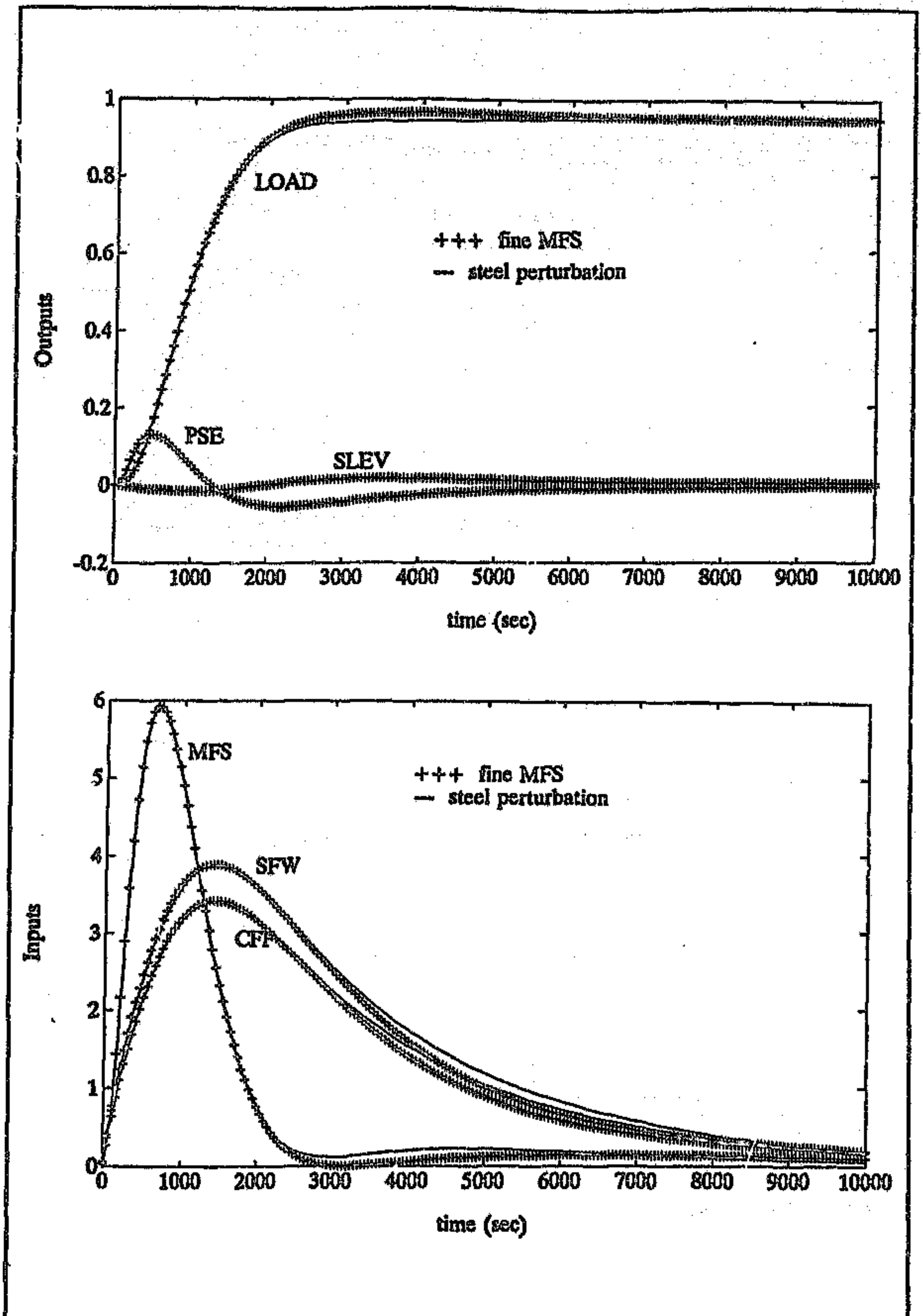

Figure 4.5: Time Simulation with a Fine MFS and a Steel Perturbation: RP Guaranteed

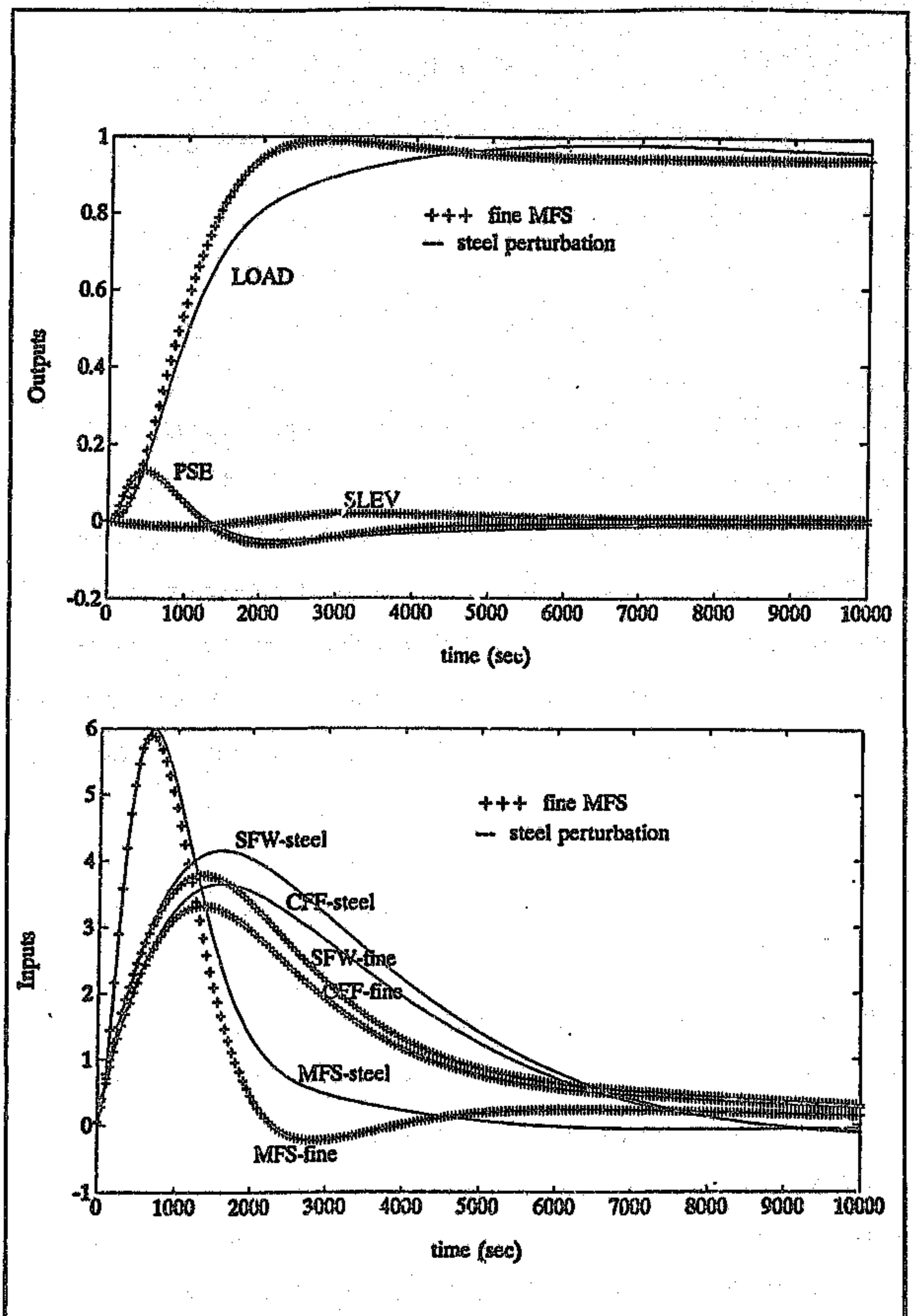

Figure 4.6: Time Simulation with a Fine MFS and a Steel Perturbation: RP not Guaranteed

CHAPTER 5

CONTROLLER IMPLEMENTATION

In this chapter an implementation of the μ-controller on an industrial ROM milling circuit is described. In Section 5.1 the platform on which the controller was implemented, is discussed. In Section 5.2 plant results are presented. This section includes a discussion of initial plant results which indicated that the μ-controller design needed to be modified. This was followed by a set of plant identification tests which led to a redesign of the μ-controller. Results achieved with this final controller are also presented and discussed. In Section 5.3 a general discussion of the implementation exercise is given.

5.1 Implementation Platform

The μ-controller as designed in Chapter 4 was implemented on Mintek's first generation experimental multivariable controller platform as described in [13]. This platform consists of a 8 MHz XT PC running the multi-tasking operating system Concurrent CP/M 86 [74]. The control, user interface, and plant interface software are written in Analog Devices' multi-tasking version of BASIC, called MACBASIC [75]. The plant interface hardware consists of μMAC-4000 I/O cards and anti-aliasing analog filters [76]. Every

5 seconds the plant output measurements are compared to the setpoints, and the resulting errors are processed by the μ-controller. The control actions calculated by the μ-controller are then sent out to the plant via the interfacing hardware. Slave PI controllers for the SFW, MFS, and CFF ensure that the control actions are implemented as requested by the μ-controller.

For the purposes of this thesis the existing Mintek platform was used with suitably modified control algorithm software. The μ-controller was discretized in MATLAB using a zero-order-hold approximation with a sampling interval of 5 seconds. The resulting discrete state-space description was then converted to a modal canonical representation [77]. The control software was thus modified to implement a controller of this form.

5.2 Plant Tests and Results

5.2.1 Initial plant test

An initial 4 hour test, shown in Figure 5.1, was conducted on the industrial ROM milling circuit with the μ-controller as designed in Chapter 4. This figure shows the plant outputs PSE, LOAD, and SLEV, and the control actions SFW, MFS, and CFF, with the dotted lines indicating the setpoints, and the solid line the actual measurement. The μ-controller was switched on for two periods; period 1 from 13:50 to 15:10, and period 2 from 15:25 to 17:20. During the first period the sump overflowed shortly after the controller was switched on, and manual corrective action had to be taken (the CFF slave controller was put onto LOCAL, and the CFF was increased from 450 m^3/h to 650 m^3/h in order to bring the SLEV down). The sump overflowed a few more times during this first period, and large PSE fluctuations occurred as a result of corrective action taken whenever this happened. It was thus decided to switch off the μ-controller and to allow the circuit settle for a short while.

During the second period no manual corrective action was taken to keep the SLEV away from extremes. Figure 5.1 shows that SLEV control was not satisfactorily, as the SLEV was at or below the low limit of the sump level indicator for most of this period. Control of the LOAD was also not as desired, and it was observed that the MFS was used mainly to keep the PSE close to its setpoint. As the MFS is the control action with the most influence on the LOAD, this would explain why the LOAD control was not adequate.

Some degree of PSE control was achieved during this second period. The μ-controller did a reasonable job of tracking a setpoint step change in the PSE from 75 to 80% $< 75\mu$m, which was made at about 16:25.

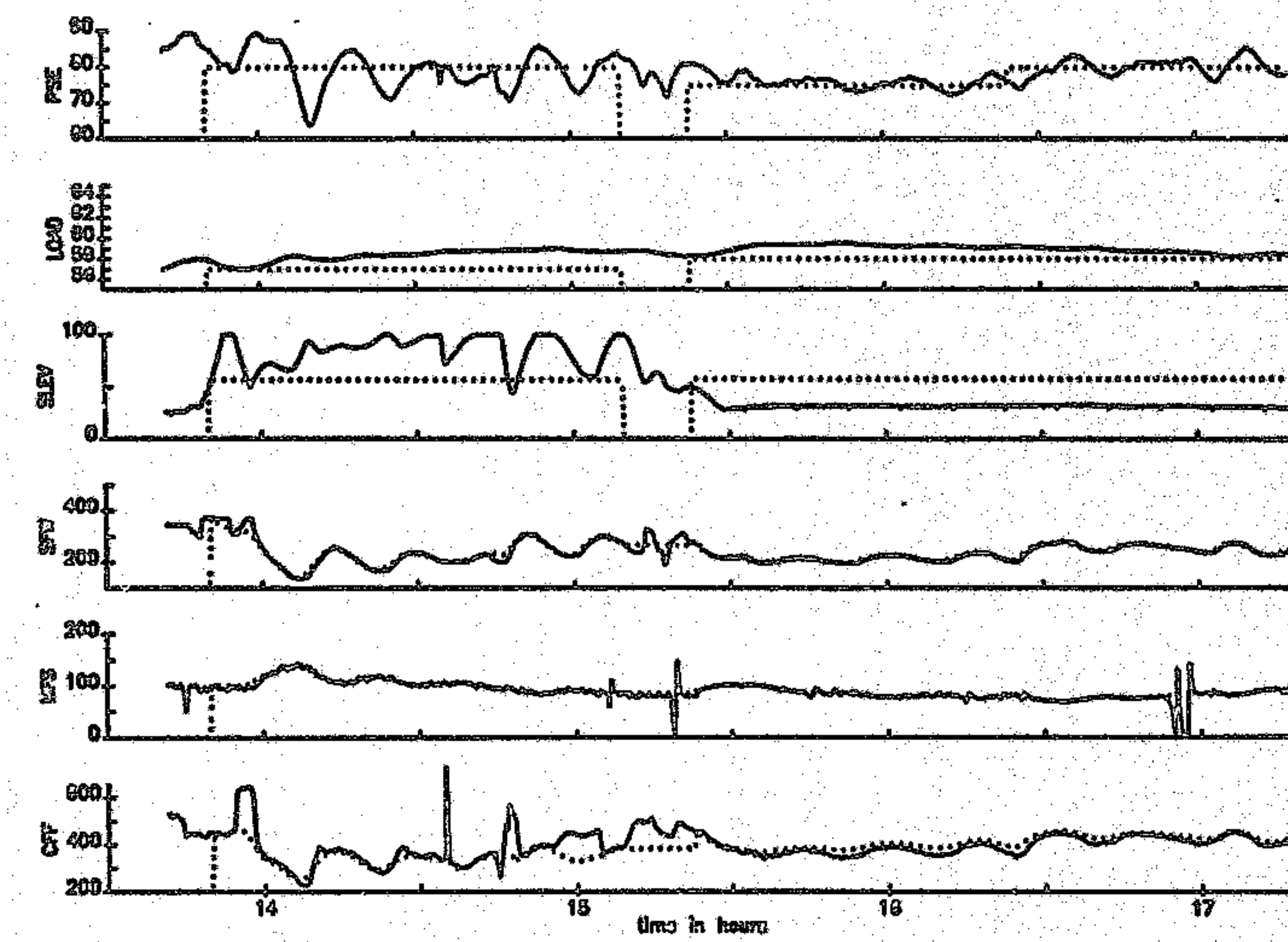

Figure 5.1: Initial μ-Controller Plant Test

This initial μ-controller test indicated that some form of PSE control was achieved, but that the LOAD and SLEV control was inadequate. This test also indicated that the CFF slave controller, and to a lesser degree the SFW slave controller, needed to be tuned more to give a faster response, as they did not follow the setpoint requested by the μ-controller accurately.

The poor SLEV control suggests that the ratio of SFW to CFF which would keep the SLEV constant, was not as the model predicted. This could be due to various factors: the CFF slave controller is not tuned correctly and is therefore not responding adequately to μ-controller requests, i.e., the ratio of SFW to CFF requested by the μ-controller, was not achieved by the physical plant; the SFW and CFF base levels are incorrect. The control of the integrator SLEV is very sensitive to the base levels of the plant inputs SFW and CFF. These base levels are obtained at the startup of the controller, and if they are incorrect because of noise or unsteady plant operation, a large effective disturbance in introduced that requires a large amount of proportional action to overcome;the uncertainty in the integral constants of the SLEV/SFW (g_{31}) and SLEV/CFF (g_{33}) transfer functions was not taken into account when the μ-controller was designed.

The inadequate LOAD control suggests that some plant changes might have occurred, as the MFS was responding more to PSE errors than to LOAD errors.

In the light of the discussions above, it was decided to re-tune the SFW and CFF slave controllers, and to also do one set of plant identification tests in order to get an indication of how much the plant has changed since the original identification tests were done. These actions are discussed in the next section.

5.2.2 Plant identification tests

Simple Ziegler-Nichols tuning [78] was used to tune the SFW and CFF slave PI controllers. After the tuning exercise the two slave controllers were considered to respond adequately to their setpoints.

Identification tests were then conducted, starting with steps in the SFW. During these steps the SLEV was not controlled, and care had to be taken not to let the sump overflow or run dry. The SFW steps are shown in Figure 5.2. A 90 minute base level was achieved before the steps commenced, in order to accurately determine steady-state gains of transfer functions with large time-constants, for e.g., LOAD/SFW. The MIW was kept constant throughout these tests.

Figure 5.3 show CFF steps (16:30 to 20:00) followed by MFS steps (20:00 to 22:00). These steps were conducted with the SLEV controlled by the SFW, and is the reason for the SFW and CFF moving together in the same direction.

Standard ARX-type models [59] were fitted to the responses obtained from the step-tests. These discrete-time models were then converted to continuous-time, to obtain a matrix of transfer functions like that in Equation (3.1). The relationships obtained from the SFW steps, i.e., PSE/SFW and SLEV/SFW, were used to remove the effects of the SFW changes made during the CFF and MFS steps.

The identification exercise showed that the nominal values of most of the gains and time-constants of the ROM circuit transfer functions, were the same as before. Some significant changes were however found. The integral constant for the transfer function LOAD/MFS (g_{22}) was 5 times smaller than the one used in the μ-controller design. Also the dead-time in the PSE/MFS (g_{12}) transfer function had increased by a factor of 7. Some minor changes (about 15%) were observed in the integral constants of the SLEV/SFW and SLEV/CFF. In addition no simple relationship, such as g_{21} and g_{23} in Chapter 3, could be found for the LOAD/SFW and LOAD/CFF transfer functions.

It is important to note that these identification tests are not comprehensive enough to accurately identify minor changes in the nominal model, and serve only to indicate where major changes have occurred. Usually at least three sets of identification tests are required to obtain a model that is adequate for controller design. Thus the minor changes observed in the sump integral constants do not warrant nominal model changes, but do indicate that these transfer functions have some uncertainty associated with them. Such uncertainty was not taken into account in the original μ-controller design, which might be one of the reasons for the inadequate SLEV control.

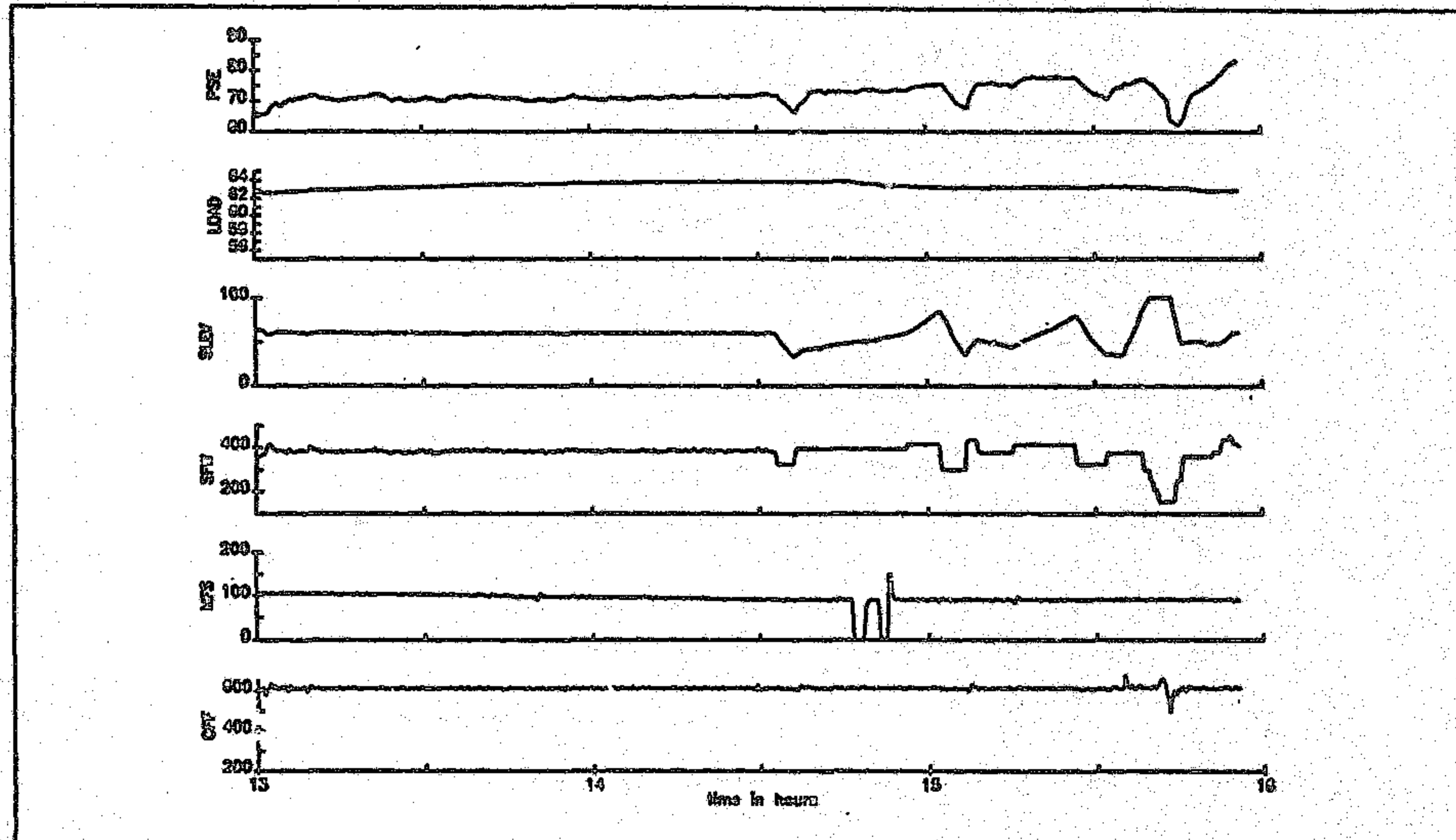

Figure 5.2: Plant Identification Test - SFW

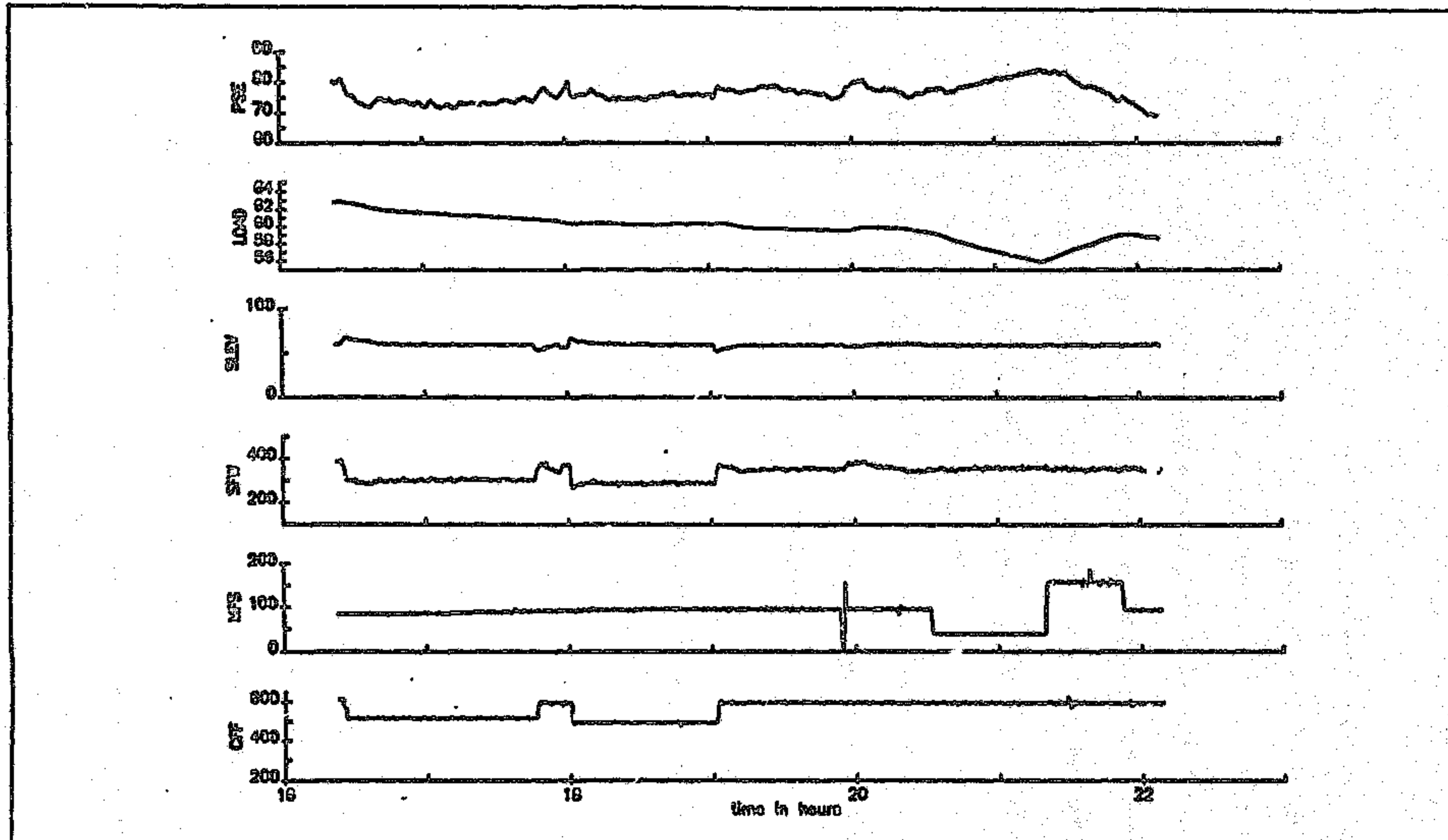

Figure 5.3: Plant Identification Test - CFF and MFS

The change in the dead-time of g_{12} (PSE/MFS) is due to a change of particle-size measuring instrument. The original identification tests were done using a ultrasound based particle-size estimator [8], whereas a derived-measurement based PSE is now in use. The new PSE uses amongst other signals the cyclone feed density (CFD) to estimate product-size [79]. The new dead-time that was found for g_{12} is of the same order as that of the dead-time found for the original CFD/MFS transfer function plus the dead-time of the PSE instrument. The large change in the LOAD/MFS integration constant is probably due to calibration changes made to the LOAD measuring instrument by plant personnel after the original identification tests were done. This calibration change, together with the change in dead-time of the PSE/MFS transfer function, [illegible] certainly have a detrimental effect on the μ-controller's ability to control the LC[illegible]

The μ-controller was redesigned to take the [illegible] into consideration, as discussed in the next section.

5.2.3 μ-Controller redesign and subsequent plant test

The redesign of the μ-controller which incorporates the changes discussed in the previous section, is described in Appendix A. The resulting plant test, which lasted for about 2 hours, is shown in Figure 5.4. This test shows that control of PSE and LOAD has improved considerably compared to the initial test described in Section 5.2.1. SLEV control was however still problematic. Good PSE and LOAD regulation was achieved from the time that the controller was switched on at 13:40 until the PSE setpoint change at 15:10. In fact the PSE control shown here compares favourably with what has been achieved with other synthesis methods such as INA [13].

The setpoint change in the PSE from 78 to 83% $<75\mu$m resulted in the sump overflowing at 15:40. The PSE setpoint was reduced from 83 to 80% $<75\mu$m to try and bring the SLEV down (the reasoning for this is given in the next paragraph). Eventually manual corrective action (reduction in SFW and increase in CFF) had to be taken to bring the SLEV down, and the test was aborted.

The reason for the sump overflowing is the following: When the PSE is below setpoint more SFW is added to bring the PSE to its setpoint. At the same time the μ-controller requests an increase in CFF to prevent the SLEV from rising. The SFW slave controller responds faster than the CFF slave controller to requests from the μ-controller. The CFF thus does not increase fast enough to compensate for the additional water that is added to the sump, i.e., the flowrate of water and slurry going into the sump is higher than the flowrate of slurry that is pumped to the cyclone, which results in the SLEV rising. If this situation continues for an extended period of time, the sump eventually overflows.

The reverse situation also occurs. When the PSE is below setpoint, the SFW is reduced without a corresponding drop in the CFF. The pump thus keeps on pumping fast whilst the SFW is decreased, which results in the SLEV going down. This phenomenon occurred at 14:35 during the run shown Figure 5.4.

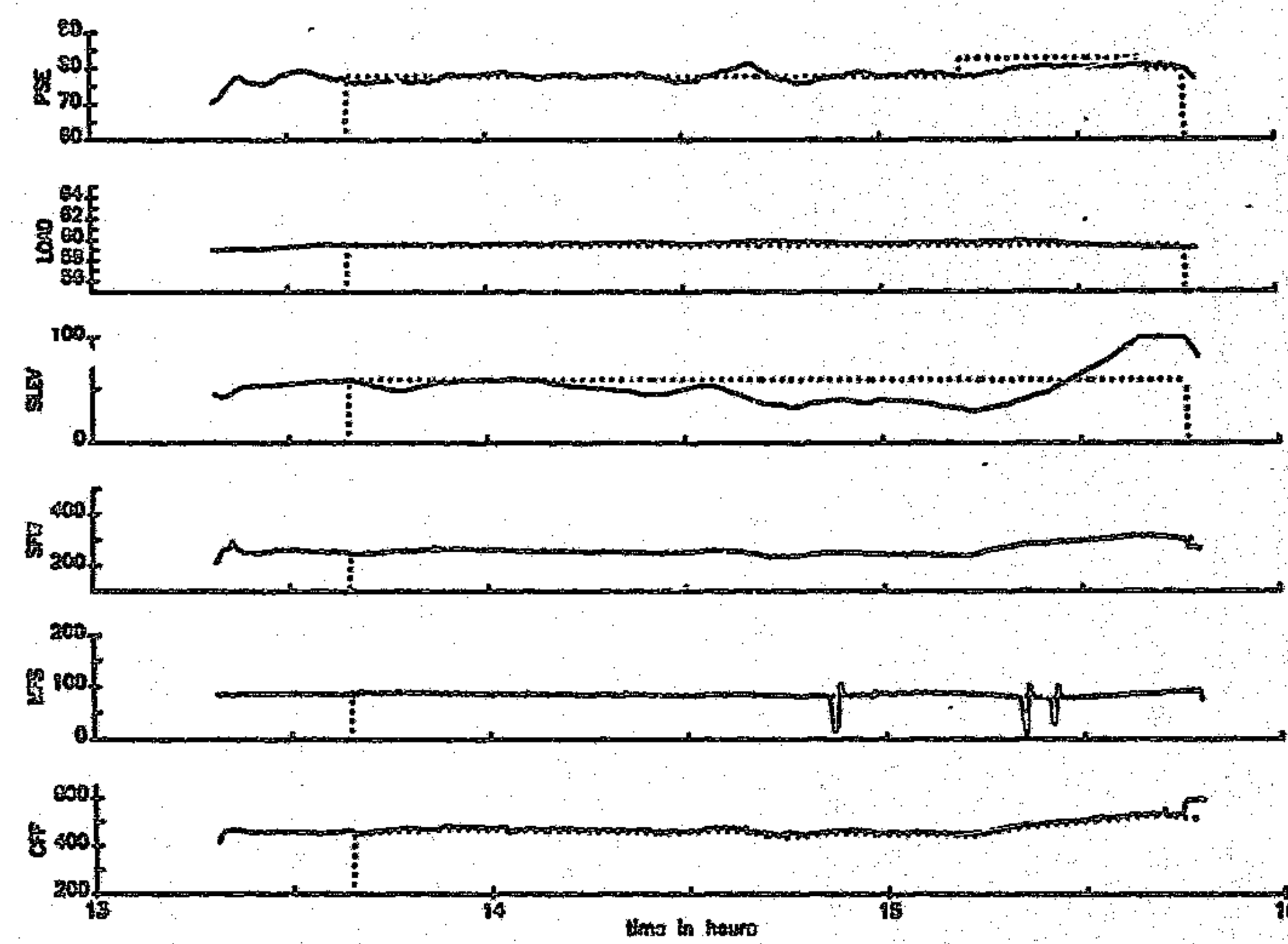

Figure 5.4: Second μ-Controller Plant Test

The poor SLEV control suggests that the physical plant goes out of the bounds described by the milling circuit model that was used for the μ-controller design. The assumption was made that the actuator dynamics were fast enough to be neglected in the controller design. This assumption is not valid as the physical SLEV/CFF transfer function, which includes the dynamics of the CFF slave controller, falls outside the parameter bounds determined for this transfer function in the milling circuit model.

A way of reducing the SLEV error would thus be to include the SFW and CFF slave controller dynamics in the nominal milling model, but the slave controllers are tuned tightly to avoid having to do this in the first place! The slave controllers' PI setting are changed regularly by plant personnel (not always for the better), which make it questionable wether the inclusion of their dynamics in the milling model will prevent the sump form overflowing or running dry in the medium to longer term.

The problem is however that the SLEV acts as an integrator, so any error will be integrated until the offset produced is large enough to build up sufficient control action. This offset will be large if the gain is small, and could perhaps become unbounded if the controller does not have the degree of freedom to correct an assumed ratio required of the SFW and CFF. The use of integral action is a possible solution to this problem.

The μ-controllers' performance will not be evaluated here against the PSE, LOAD, and SLEV error weights, as the SLEV control problem prevented significant setpoint changes from being made in the plant outputs.

5.3 Concluding Remarks

The plant test shown in Figure 5.4 indicates that the μ-controller could be made to work on an industrial ROM milling circuit, provided that the SLEV control problem can be overcome. A possible solution to this problem is to include the dynamics of the SFW and CFF slave controllers in the nominal milling model. It is however alarming that the μ-controller is so sensitive to the PI settings of the SFW and CFF slave controllers. This sensitivity can fortunately be explained, and requires careful handling in applications.

The μ-controller in its current form is unable to deal with the problem of instrument calibration changes such as the one observed in the LOAD measuring instrument. Because calibration changes happen frequently on industrial milling circuits (although not usually as large as the LOAD calibration change), it is essential for a controller to deal with such changes.

Some form of integral action is required to eliminate steady-state errors caused by calibration errors, such as making the value A in the error weighting function very small. However the smaller A gets, the more difficult it is to achieve robust performance. The existing model will also have to be expanded to describe all observed input-output behaviours of the milling circuit. In addition, safety jacket structures to deal with, for example, control action saturation, will have to be built around the μ-controller to make it rugged enough for industrial use. It is beyond the scope of this thesis to develop the μ-controller into a ruggedized full-blown practical industrial controller, and the matter will thus not be pursued any further.

CHAPTER 6

CONCLUSIONS AND RECOMMENDATIONS

This chapter gives a brief summary of the most important results of the research. The study is assessed and the significance and limitations of the work are discussed. Finally some suggestions are made for possible future research.

6.1 Assessment of Study

The significance of the study reported in this thesis is that, for the first time, it has been shown that the ROM mill control problem can be formalized in terms of the general synthesis and analysis framework. Motivation for this approach based on practical considerations, has been provided. Another key contribution of this work is that the resulting μ-controller was tested on a real industrial ROM milling circuit. It showed promising performance and confirmed the feasibility of the proposed approach. Such practical tests constitute a large leap from computer simulations studies, and are considered essential in evaluating a controller's applicability for industrial implementation.

The work described in this thesis can be divided into three sections: casting the ROM milling control problem in a general synthesis and analysis framework, synthesis and analysis of the μ-controller, and the practical implementation of the controller on an industrial ROM milling circuit.

The μ-methodology was applied to a ROM milling circuit model with physically motivated performance specifications. The resulting controller was implemented on an industrial milling circuit. Plant tests showed that good PSE and LOAD regulation can be achieved with the μ-controller, but that SLEV control is inadequate. The reasons for the poor SLEV control are analyzed in Chapter 5, and suggestions are made as to how they could be overcome. The μ-controller's performance is not evaluated against the PSE, LOAD, and SLEV error weights, as the SLEV control problem prevented significant setpoint changes from being made in the plant outputs.

The promising initial results indicate that with enough effort, the μ-controller could be made to work on an industrial milling circuit. An interesting question is whether the effort in establishing a μ-controller on an industrial ROM milling circuit is justified. From a commercial point of view the answer to this question is probably "no", for the following reasons: Existing controller design methods such as INA, can with just a nominal plant model and some on-line tuning achieve adequate control of an ROM milling circuit. The μ-methodology requires significantly more modelling input to quantify the uncertainty. It is considered unlikely that in practice even a major modelling effort would result in a model which can describe all the observed input-output behaviours of a ROM milling circuit. On-line tuning will therefore still be required to achieve good control.

This is certainly not an attempt to detract from the μ-theory. The μ-theory is considered to be very powerful, but it makes no statement about the performance or stability of the actual physical system. It needs to be supplied with the right information, and this is where the problem arises. The uncertainty description of the milling circuit that is used in this thesis, was derived from *over a hundred* models that were fitted to individual responses of experimental runs. It is somewhat alarming that even such a significant modelling effort is not sufficient to enable the μ-controller to perform as designed (admittedly, the μ-controller would have performed better if the CFF slave controller's dynamics were included in the nominal milling model). The other disturbing factor regarding the μ-controller is its sensitivity to instrument calibration changes and its inability to deal with ever-changing slave controller PI settings. Some form of integral action is required to eliminate steady-state errors caused by calibration changes, such as making the value A in the error weighting function very small. However the smaller A gets, the more difficult it is to achieve robust performance.

In defence of the μ-controller it must also be said that the plant tests were limited. The μ-controller should ideally be evaluated over a period of weeks and months. Also the tracking ability of this controller should be evaluated further, and based on long-term tests, the applicability of the performance specifications and the uncertainty weights should be determined. Such extensive tests are however beyond the scope of this thesis.

The results presented in this thesis confirm that the strength of the μ-methodology lies in analysis and not synthesis. Its analysis power is demonstrated by the fact that one can determine the effect of model parameter variations and different performance specifications all at once. μ-Analysis could thus be used to analyze for example, the sensitivity of an INA controller to different plant parameter variations. Such a process might indicate that more emphasis should be placed on identifying certain transfer functions, i.e., it might turn out that it is not necessary from a robustness point of view to accurately determine the LOAD/SFW transfer function. On the other hand, the controller might be very sensitive to changes in the parameters of another transfer function such as the PSE/SFW transfer function. Such an analysis study could be very useful in saving time in establishing a model for controller design. It could also suggest improvements to mechanistic milling models that are currently employed.

6.2 Suggestions for Future Research

As stated in the previous section, the μ-theory is considered to be very powerful, but it needs to be supplied with the right information. This clearly indicates that effort should be put into developing identification methods that can accurately determine not only nominal MIMO models, but their associated uncertainty descriptions as well. Some progress has already been made in this regard and the July 1992 issue of the IEEE Transactions on Automatic Control was dedicated to this topic. In this issue Smith and Doyle [80] make a connection between robust control and identification, and give a necessary condition for a model to be able to describe all observed input-output behaviours of a system.

The identification problem can of course also be approached from a mechanistic modelling point of view, and efforts should continue to gain fundamental knowledge of the processes that occur in a ROM milling circuit.

More plant tests should be conducted with the μ-controller, and the relevance of the uncertainty description and the performance specifications should be evaluated. Methods which incorporate some form of on-line tuning in the μ-methodology should also be investigated, as this could have a considerable impact on the amount of identification effort required.

As stated several times in this thesis, large disturbances enter the milling circuit via the ROM feed. Instrumentation should thus be developed to provide a reliable measurement of such disturbances, and plant tests should be performed to determine what should be done with such a measurement once it is available. Some progress has already been made in this regard using vision-based systems to estimate rock-size on a mill feed belt [81]. It is possible that such a measurement could be linked in a feed-forward manner to the MIW such that the rheology inside the mill is optimized for good grinding.

A APPENDIX A

This appendix describes the redesign of the μ-controller. It includes a description of the weights used in the design, μ-synthesis and analysis results, and a state-space description of the reduced order μ-controller.

A.1 Uncertainty, Performance and Control Weights

For this design the LOAD/SFW (g_{21}) and LOAD/CFF (g_{23}) transfer functions were omitted, and 15% integral constant uncertainty was added to the transfer functions of the SLEV/SFW (g_{31}) and SLEV/CFF (g_{33}). The nominal integral constant for the LOAD/MFS transfer function (g_{22}) was decreased by a factor of 5, and the dead-time associated with the PSE/MFS transfer function was increased by a factor of 7. Five uncertainty weights were used i.e., w_1, w_3, w_4, w_5, and w_6. These weights are as shown in equations (3.15) to (3.17), with one exception; ω_b was made 1/8 to accommodate the fact that control action is taken every 5 seconds.

The "new" nominal plant with uncertainty description is shown in Figure A.1.

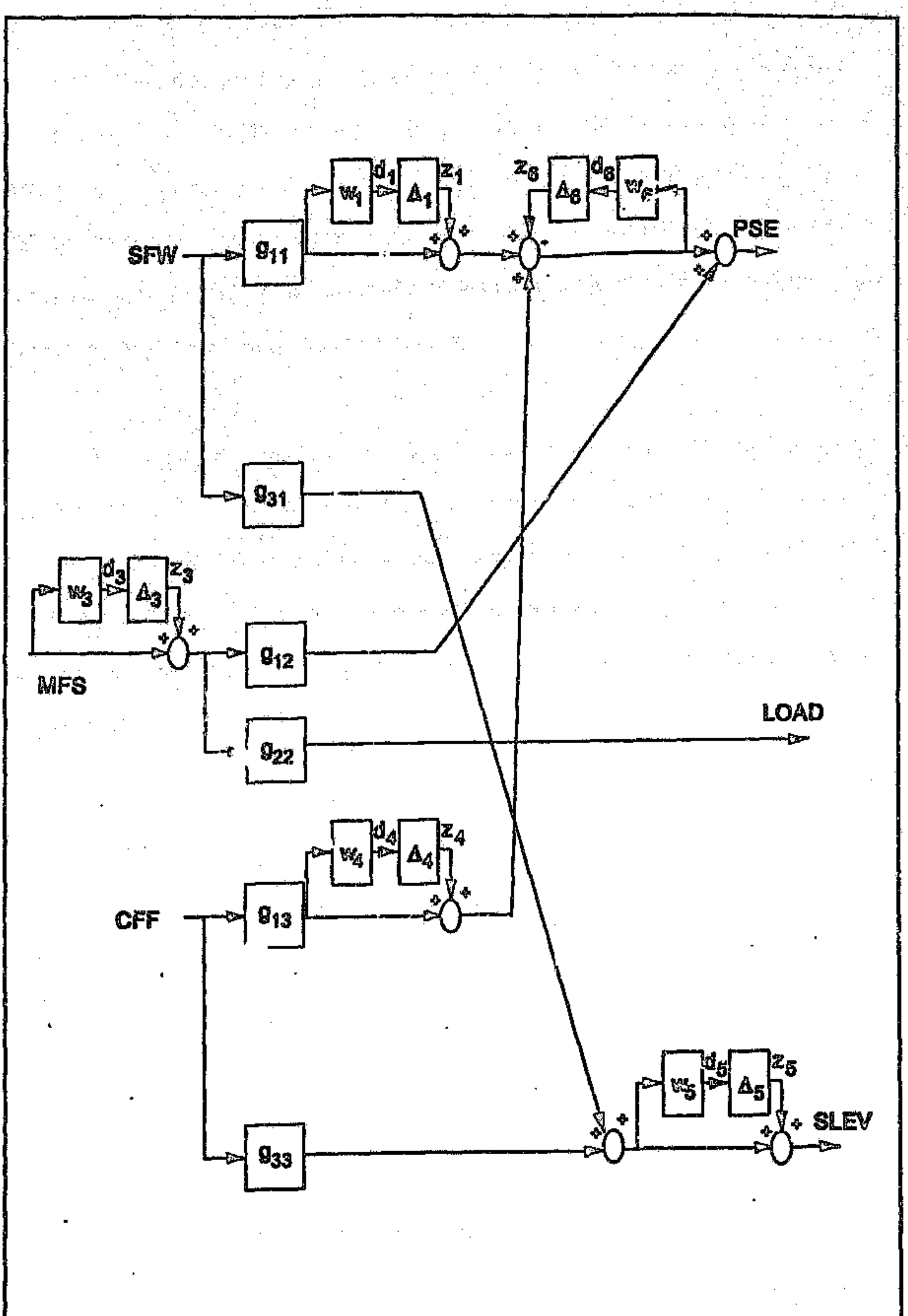

Figure A.1: New Nominal Plant with Uncertainty Description

Some changes were also made to the PSE error weight. The value A in the PSE error weight (see (3.19)) was increased to 0.1 from 0.05, to make it the same as that of the LOAD error weight. This was done because the LOAD is controlled over a range of 10%, whereas PSE control is done over a range of 20%. The change in PSE error weight thus amounts to output scaling which takes the range of control of a particular variable into account. The LOAD and SLEV error weights were left as is.

The MFS control weight was changed to scale this input to be in the same units as the SFW and CFF, i.e., m^3/h instead of t/h. The control weights were also scaled to incorporate the ranges over which the control actions operate, i.e., SFW $\pm$ 125 m^3/h, MFS $\pm$ 80 t/h, and CFF $\pm$ 125 m^3/h. The bandwidth of the control weight was also changes to accommodate the fact that control action is taken ever[illegible] seconds. The new control weight W_u is given as,

$$W_u = w_{ui} I_3$$

$$w_{ui} = \frac{8s + 0.005}{8s + 1}; \quad i=1,2 \tag{A.1}$$

$$w_{u3} = \frac{8s + \left(\frac{80}{125 * 2.7}\right)0.005}{8s + 1}$$

where 2.7 is the density of the ore in t/m^3.

A.2 μ-Synthesis and Analysis Results

Robust performance was achieved after 2 DK iterations with $\|M_{22}\|_\infty < 1.0$,

$\|\mu(M_{11})\|_\infty < 0.3$, and $\|\mu(M)\|_\infty < 1.02$. Figure A.2 shows the plots of $\mu(F_l(P,K))$ (both upper and lower bound), as well as the μ plot of M_{11} for robust stability and the $\bar{\sigma}$ plot of M_{22} for nominal performance. The controlled system achieves nominal performance and robust stability as indicated. Robust performance is almost achieved, with the μ plot of M, with respect to the block structure in Figure 2.5, peaking at a value of 1.02.

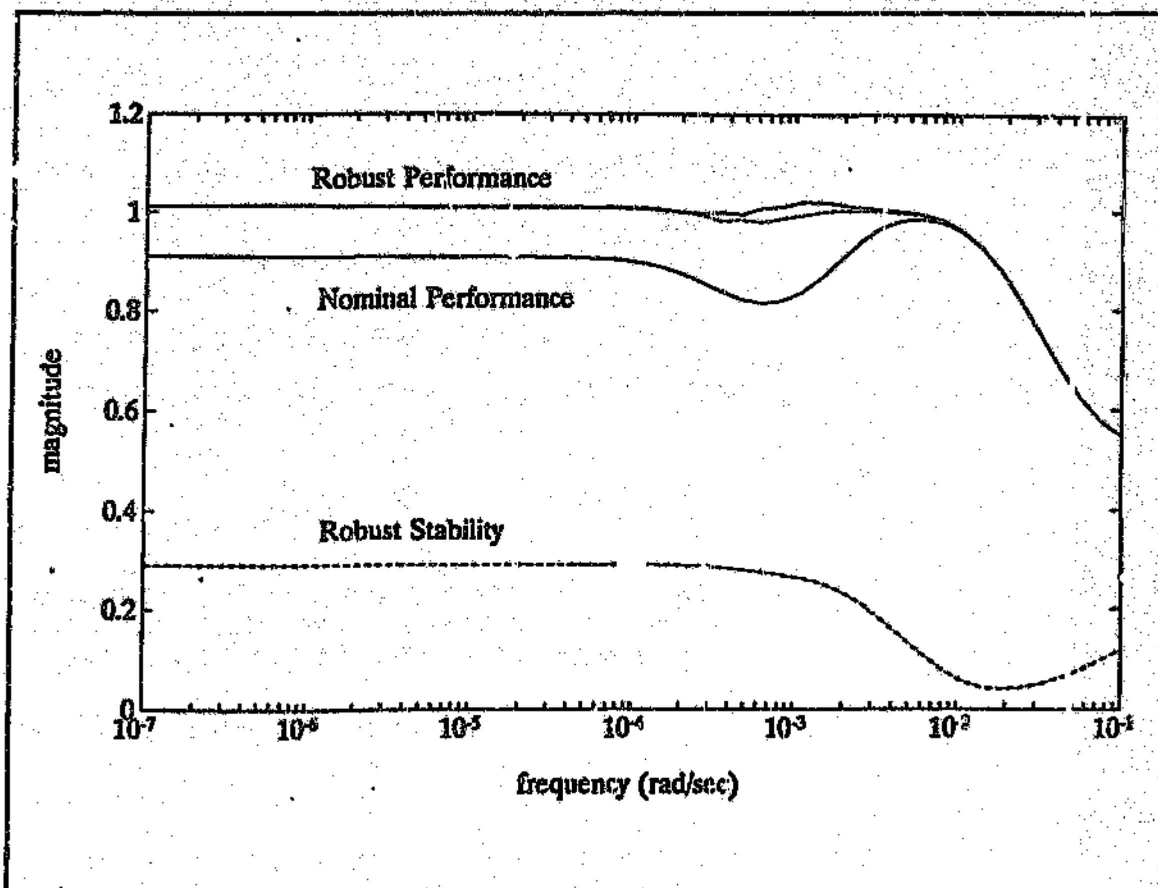

Figure A.2: Performance and Robustness Analysis of the Controlled System

A.3 State-Space Description of the Reduced Order μ-Controller

The μ-synthesis process resulted in a 32-state controller which was reduced to 12 states without losing the achieved level of robust performance. The 12 state controller was then converted to a discrete-time modal canonical state-space description as before. The discrete-time state-space description is shown below in the form,

$$x[k+1] = \Phi x[k] + \Gamma e[k]$$
$$u[k] = Cx[k] + De[k]$$

with Φ being a 12 x 12 matrix having only diagonal, upper and lower diagonal terms. The 12 diagonal terms are,

diag(Φ)=

[8.7882262E-01, 9.5169161E-01, 9.5169161E-01, 9.6512643E-01,
9.8508110E-01, 9.8508110E-01, 9.9565959E-01, 9.9637024E-01,
9.9944382E-01, 9.9926251E-01, 9.9972235E-01, 9.9999480E-01]

and the 11 upper diagonal terms are,

upperdiag(Φ) =

[0.0000000E+00, 2.5355977E-02, 0.0000000E+00, 0.0000000E+00,
1.7558486E-0[illegible], 0.0000000E+00, 0.0000000E+00, 0.0000000E+00,
0.0000000E+00, 0.0000000E+00, 0.0000000E+00]

The lower diagonal terms are given by,

lowerdiag(Φ) = - upperdiag(Φ)

The 12 x 3 Γ matrix is,

1.3514808E-02,	-1.8039928E+00,	-1.4957170E-02
-2.2263361E+00,	-2.4041768E-01,	1.3115054E-01
-9.0769077E-01,	6.5452338E-01,	1.0544791E-01
-9.3704678E-0[illegible],	9.0210162E-03,	2.2811913E-01

2.8568221E-02,	1.0412695E+01,	8.2967905E-03
-1.1480505E-01,	9.6627428E-02,	3.7855838E-03
-1.3158877E-01,	-1.7018330E+00,	-5.8213929E-03
1.7031531E-01,	-1.7603067E-01,	-1.1298962E-03
-7.1590220E-01,	1.8296749E-04,	-7.8894152E-03
5.9939681E-03,	-2.0899848E-03,	2.9616990E-02
-5.5693239E-04,	-2.1993800E-01,	-2.0508974E-04
1.1245586E-02,	3.8110481E-04,	9.8107825E-05

The 3 x 12 C matrix is given in terms of its 3 rows by,

row1 = [2.0222076E-02,-1.[illegible]780731E-02, 1.1005257E-01,-1.9108652E-02,-2.6347211E-02, 8.1034987E-02,
-1.4031186E-01,-2.9271139E-02,-1.1084911E-01,-5.9793329E-03,3.5177271E-02,-1.7268165E-03]

row2 = [2.6235928E-01,-7.7883441E-04,-5.5422270E-03, 1.6790879E-02, 6.7862203E-02,-8.9941153E-03
5.0936728E-02,-2.8873772E-02,-2.1894306E-03,-1.5673703E-03,3.0859721E-02, 6.2733011E-06]

row3 = [1.8172307E-02,-1.0363255E-02, 9.3339339E-02,-6.6604147E-02,-2.2227933E-02, 6.9009148E-02
-1.1871[illegible]4E-01,-2.5262822E-02,-9.3767794E-02,2.2468081E-03, 2.9749230E-02,-1.4600085E-03]

The 3 x [illegible] matrix is given by,

1.18[illegible]95E-02,	9.6938847E-04,	-7.5106805E-03
-5.5768567E-03,	-4.5774427E-04,	3.5465358E-03
4.4590287E-03,	3.6599377E-04,	-2.8356664E-03

REFERENCES

1. Hulbert, D.G., The state of the art in the control of milling circuits, *Preprints of the 6th IFAC Symp. on Automation in Mining, Mineral and Metal Processing*, Buenos Aires, 1989.

2. Bode, H.W., *Network Analysis and Feedback Amplifier Design*, Princeton: Van Nostrand, 1945.

3. Horowitz, I.M., *Synthesis of Feedback Systems*, New York: Academic Press, 1963.

4. Doyle, J.C., and Stein, G., Multivariable feedback design: Concepts for a classical/modern synthesis, *IEEE Trans. Automat. Contr.*, Vol. 26, Feb. 1981, pp. 4-16.

5. Doyle, J.C., Analysis of feedback systems with structured uncertainty, *IEE Proceedings-D*, Vol.129, No.6, Nov. 1982, pp. 242-250.

6. Doyle, J.C., Synthesis of robust controllers and filters, *22nd IEEE Decision and Control Conf.*, 1983, pp. 109-114.

7. Milich, D.A., Athans, M., Valavani, L., and Stein, G., A method for designing robust multivariable feedback systems, *27th IEEE Decision and Control Conf.*, 1988, pp. 2150-2156.

8. Cushman, C.R., Hale, J.C., and Anderson, V.A., *Particle Size and Percent Solids Monitors*, U.S. Patent No. 3,779,070. 1973.

9. Hulbert, D.G., Koudstaal, J., Braae, M., and Gossman, G.I., in O'Shea, J., and Polis, M. (Eds.), Multivariable control of an industrial grinding circuit, *3rd IFAC Symp. Automation in Mining, Mineral, and Metal Processing*, London: Pergamon Press, 1981, pp. 817-825.

10. Jämsä, S-L., Melama, H. and Penttinen, J. in Westerlund, T., (Ed.), "Design and experimental evaluation of a multivariable grinding circuit control system", *4th IFAC Symposium on Automation in Mining, Mineral and Metal Processing, 1983, Espoo, Finland.* Oxford: Pergamon Press, 1984, pp. 189-197.

11. Jackson, O.A.E., A review of modern milling practice at the South African gold and uranium mines, *7th Common. Min. and Metall Congr.*, Vol. 3, Johannesburg: South African Institute of Mining and Metallurgy, 1961, pp. 937-978.

12. Flook, W.R., Automatic control of feed of autogenous grinding media, *J. S. Afr. Inst. Min. Metall.*, Vol. 75, 1976, pp. 60-64.

13. Hulbert, D.G., Craig, I.K., Coetzee, M.L., and Tudor, D., Multivariable control of a run-of-mine milling circuit, *J.S. Afr. Inst. Min. Metall.*, Vol. 90, Jul. 1990, pp. 173-181.

14. Rosenbrock, H.H., *Computer-aided control system design*, London: Academic Press, 1975.

15. MacFarlane, A.G.J., and Kouvaritakis, B., A design technique for linear multivariable feedback-systems, *Int. J. Control*, Vol. 25, 1977, pp. 837-879.

16. Postlethwaite, I., and MacFarlane, A.G.J., *A complex variable approach to the analysis of linear multivariable feedback systems*, Berlin:Springer-Verlag, 1979.

17. Flook, W.R. and Plasket, R.P., in H.W. Glenn (ed.), Design and control practice for run-of-mine mills in Union Corporation Ltd., *Proc. 12th CMMI CONGRESS*, Johannesburg:S. Afr. Inst. Min. Metall., 1982, pp. 529-550.

18. Williamson, J.E., The automatic control of grinding medium in pebble mills, *J. S. Afr. Inst. Min. Metall.*, Vol. 60, 1960, pp. 333-345.

19. Pauw, O.G., King, R.P., Garner, K.C., and Van Aswegen, P.C., The control of pebble mills at Buffelsfontein Gold Mine by use of a multivariable peak-seeking controller, *J. S. Afr. Inst. Min. Metall.*, Vol. 85, 1985, pp. 89-96.

20. Herbst, J.A., Pate, W.T., and Oblad, A.E., Model-based control of mineral processing operations, *Powder Technology*, Vol. 69, 1992, pp. 21-32.

21. Mular, A.L., Automatic control of conventional and semi-autogenous grinding circuits, *CIM Bulletin*, Vol. 82, Feb. 1989, pp. 68-74.

22 Craig, I.K., Hulbert, D.G., Metzner, G., and Moult, S., Optimized multivariable control of an industrial run-of-mine milling circuit, *J.S. Afr. Inst. Min. Metall.*, Vol. 92, Jun. 1992, pp.169-176.

23. Craig, I.K., Hulbert, D.G., Metzner, G., and Moult, S., Extended particle-size control of an industrial run-of-mine milling circuit, *Powder Technology*, Vol. 73, 1992, pp. 203-210.

24. Barker, I.J., and King, R.P., in Lancaster, F.H. (ed.), A real-time recursive filter applied to a milling circuit to estimate particle-size distributions. *2nd IFAC Symposium on Automation in Mining, Mineral and Metal Processing*. Pretoria:South African Council for Automation and Computation, 1977, pp. 263-275.

25. Herbst, J.A., Rajamani, K., and Pate, W.J., in O'Shea, J., and Polis, M. (Eds.), Identification of ore hardness disturbances in a grinding circuit using a Kalman filter. *3rd IFAC Symposium on Automation in Mining, Mineral and Metal Processing*, Oxford. Pergammon Press, 1980, pp. 333-348.

26. Metzner, G., and MacLeod, I.M., The application of multivariable adaptive control to an industrial run-of-mine milling process, *IFAC Conf. on Intelligent Tuning and Adaptive Control*, Singapore, 1991.

27. Dorato, P. (ed.), *Robust Control*, New York: IEEE Press, 1987.

28. Dorato, P., and Yedavalli, P.K. (eds.), *Recent Advances in Robust Control*, New York:IEEE Press, 1990.

29. Horowitz, I.M., Invited paper. Survey of quantitative feedback theory (QFT), *Int. J. Control*, Vol. 53, 1991, pp. 255-291.

30. Doyle, J.C., Quantitative feedback theory and robust control, *Proc. American Control Conf.*, Seattle, WA, 1986, pp. 1691-1695.

31. Laughlin, D.L., Jordan, K.G., and Morari, M., Internal model control and process uncertainty: Mapping uncertainty regions for SISO controller design, *Int. J. Control*, Vol. 44, 1986, pp. 1675-1698.

32. Garcia, C.E., and Morari, M., Internal Model Control - 1. A unifying review and some new results, *Ind. Eng. Chem. Process Des. & Dev.*, Vol. 21, 1982, pp. 308-323.

33. Safanov, M.G., Stability margins of diagonally perturbed multivariable feedback systems, *IEE Proceedings-D*, Vol. 129, 1982, pp. 251-256.

34. Wei, K., and Yedavalli, R.K., Robust stabilization for linear systems with both parameter and unstructured uncertainty, *IEEE Trans. Automat. Contr.*, Vol. 34, 1989, pp. 149-156.

35. Hollot, C.V., Looze, D.P., and Bartlett, A.C., Parametric uncertainty and unmodeled dynamics: Analysis via parameter space methods, *Automatica*, Vol. 26, No. 2, 1990, pp. 269-282.

36. Barmish, B.R., New Tools for robust analysis, *27th IEEE Decision and Control Conf.* 1988, pp. 1-6.

37. Fan, M.K.H., Tits, A.L., and Doyle, J.C., Robustness in the presence of mixed parametric uncertainty and unmodeled dynamics, *IEEE Trans. Automat. Contr.*, Vol. 36, Jan. 1991, pp. 25-38.

38. Sánches Peña, R.S., and Sideris, A., Robustness with real parametric and structured complex uncertainty., *Int. J. Control*, Vol. 52, No. 3, 1990, pp. 753-765.

39. Rohrs, C.E., Valavani, L., Athans, M., and Stein, G., Robustness of continuous time adaptive control algorithms in the presence of unmodeled dynamics, *IEEE Trans. Automat. Contr.*, Vol. 30, Sep. 1985, pp. 881-889.

40. Krause, J.M., Stein, G., and Khargonekar, P.P., Sufficient conditions for robust performance of adaptive controllers with general uncertainty structure, *Automatica*, Vol. 28, No. 2, 1992, pp. 277-288.

41. Doyle, J.C., Structured uncertainty in control systems design, *24th IEEE Decision and Control Conf.* 1985, pp. 260-265.

42. Doyle, J.C., A review of μ for case studies in robust control, *IFAC Triannual World Congress*, Munich, West Germany, 1987, pp. 395-402.

43. Doyle, J.C., Lenz, K., and Packard, A., Design examples using μ-synthesis: Space shuttle lateral axis FCS during reentry, *25th IEEE Decision and Control Conf.*, 1986, pp. 2218-2223.

44. Smith, R.S., Doyle J.C., Morari, M., and Skjellum, A., A case study using μ: Laboratory process control problem, *IFAC Triannual World Congress*, Munich, West Germany, 1987, pp. 403-415.

45. Skogestad, S., Morari, M., and Doyle, J.C., Robust control of ill-conditioned plants: High-purity distillation, *IEE Trans. Automat. Contr.*, Vol. 33, Dec. 1988, pp 1092-1105.

46. Steinbach, M., Terlouw, J.C., Bosgra, O.H., and Smit S.G., Uncertainty modelling and structured singular-value computation applied to an electromechanical system, *IEE Proceedings-D*, Vol. 139, May 1992, pp. 301-307.

47. Doyle, J.C., Glover, K., Khargonekar, P., and Francis, B.A., State-space solutions to the standard H_2 and H_∞ control problems, *IEEE Trans. Automat. Contr.*, Vol. 34, Aug. 1989, pp. 831-847.

48. Francis, B.A., *A course in H_∞ control theory*, Lecture notes in control and information sciences, Berlin:Springer Verlag, 1987.

49. Glover, K., and Doyle, J.C., State-space formulae for all stabilizing controllers that satisfy an H_∞-norm bound and relations to risk sensitivity, *Systems & Control Letters*, Vol. 11, 1986, pp. 167-172.

50. Packard, A., Fan, M.K.H., and Doyle, J.C., A power method for the structured singular value, *27th IEEE Decision and Control Conf.* 1988, pp. 2132-2137.

51. Osborne, E.E., On pre-conditioning of matrices, *J. Ass. Comput. Mach.*, Vol. 7, 1960, pp. 338-345.

52. Morari, M., and Zafiriou, E., *Robust Process Control*, Englewood Cliffs: Prentice Hall, 1989.

53. Youla, D.C., Jabr, H.A., and Bongiorno, J.J., Modern Weiner-Hopf Design of optimal controllers, Part II: The multivariable case, *IEEE Trans. Automat. Contr.*, Vol. 21, Jun. 1976, pp. 319-338.

54. Balas, G.J., Doyle, J.C., Glover, K., Packard, A.K., and Smith, R., *Manual to μ-Analysis and Synthesis Toolbox*, Natick: The Mathworks, 1991.

55. Stanley G.G. (ed.), *The extractive metallurgy of gold in South Africa*, Vol. 1, Johannesburg: South African Institute of Mining and Metallurgy, 1987.

56. Lynch, A.J., and McKee, D.J., in Haughton, L.F. (ed.), The modelling and control of mineral processing plants, *Proc. Mintek 50, Int. Conf. on Mineral Science and Technology*, Vol. 1, 1984, pp 77-85.

57. Austin, L.G., A review: Introduction to the mathematical description of grinding as a rate process, *Powder Technology*, Vol. 5, 1971, pp. 1-17.

58. Stanley, G.G., Mechanisms in the autogenous mill and their mathematical representation, *J. S. Afr. Inst. Min. Metall.*, Vol. 75, 1974, pp. 77-98.

59. Ljung, L., *System identification: Theory for the user*, Englewood Cliffs: Prentice Hall, 1987.

60. Wigdorowitz, B., and MacLeod, I.M., Application of equilibrium surface modelling methodology in designing a controller for a Van der Pol oscillator, *Int. J. Control*, Vol. 53, No. 5, 1991, pp. 1055-1065.

61. Duckworth, G.A., and Lynch, A.J., The effect of some operating variables on autogenous grinding circuits and their implications for control, *14th International Mineral Processing Congress*, Ottowa: Canadian Institute of Mining and Metallurgy, 1982, pp. III-1.1 to III-1.21.

62. Rhumer, W.T., *Handbook on the estimation of metallurgical process costs*, 2nd edition, Mintek Special Publication No. 14, Randburg: Mintek, 1991.

63. Laughlin, D.L., Rivera, D.E., and Morari, M., Smith predictor design for robust performance, *Int. J. Control*, Vol. 46, 1987, pp. 477-504.

64. Lundström, P., Skogestad, S., and Wang, Z-Q., Performance weight selection for H-infinity and μ-control methods, *Trans. Inst. MC* ,Vol. 13, No. 5, 1991, pp. 241-252.

65. Chiang, R.Y., and Safanov, M.G., *Robust-Control toolbox for MATLAB. User's guide*, South Natick: The MathWorks, 1988.

66. Chiang, R.Y., Safanov, M.G., and Takawy, J.A., H-infinity flight control design with large parametric robustness, *Proc. American Control Conference*, San Diego, CA, 1990, pp. 2496-2501.

67. Yue, A., and Postlethwaite, I., Improvement of helicopter handling qualities using H_∞-optimisation, *IEE Proceedings-D*, Vol.137, No.3, May 1990, pp. 115-129.

68. Strang, G., *Linear Algebra and its applications*, New York: Harcourt, Brace and Jovanovich, 1980.

69. Stein, G., and Doyle, J.C., Beyond singular values and loop shapes, *AIAA J. Guidance, Control and Dynamics*, Vol. 14, Jan-Feb. 1991, pp. 5-16.

70. De Zouza, C.E., Goodwin, G.C., Mayne, D.Q., and Palaniswami, M, An adaptive control algorithm for linear systems having unknown time delay, *AUTOMATICA*, Vol. 24, No. 3, 1988, pp.327-341.

71. Enns, D., *Model reduction for control system design*, Ph.D. thesis, Stanford University, 1984.

72. Glover, K., All optimal Hankel-norm approximations of linear multivariable systems and their L_∞ error bounds, *Int. J. Control*, Vol. 39, No. 6, 1984, pp. 1115-1193.

73. Davidson, I.W.D., Private Communication.

74. Concurrent CP/M Operating System Guide, Digital Research Inc., 1984.

75. MACBASIC 120 Programming, Analog Devices Inc., 1985.

76. μMAC-4000 User's Manual, Analog Devices Inc., 1985.

77. Kailath, T., *Linear Systems*, Prentice-Hall, 1980.

78. Stephanopoulos, G., *Chemical Process Control: An introduction to theory and practice*, Englewood Cliffs: Prentice Hall, 1984.

79. Mintek Bulletin, No. 57, Jan. 1993.

80. Smith, R.S., and Doyle, J.C., Model Validation: A Connection between robust control and identification, *IEEE Trans. Automat. Contr.*, Vol. 37, Jul. 1992, pp. 942-952.

81. Lange, T.B.L., *Measurement of the size distribution of rocks on a conveyor belt using machine vision*, Ph.D thesis, University of the Witwatersrand, 1990.